Longer-term simulations of projected changes in lake DOM concentrations related to climate change

Deliverable 5.2



Authors: Ricardo Paíz, Daniel Mercado-Bettín, Rafael Marcé, Eleanor Jennings, Valerie McCarthy

Date: 06/10/2026

Funded by the European Union

GRANT AGREEMENT NUMBER	101081728		
FULL TITLE / ACRONYM	INNOVATIVE TOOLS TO CONTROL ORGANIC MATTER AND DISINFECTION BYPRODUCTS IN DRINKING WATER / intoDBP		
START DATE	May 2023	**DURATION**	40 months
END DATE	September 2026		
PROJECT URL	**https://intodbp.eu/**		
DELIVERABLE	**D5.2**		
WORK PACKAGE	**WP5**		
CONTRACTUAL DATE OF DELIVERY	**30-09-2026**		
ACTUAL DATE OF DELIVERY	**06-10-2026**		
NATURE	**REPORT**	**DISSEMINATION LEVEL**	**PUBLIC**
LEAD BENEFICIARY	**DCU/CSIC**		
RESPONSIBLE AUTHOR	**Ricardo Paíz, Daniel Mercado-Bettín, Rafael Marcé, Eleanor Jennings, Valerie McCarthy**		
CONTRIBUTIONS FROM	**DCU & CSIC**		

ABSTRACT

DOC is a widely used proxy for dissolved organic matter (DOM), which is relevant to drinking water applications, including the formation of disinfection by-products (DBPs). This deliverable introduces the deployment of a process-based lake model to simulate long-term dissolved organic carbon (DOC) concentrations in an Irish lake and a Spanish reservoir. For this purpose, the General Lake Model (GLM) coupled with the Aquatic EcoDynamics (AED) set of modules was calibrated using local observations and globally available climate data to reproduce historical variations in water temperature and DOC, providing the basis for longer-term simulations. Future dynamics were projected under three climate change scenarios for each site using an ensemble of five global climate models, allowing climate-driven variability and associated uncertainty to be characterised. Our results provide an indication of how DOM levels may evolve in these source waters under future climatic conditions. This information has the potential to support water managers and relevant authorities in evaluating long-term adaptation strategies at catchment, source-water and treatment scales, including mitigation actions addressing the formation of DBPs and subsequent human exposure.

Disclaimer

Any dissemination of results reflects only the author's view and the European Commission is not responsible for any use that may be made of the information it contains.

© intoDBP Consortium, 2022

This deliverable contains original unpublished work except where clearly indicated otherwise. Acknowledgement of previously published material and of the work of others has been made through appropriate citation, quotation, or both. Reproduction is authorised provided the source is acknowledged.

Table of contents

List of figures 6

List of abbreviations 10

Executive summary 12

1. Introduction 14

1.1 Background 14
1.2 Objectives 18

2. Methods 19

2.1 Study sites 19
2.2 The model 21
2.3 Observational input data 25
2.4 Future climate projections and derived boundary conditions. 29
2.5 Modelling workflow 33

3. Results 42

3.1 Historical dynamics and model calibration 42
3.2 Future climate 52
3.3 Response of thermal structures 60
3.4 Future change in DOC concentrations 69

4. Discussion 80

4.1 Implications for water management 83
4.2 Modelling ahead 85

5. Conclusions 88

References 89

List of figures

Figure 1. Location of the study catchments including river network and topographic elevation. 18
Figure 2. Location of the study catchments including grouped land cover classifications and river network. 19
Figure 3. GLM simulation domain, input information and key simulated processes (Hipsey et al., 2019). 21
Figure 4. Schematic of the surface heat fluxes impacting the surface mixed layer as conceptualised in the General Lake Model (GLM) (Hipsey et al., 2014). 23
Figure 5. Modelling workflow implemented at each study site. The workflow comprised six sequential steps. 33
Figure 6. Daily observed and simulated water temperature profiles at Lough Feeagh during GLM calibration and validation. Model performance are indicated for calibration and validation, respectively. 42
Figure 7. Daily observed and simulated water temperature at different depths for Lough Feeagh during GLM calibration and validation. Model performance are indicated for calibration and validation, respectively. 43
Figure 8. Daily observed and simulated water temperature profiles at Sau Reservoir during GLM calibration and validation. Model performance are indicated for calibration and validation, respectively. 44
Figure 9. Daily observed and simulated water temperature at different depths for Sau Reservoir during GLM calibration and validation. Model performance are indicated for calibration and validation, respectively. 46
Figure 10. Daily observed and simulated DOC concentration at the surface layer (0.9 m) for Lough Feeagh during GLM-AED calibration and validation. Model performance are indicated for the best parameter set obtained during calibration and employed during validation, respectively. The light blue band around the optimised run denotes the local parameter ensemble uncertainty band. 48
Figure 11. Monthly observed and simulated DOC concentration at the surface layer (0.9 m) for Lough Feeagh during GLM-AED calibration and validation. Model performance are indicated for the best parameter set obtained during calibration and employed during validation, respectively. The light blue band around the optimised run denotes the local parameter ensemble uncertainty band. 48
Figure 12. Daily observed and simulated DOC concentration at the surface layer (0 – 5 m average) for Sau Reservoir during GLM-AED calibration and validation. Model performance are indicated for the best parameter set obtained during calibration and employed during validation, respectively. The light blue band around the optimised run denotes the local parameter ensemble uncertainty band. 50
Figure 13. Monthly observed and simulated DOC concentration at the surface layer (0 – 5 m average) for Sau Reservoir during GLM-AED calibration and validation. Model performance are indicated for the best parameter set obtained during calibration and employed during validation, respectively. The light blue band around the optimised run denotes the local parameter ensemble uncertainty band. 50

Figure 14. Boxplot distributions of average annual air temperature for the baseline period, and for the SSP126, SSP370 and SSP585 scenarios during the three analysed independent future periods for Lough Feeagh. 52
Figure 15. Boxplot distributions of average annual precipitation for the baseline period, and for the SSP126, SSP370 and SSP585 scenarios during the three analysed independent future periods for Lough Feeagh. 52
Figure 16. Boxplot distributions of average annual shortwave radiation for the baseline period, and for the SSP126, SSP370 and SSP585 scenarios during the three analysed independent future periods for Lough Feeagh. 53
Figure 17. Average calendar month air temperature value for the baseline period, and for the SSP126, SSP370 and SSP585 scenarios during the three analysed independent future periods for Lough Feeagh. 54
Figure 18. Average calendar month precipitation value for the baseline period, and for the SSP126, SSP370 and SSP585 scenarios during the three analysed independent future periods for Lough Feeagh. 55
Figure 19. Average calendar month shortwave radiation value for the baseline period, and for the SSP126, SSP370 and SSP585 scenarios during the three analysed independent future periods for Lough Feeagh. 55
Figure 20. Boxplot distributions of average annual air temperature for the baseline period, and for the SSP126, SSP370 and SSP585 scenarios during the three analysed independent future periods for Sau Reservoir. 56
Figure 21. Boxplot distributions of average annual precipitation for the baseline period, and for the SSP126, SSP370 and SSP585 scenarios during the three analysed independent future periods for Sau Reservoir. 56
Figure 22. Boxplot distributions of average annual shortwave radiation for the baseline period, and for the SSP126, SSP370 and SSP585 scenarios during the three analysed independent future periods for Sau Reservoir. 57
Figure 23. Average calendar month air temperature value for the baseline period, and for the SSP126, SSP370 and SSP585 scenarios during the three analysed independent future periods for Sau Reservoir. 57
Figure 24. Average calendar month precipitation value for the baseline period, and for the SSP126, SSP370 and SSP585 scenarios during the three analysed independent future periods for Sau Reservoir. 58
Figure 25. Average calendar month shortwave radiation value for the baseline period, and for the SSP126, SSP370 and SSP585 scenarios during the three analysed independent future periods for Sau Reservoir. 58
Figure 26. Future projections of average calendar month water temperature profiles for Lough Feeagh for the SSP126, SSP370 and SSP585 scenarios during the three analysed independent future periods. 61
Figure 27. Model-based anomalies of average calendar month water temperature profiles for Lough Feeagh for the SSP126, SSP370 and SSP585 scenarios during the three analysed independent future periods. 62
Figure 28. Future projections of average water temperature at different depths for Lough Feeagh for the historical reference, and for the SSP126, SSP370 and SSP585 scenarios during the three

analysed independent future periods. Light coloured bands denote GCM-derived uncertainty for each scenario, respectively. 63
Figure 29. Future projections of average calendar month water temperature profiles for Sau Reservoir for the SSP126, SSP370 and SSP585 scenarios during the three analysed independent future periods. 65
Figure 30. Model-based anomalies of average calendar month water temperature profiles for Sau Reservoir for the SSP126, SSP370 and SSP585 scenarios during the three analysed independent future periods. 66
Figure 31. Future projections of average water temperature at different depths for Sau Reservoir for the historical reference, and for the SSP126, SSP370 and SSP585 scenarios during the three analysed independent future periods. Light coloured bands denote GCM-derived uncertainty for each scenario, respectively. 67
Figure 32. Boxplot distributions of average annual surface DOC for Lough Feeagh for the baseline period, and for the SSP126, SSP370 and SSP585 scenarios during the three analysed independent future periods. 68
Figure 33. Boxplot distributions of model-based anomalies of average annual surface DOC for Lough Feeagh for the baseline period, and for the SSP126, SSP370 and SSP585 scenarios during the three analysed independent future periods. 69
Figure 34. Average calendar month DOC concentration value for the surface layer of Lough Feeagh for the baseline period, and for the SSP126, SSP370 and SSP585 scenarios during the three analysed independent future periods. 70
Figure 35. Future projections of average calendar month DOC concentration profiles for Lough Feeagh for the SSP126, SSP370 and SSP585 scenarios during the three analysed independent future periods. 71
Figure 36. Model-based anomalies of average calendar month DOC concentration profiles for Lough Feeagh for the SSP126, SSP370 and SSP585 scenarios during the three analysed independent future periods. 72
Figure 37. Future projections of average DOC concentration at different depths for Lough Feeagh for the historical reference, and for the SSP126, SSP370 and SSP585 scenarios during the three analysed independent future periods. Light coloured bands denote GCM-derived uncertainty for each scenario, respectively. 73
Figure 38. Boxplot distributions of average annual surface DOC for Sau Reservoir for the baseline period, and for the SSP126, SSP370 and SSP585 scenarios during the three analysed independent future periods. 74
Figure 39. Boxplot distributions of model-based anomalies of average annual surface DOC for Sau Reservoir for the baseline period, and for the SSP126, SSP370 and SSP585 scenarios during the three analysed independent future periods. 74
Figure 40. Average calendar month DOC concentration value for the surface layer of Sau Reservoir for the baseline period, and for the SSP126, SSP370 and SSP585 scenarios during the three analysed independent future periods. 75
Figure 41. Future projections of average calendar month DOC concentration profiles for Sau Reservoir for the SSP126, SSP370 and SSP585 scenarios during the three analysed independent future periods. 76

Figure 42. Model-based anomalies of average calendar month DOC concentration profiles for Sau Reservoir for the SSP126, SSP370 and SSP585 scenarios during the three analysed independent future periods. 77
Figure 43. Future projections of average DOC concentration at different depths for Sau Reservoir for the historical reference, and for the SSP126, SSP370 and SSP585 scenarios during the three analysed independent future periods. Light coloured bands denote GCM-derived uncertainty for each scenario, respectively. 78

List of abbreviations

Abbreviation	Full Description
AWQMS	Automatic Water Quality Monitoring Station
C	Carbon
CDOM	Chromophoric Dissolved Organic Matter
CMIP	Coupled Model Intercomparison Project
CO_2	Carbon Dioxide
CORINE	Coordination of Information on the Environment
DBP	Disinfection By-product
DOC	Dissolved Organic Carbon
DOM	Dissolved Organic Matter
EPA	Environmental Protection Agency
EU	European Union
FAO	Food and Agriculture Organization of the United Nations
FDOM	Fluorescent Dissolved Organic Matter
GCM	Global Climate Model
GHG	Greenhouse Gas
GLEON	Global Lake Ecological Observatory Network
GLM	General Lake Model
GLUE	The Generalised Likelihood Uncertainty Estimation Method
GWLF	The Generalised Watershed Loading Functions Model
GWLF-DOC	The Generalised Watershed Loading Functions Model with an Integrated DOC Module
HAA	Haloacetic Acids
HFM	High Frequency Monitoring
IPCC	Intergovernmental Panel on Climate Change
ISIMIP	Inter-Sectoral Impact Model Intercomparison Project
NOAA	National Oceanic and Atmosphere Administration
NSE	Nash-Sutcliffe Efficiency
OC	Organic Carbon
PET	Potential Evapotranspiration
QA	Quality Assurance
QC	Quality Control
r^2	Coefficient of Determination
RCP	Representative Concentration Pathway
RMSE	Root Mean Square Error
SA	Sensitivity Analysis
SSP	Shared Socioeconomic Pathway

THMs	Trihalomethanes
TOC	Total Organic Carbon
UK	United Kingdom
USA	United States of America
WFD	Water Framework Directive
WHO	World Health Organisation

Executive summary

Dissolved organic carbon (DOC) is widely used as a proxy for dissolved organic matter (DOM) and provides a measurable indicator of its concentration and variability in freshwater systems. The amount of DOM impacts raw water treatability and the formation of disinfection by-products (DBPs) in treated drinking water, some of which have been associated with potential adverse health effects dependent both on the type of DBP and the exposure conditions.

The dynamics of DOM are influenced by interactions between climate, land use, soil characteristics and hydrological conditions, which regulate the production, mobilisation and transport of organic matter from catchments into rivers, lakes and reservoirs. These processes can result in considerable variation in source-water quality over time and between sites. The complexity and amount of processes that control DOM not only make it difficult to understand DOM dynamics in some systems, but also to elucidate how these dynamics may evolve in the future. As part of the work undertaken in WP5 of the intoDBP project, a modelling and long-term projection framework was developed to simulate DOC in two contrasting freshwater systems: Lough Feeagh, a humic lake in Ireland, and Sau Reservoir, a regulated dam system in Spain. The framework uses the General Lake Model (GLM) coupled with the Aquatic EcoDynamics (AED) set of modules (GLM-AED), a widely applied process-based model for simulating physical and biogeochemical dynamics of lakes and reservoirs. The model was calibrated using local sensor observations and globally-available meteorological forcing data to simulate thermal and DOC dynamics at each site. Simplified representations of catchment, soil and inflow processes were incorporated to account for the environmental conditions controlling aspects of delivery and behaviour of DOC within each water body.

The future long-term simulations were generated using climate data from an ensemble of five global climate models under three Shared Socioeconomic Pathways: SSP126, SSP370 and SSP585 (IPCC et al., 2023). These scenarios represent different futures of global climatic conditions, socio-economic development and human adaptation to climate change. The numerical component of each scenario indicates the approximate radiative forcing reached by 2100 and corresponds to the forcing levels associated with RCP2.6, RCP7.0 and RCP8.5, respectively. Selected periods extending to the end of the century

were compared with a historical climatological baseline, allowing potential changes in DOC concentrations and their seasonal dynamics to be evaluated. The ensemble approach also provided an indication of the variability and uncertainty associated with the future climate projections.

Our work demonstrates that process-based modelling can be employed to reproduce broad DOC dynamics across two freshwater systems with markedly different physical, climatic and catchment characteristics. The future simulations show that surface DOC concentrations will likely increase compared with the historical baseline, particularly under the higher forcing scenarios and during the end of the century. The magnitude, seasonal patterns and changes with depth differed between the lake and reservoir. These differences highlight the importance of local water quality monitoring and of considering hydrodynamic conditions, catchment inputs and reservoir operations when estimating future changes in DOC. This information has the potential to support the evaluation and implementation of long-term adaptation and mitigation strategies at catchment, source-water, treatment and distribution scales. In addition, these results help to bridge the gap between environmental modelling and water management by providing information on future conditions effecting the precursors of DBP formation that may be relevant to DBP formation and potential human exposure, therefore contributing to a safer and more resilient drinking water supply.

1. Introduction

1.1 Background

Lakes and reservoirs play a central role in freshwater ecosystems and support a wide range of ecosystem services, including drinking water supply (Inácio et al., 2022; Montenegro-Díaz et al., 2025). Across Europe, many communities depend on these water bodies as primary or supplementary sources of raw drinking water (Flem et al., 2015). The capacity of lakes and reservoirs to provide this service, however, depends largely on the quantity and quality of the water they receive and on the physical and biogeochemical processes occurring within them. These water bodies are therefore not isolated systems but are closely connected to their surrounding catchments through rivers, runoff, groundwater and the transport of dissolved and particulate materials (Shan et al., 2019; Xie et al., 2024).

Dissolved organic matter (DOM) is one of the principal components transferred from terrestrial environments into freshwater systems (Jennings et al., 2010; Adler et al., 2021). The production, mobilisation and transport of DOM are regulated by interactions arising from various land cover, land use, soil characteristics, and meteorological factors such as temperature as well as water availability and catchment hydrology (Evans et al., 2006; Wit et al., 2021). Organic matter produced and stored within soils can be transported into water bodies during rainfall and runoff events, through subsurface pathways or following changes in hydrological connectivity (Clark et al., 2009; Adler et al., 2021). These processes vary considerably between catchments and can result in marked spatial and temporal differences in the amount and composition of DOM entering lakes and reservoirs (Jennings et al., 2010; Paíz et al., 2025a; Mercado-Bettín et al., 2026).

Climate variability further influences these dynamics by modifying both the production of organic matter in soils and its transport towards freshwater systems (Anderson et al., 2023; Wu and Yao, 2024). Changes in air temperature and precipitation can affect soil decomposition, moisture conditions, water-table levels and the magnitude and timing of catchment runoff. Prolonged dry periods, drought–rewetting cycles, intense rainfall and flooding can all alter DOC mobilisation and produce substantial changes in its

concentration and seasonal distribution (Blaurock et al., 2021; Dong et al., 2021; Wu et al., 2023). These effects are expected to become increasingly relevant under climate change. Many projections indicate that DOC concentrations or their variability may increase under warmer and more hydrologically variable conditions, particularly in scenarios characterised by greater warming and limited mitigation efforts (Naden et al., 2010; Paíz et al., 2025a).

Once organic matter reaches a lake or reservoir, its behaviour is further regulated by processes occurring within the water body. Hydrodynamic conditions determine how water, heat and dissolved substances are distributed through the water column. Water temperature, thermal stratification, vertical mixing, inflow dynamics, residence time and reservoir operation can influence where organic matter accumulates and how long it remains within the system (Evans et al., 2005; Rodríguez-Cardona et al., 2022). At the same time, microbial degradation, photochemical reactions, biological production and interactions with sediments can modify both the quantity and composition of DOM. For example, sunlight can reduce DOM colour through photobleaching and contribute to DOC breakdown near the surface. Microbial mineralization in the water column and sediments can also lower DOC concentrations by converting organic carbon into inorganic forms, while sediment release and biological production can add DOC to the water (Gonsior et al., 2013, 2014; Lavonen et al., 2015). Lakes and reservoirs may therefore respond differently to similar external inputs, depending on their morphology, hydrological regime, thermal structure and internal biogeochemical conditions (Luo et al., 2022; Kajan et al., 2023). Understanding catchment inputs alone can be consequently insufficient without also considering how the receiving water body processes and transforms them.

These dynamics are particularly important when lakes and reservoirs are used as drinking-water sources (Anderson et al., 2023). Elevated or highly variable DOM concentrations can increase treatment requirements and reduce the efficiency of processes used to remove organic material from raw water (Köhler et al., 2016; Piai et al., 2024). If part of this material remains during disinfection, it can react with disinfectants such as chlorine and form disinfection by-products (DBPs) (Srivastav et al., 2020; Franklin et al., 2021). These include trihalomethanes (THMs) and haloacetic acids

(HAAs), among a broader range of compounds with differing chemical characteristics and potential toxicity (Villanueva et al., 2023). Long-term exposure to some DBPs has been associated with adverse human-health effects, making their occurrence an important concern for drinking-water providers and regulatory authorities. Considerable attention is therefore emerging towards monitoring DBPs, preventing regulatory exceedances and reducing both their formation and subsequent human exposure (Diana et al., 2019; Kumari and Gupta, 2022).

Strategies for controlling DBPs can be implemented at several stages of the drinking-water cycle (Kritzberg et al., 2020; Anderson et al., 2023). These include improving organic matter removal during treatment, adjusting disinfection practices, reducing water residence times within distribution systems and applying additional treatment at centralised or household scales (Wang et al., 2024; Zimmermann et al., 2025). Their feasibility and effectiveness, however, differ among water supplies and can be constrained by infrastructure, costs and operational capacity. A complementary and preventive approach is to address the problem at catchment and source-water scales (Kritzberg et al., 2020; DeMont et al., 2021). Actions that reduce organic matter mobilisation from the catchment, improve the quality of inflows or manage conditions within the water body can decrease the burden placed on downstream treatment (Xiao et al., 2024). In principle, maintaining raw water at a quality that does not compromise treatability can support more efficient treatment and distribution while reducing the conditions that favour DBP formation (DeMont et al., 2021; Villanueva et al., 2023).

Effective planning therefore requires information on how source-water quality may change across different time scales. Short-term information can support operational responses (Carey et al., 2022; Klante et al., 2022), while long-term projections are needed to evaluate investments, catchment interventions, treatment upgrades and adaptation strategies that may take several years or decades to implement (Anderson et al., 2023). Historical observations remain essential for describing past conditions, but they may not fully represent the climatic and hydrological conditions that water bodies will experience in the future (Clark et al., 2010). Quantifying how DOM concentrations may increase, decrease or change seasonally under alternative climate scenarios can

provide a stronger basis for evaluating these longer-term decisions (Anderson et al., 2023; Wu and Yao, 2024).

Process-based modelling provides a pathway for generating this information by integrating meteorological forcing, hydrology, lake physics and water-quality processes within a consistent framework (Cuddington et al., 2013; Chen et al., 2021). Models can first be evaluated against observations to determine their capacity to reproduce historical hydrodynamic and DOM dynamics. They can then be driven with projected climate conditions to investigate how these dynamics may evolve under alternative futures (e.g., Ayala et al. 2020, 2023). The use of multiple climate scenarios and global climate models further allows the range of potential responses and the uncertainty arising from future climatic conditions to be characterised and communicated (Hattermann et al., 2018; Her et al., 2019a; Paíz et al., 2025a).

Within this context, this deliverable presents the deployment of the General Lake Model (GLM) coupled with the Aquatic EcoDynamics (AED) set of modules (GLM-AED) (Hipsey et al., 2013, 2014) to simulate historical and future thermal and DOC dynamics in two contrasting freshwater systems: an Irish lake and a Spanish reservoir. This approach builds on previous modelling research conducted in these systems and their surroundings. GLM and AED are also openly available, open source tools that have been applied across a wide range of freshwater environments. Their established use, accessibility and adaptable structure enhance the reproducibility of the modelling workflow and provide a scalable framework that can be transferred to other freshwater systems where suitable data are available. The modelling framework combines local sensor observations with globally available climate data and future climate projections to evaluate changes relative to a historical baseline. Through this work, we advance the application of environmental modelling to long term freshwater management by illustrating how thermal conditions and DOM dynamics may evolve in two contrasting systems. The resulting site specific projections can support the development and evaluation of adaptation and mitigation strategies, contributing to safer and more resilient drinking water supplies.

1.2 Objectives

The main aim of this deliverable was to implement a modelling workflow capable of simulating broad DOM dynamics in source waters and projecting long-term future levels with associated uncertainty. The workflow utilised DOC as a proxy for DOM and was designed to capture large-scale temporal variability using the General Lake Model (GLM) coupled with the Aquatic EcoDynamics (AED) set of modules (GLM-AED), a freely available, open-source and widely applied modelling tool for lakes and reservoirs. The framework was tested in two contrasting systems that differ markedly in their organic matter levels and in the environmental processes controlling their dynamics.

The specific objectives were:

1. To calibrate the physical and biogeochemical components of the model, relevant to simulate DOC at each site, and to evaluate its capacity to reproduce broad historical dynamics.
2. To project DOM dynamics using DOC as a proxy under three climate change scenarios, here three Shared Socioeconomic Pathways (SSP126, SSP370 and SSP585), using an ensemble of global climate models to characterise the magnitude, variability and uncertainty of potential future changes.
3. To present the results in a form that provides quantitative information for water managers and relevant authorities when evaluating long-term adaptation and mitigation strategies in, but not limited to, the study sites. These may include actions at catchment, source-water and treatment scales aimed at reducing DBP formation and subsequent human exposure.

2. Methods

2.1 Study sites

This study focused on two contrasting freshwater systems: Lough Feeagh in western Ireland and Sau Reservoir in northeastern Spain (Figure 1). The sites differ markedly in their morphology, hydroclimatic conditions, landcover (see Figures 1 and 2), degree of human influence and dissolved organic matter dynamics (see Mercado-Bettín et al. 2026). They therefore provide an appropriate basis for evaluating the capacity of the process-based modelling framework to reproduce and project DOC concentrations under contrasting environmental conditions.

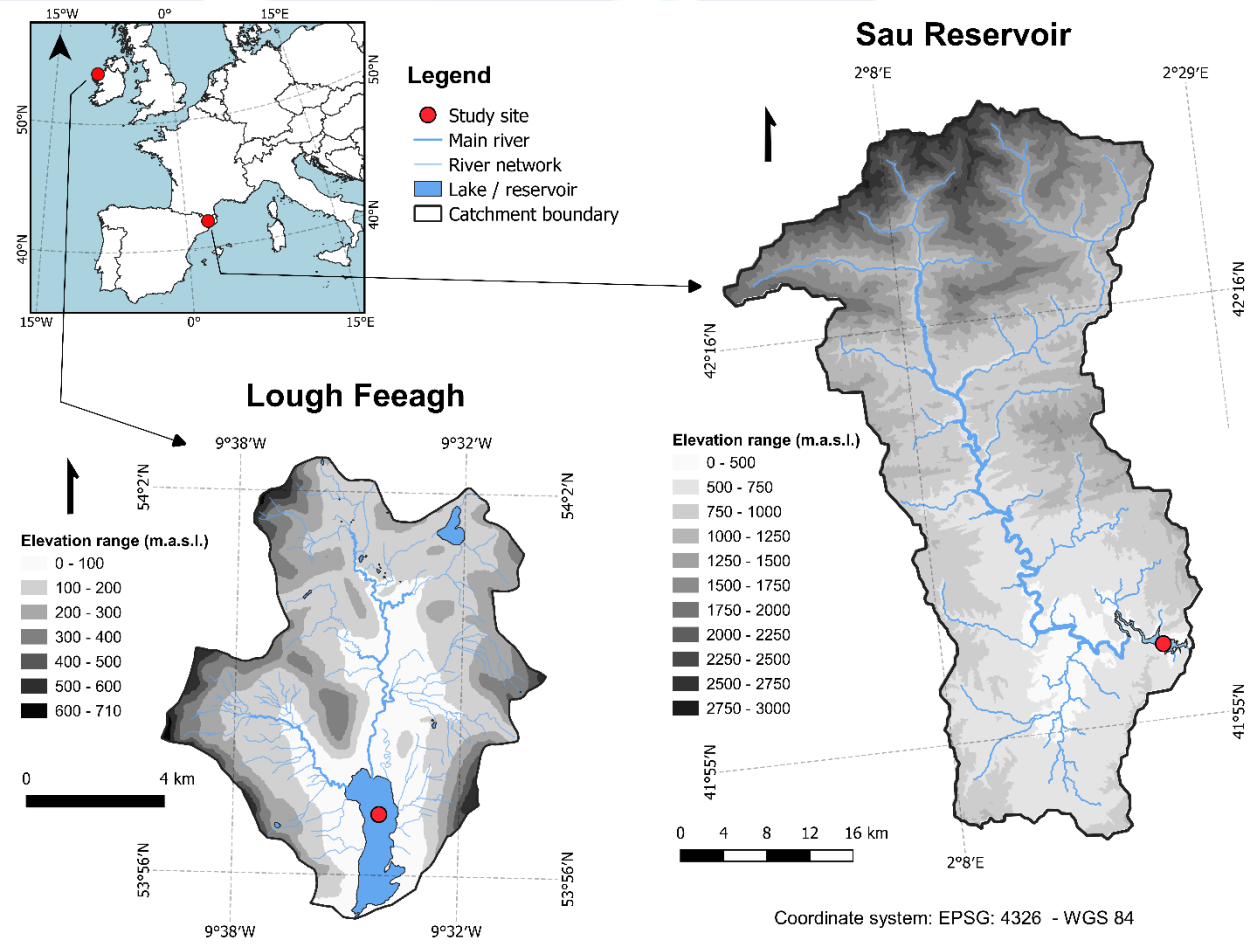


Figure 1. *Location of the study catchments including river network and topographic elevation.*

Lough Feeagh is a humic, monomictic and oligotrophic lake with a surface area of 3.95 km² and a maximum depth of 46.8 m. It is located within the Burrishoole catchment, a relatively small catchment of approximately 84 km² dominated by peatland, an organic-rich soil. The lake receives most of its water from the Black and Glenamong rivers (see Figure 1). Its climate is temperate, characterised by relatively cool conditions and frequent rainfall throughout the year, supporting sustained hydrological connectivity between the catchment and the lake (Doyle et al., 2019). DOM dynamics are consequently governed mainly by natural processes, including soil temperature, catchment discharge, drought and the mobilisation of terrestrially derived carbon (Doyle et al., 2023). Although carbon inputs occur throughout the annual cycle, they exhibit a clear seasonal pattern associated with variations in climate and hydrology (Ryder et al., 2012; Jennings et al., 2020).

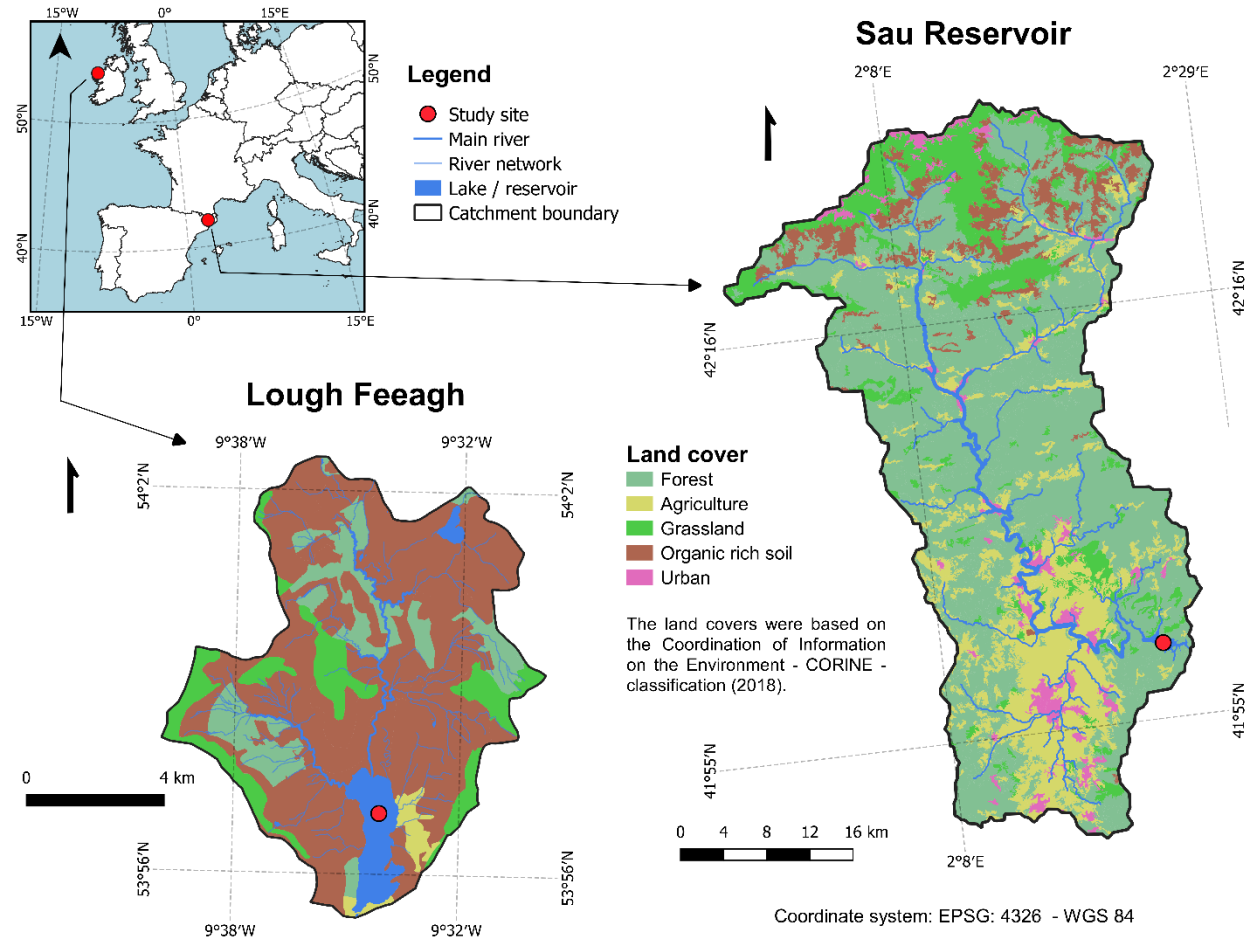


Figure 2. *Location of the study catchments including grouped land cover classifications and river network.*

Sau Reservoir is a eutrophic and heavily regulated system with a surface area of approximately 5.8 km² and a maximum depth of 70 m. It is primarily fed by the Ter River and drains a much larger catchment of approximately 1,525 km², characterised by diverse land uses, variable topography and a greater degree of human influence (see Figure 2). The reservoir is subject to water abstraction and forms part of the drinking-water supply system serving the metropolitan area of Barcelona. Its Mediterranean climate, with hot and dry summers and milder, wetter winters, strongly regulates water availability, reservoir volume, thermal stratification and organic matter transport. In addition to natural catchment and soil processes, DOM dynamics are influenced by wastewater discharges, agricultural runoff and reservoir operation (Marcé et al., 2021).

2.2 The model

The General Lake Model (GLM) (Hipsey et al., 2014, 2017, 2019) was used to simulate the hydrodynamic conditions of Lough Feeagh and Sau Reservoir. GLM is an open-source, one-dimensional process-based model developed to reproduce the water balance, thermal structure and vertical mixing of lakes, reservoirs and other standing water bodies. Its relatively low computational requirements and suitability for simulations extending from months to decades make it particularly appropriate for long-term modelling applications. GLM simulates vertical profiles of water temperature, salinity and density by integrating meteorological forcing, surface heat exchange, inflows, outflows and mixing processes. As a one-dimensional model (1-D), it assumes that horizontal variability is limited and that the principal gradients occur vertically through the water column. This assumption allows the model to represent seasonal stratification and mixing efficiently (Bruce et al., 2018), while avoiding the computational demands of two- or three-dimensional modelling approaches.

GLM was coupled with the Aquatic EcoDynamics (AED) (Hipsey et al., 2013, 2019) modules to simulate water-quality processes. In this study, the coupling was used to represent DOC as a measurable proxy for dissolved organic matter DOM. The simulated physical environment therefore provided the basis for representing the entry, vertical distribution, transformation and removal of DOC within each water body.

GLM requires information describing water-body morphology, initial water-column conditions and meteorological forcing. The principal meteorological inputs include shortwave and longwave radiation, air temperature, relative humidity, wind speed, precipitation and cloud cover. Inflow and outflow data can also be incorporated, including discharge, water temperature, salinity and water-quality concentrations (see Hipsey et al. 2019). Model time steps, output frequencies, vertical resolution and process-related parameters are specified through the GLM and AED configuration files in Supplementary Material A.

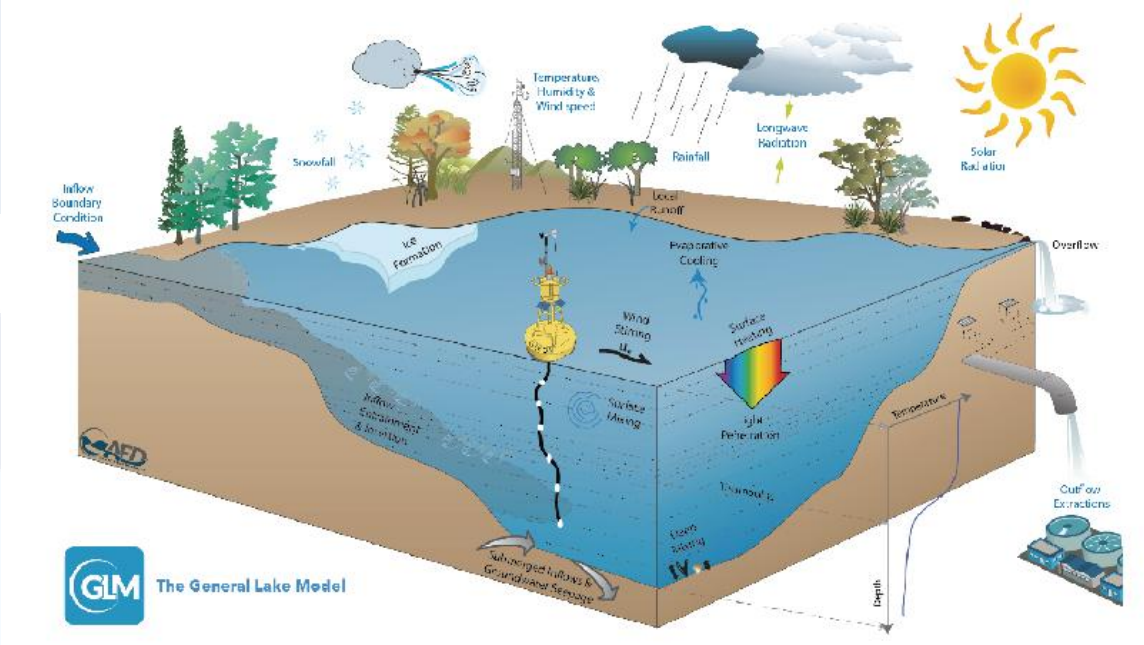


Figure 3. *GLM simulation domain, input information and key simulated processes (Hipsey et al., 2019).*

2.2.1 Layer structure

The water column in GLM is represented through a flexible Lagrangian layer structure (Hipsey et al., 2019). Each layer acts as an internally homogeneous control volume with a defined temperature, salinity, density and concentration of associated water-quality variables. Rather than retaining a fixed vertical grid, the thickness and number of layers change during the simulation in response to surface heating and cooling, inflows, outflows and mixing. Density is calculated from the temperature and salinity of each layer. When sufficient energy is available to overcome the density difference between adjacent layers, these layers can merge and mix. Conversely, the model increases vertical resolution where strong density gradients occur. During stratified periods, this produces

finer layers around the thermocline and thicker layers within relatively well-mixed regions of the water column (Bruce et al., 2018).

Layer volumes and surface areas are determined from a user-defined hypsographic relationship between water depth, area and volume. This allows changes in water level and storage to be represented consistently with the morphology of each lake or reservoir.

2.2.2 Water and surface energy balance

GLM maintains a water balance by accounting for precipitation, evaporation, snowfall, catchment runoff, river inflows, withdrawals, overflow and seepage, depending on their inclusion in the site configuration. Precipitation and evaporation act directly on the surface layer, while seepage occurs at the lake bottom. Inflows and outflows can affect multiple layers according to their magnitude, location and density.

Water temperature is primarily regulated through the surface energy balance. GLM calculates the net exchange of energy between the atmosphere and the water surface by accounting for incoming shortwave and longwave radiation, outgoing longwave radiation, sensible heat and latent heat. The general heat budget equation in GLM used to determine the net cooling and heating for the lake system is given by:

$$\left[\frac{c_p}{A_s z_{sml}}\right]\frac{dT_s}{dt} = \emptyset_{SW_s} - \emptyset_E + \emptyset_H + \emptyset_{LWin} - \emptyset_{LWout}$$

where c_p is the specific heat capacity of air, A_s is the surface area of the lake, z_{sml} is the depth of the surface mixed layer, T_s is the surface temperature of the surface mixed layer, $\emptyset_{SW_s}$ is the shortwave radiation penetration into the lake, $\emptyset_E$ is the latent heat, $\emptyset_H$ is the sensible heat , $\emptyset_{LWin}$ is the incoming longwave radiation and $\emptyset_{LWout}$ is the outgoing longwave radiation (Hipsey et al., 2019). Heat exchange with bottom sediments can also be represented through different sediment zones. This allows the model to account for differences in thermal interactions between sediments and the overlying water across shallow and deep areas of the water body. Each of the components that impact the lake general heat budget in GLM are described in detail by Hipsey et al. (2014, 2019).

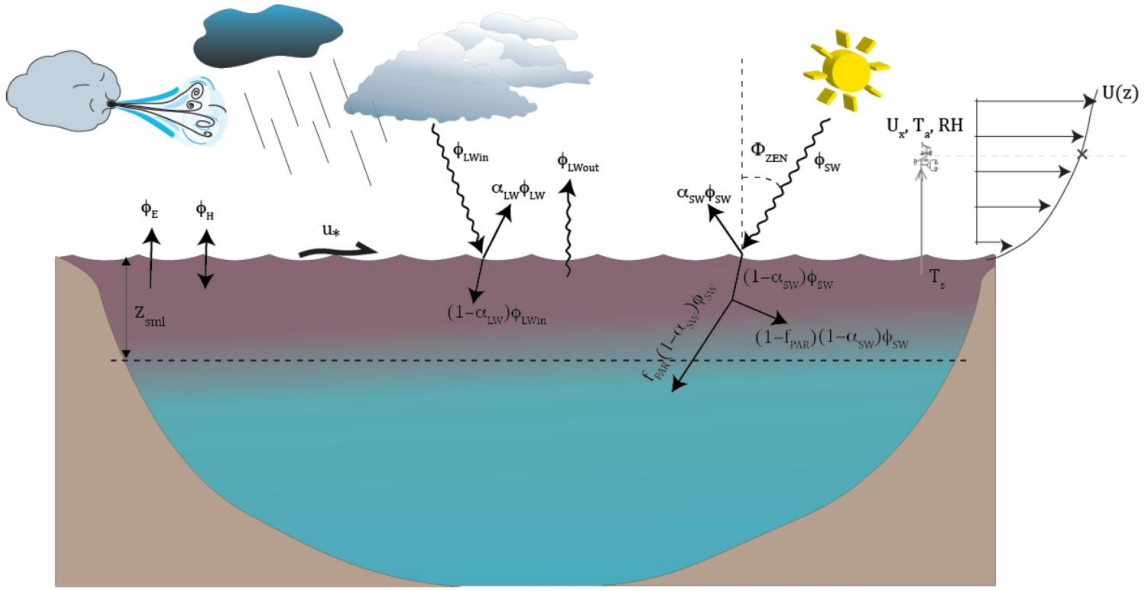


Figure 4. *Schematic of the surface heat fluxes impacting the surface mixed layer as conceptualised in the General Lake Model (GLM) (Hipsey et al., 2014).*

2.2.3 Stratification, mixing and hydrological exchanges

Vertical mixing in GLM is simulated using an energy-balance approach. The model estimates the turbulent energy generated by wind stirring, convective overturn, shear between adjacent layers and internal billowing. Mixing occurs when the available energy is sufficient to overcome the potential energy associated with density differences in the water column. These processes allow the model to reproduce the formation, persistence and breakdown of thermal stratification. They are particularly relevant to DOC simulation because stratification and mixing impact on the transport and redistribution of dissolved material between surface and deeper waters.

River inflows are incorporated according to their discharge, temperature, salinity and density. As inflowing water enters the lake or reservoir, it entrains surrounding water and moves vertically until reaching a depth of approximately neutral buoyancy, where it is inserted into the water column. Outflows can be defined at specific depths and remove water and associated dissolved constituents from the adjacent layers. These mechanisms are important for representing the delivery, internal distribution and export of DOC, particularly where inflow characteristics or withdrawal depths vary over time.

2.2.4 Aquatic EcoDynamics (AED) and DOC simulation

The AED set of modules extend GLM beyond hydrodynamics by simulating biogeochemical and water-quality variables within the dynamically changing water-column layers (Hipsey et al., 2013, 2019). GLM provides the physical conditions that regulate these processes, including water temperature, layer volume, stratification, mixing, inflow insertion and outflow removal.

For this study, the AED organic matter component was used to represent DOC concentrations. This component requires DOC concentrations in the incoming water to be specified, which, together with inflow volumes, determine DOC inputs from the catchment. It can represent processes such as the breakdown of particulate organic matter into DOC, microbial mineralization and exchange with sediments, depending on the model configuration. External DOC in this study entered the model through the configured inflows and was subsequently distributed according to the hydrodynamic conditions simulated by GLM. Its concentration within the water body was influenced by inflow loading, dilution, vertical transport, mixing, residence time and the biogeochemical processes included in the AED configuration. This coupled structure was used first to reproduce the historical thermal and mixing conditions of each site and subsequently to simulate their DOC dynamics. The model therefore provided a process-based representation of how external climatic and hydrological forcing interacts with internal lake and reservoir processes to regulate DOM levels over time. A detailed description of the different modules of AED employed in this study is provided in the following repository.

2.3 Observational input data

Historical datasets were compiled separately for Lough Feeagh and Sau Reservoir to configure the models, define boundary conditions and evaluate simulated water temperature and DOC. These datasets included local water-temperature and water-quality observations, historical meteorological forcing, inflow and outflow information, water-body morphology and, for Sau Reservoir, operational withdrawal data. Future input data including future climate projections for the long-term simulations of DOC are described separately in Section 2.4.

2.3.1 Target variables (water temperature and DOC)

Water-temperature observations were used to evaluate the physical component of GLM and its capacity to reproduce the thermal structure of each water body. At Lough Feeagh, water temperature was monitored at 13 depths: 0.9, 2.5, 5, 8, 11, 14, 16, 18, 20, 22, 27, 32 and 42 m. Measurements were collected at 2 min intervals as part of the its Automatic Water Quality Monitoring System (AWQMS) (Marine Institute, 2017). Surface temperature at 0.9 m was measured using a Hach Environmental Hydrolab Data Sonde X5, while temperatures at the remaining depths were measured using platinum resistance thermometers (see Paíz et al. 2025b for more details). Quality-controlled observations corresponding to the historical period from 2005 to 2019 were retained and aggregated to daily values for model evaluation. The availability of measurements across the water column allowed the model to be evaluated under both mixed and stratified conditions.

For Sau Reservoir, water-temperature profile observations followed the dataset described by Mercado-Bettín et al. (2021) and covered the period from 1997 to 2018. The original dataset consisted of approximately 78,800 valid temperature measurements collected during 285 vertical profiling campaigns, with observations extending from the surface to approximately 58 m depth. Because the vertical sampling resolution varied among profiles and was considerably denser than required for model evaluation, observations were standardised to a common set of representative depths. Measurements between the surface and 20 m were grouped at 2 m intervals, corresponding to target depths of 0, 2, 4, 6, 8, 10, 12, 14, 16, 18 and 20 m, while deeper observations were grouped at 5 m intervals at 25, 30, 35, 40, 45, 50 and 55 m. Each individual measurement was assigned to its nearest target depth, and when multiple measurements from the same profile were associated with the same target depth, their mean temperature was retained (see Supplementary Material A). This procedure resulted in 4,284 date–depth temperature observations distributed across 18 representative depths. The resulting dataset provided consistent vertical coverage for evaluating simulated temperature dynamics from surface waters to the deeper reservoir layers while retaining the temporal information contained in the original field profiles.

DOC was used as a quantitative proxy for DOM at both sites, although the observational basis differed according to the monitoring information available. At Lough Feeagh, a sensor-derived DOC proxy was obtained from fluorescent dissolved organic matter (fDOM) measurements collected at 0.9 m depth using a Seapoint UV fluorometer. Raw measurements were recorded at 2 min intervals and subsequently aggregated to daily values. The fluorescence signal was corrected for temperature quenching relative to a reference temperature of 20 °C following the sensor-specific procedure described in Mercado-Bettín et al. (2026). The corrected fDOM signal was then expressed as an equivalent DOC concentration in mg C L^{-1} using an established local relationship (Ryder et al., 2012; Mercado-Bettín et al., 2026). The resulting daily DOC proxy covered the period from 5 March 2010 to 19 November 2019 and comprised 3,002 daily observations.

For Sau Reservoir, DOC concentrations were determined through laboratory analysis of water samples collected at the central monitoring location. The observational dataset extended from 1 February 1995 to 3 December 2020 and consisted of vertical profiles spanning the surface to approximately 56 m depth. Sampling was conducted approximately monthly, although both the number of samples and the exact sampling depths varied among monitoring dates. The complete dataset contained 1,950 DOC measurements collected on 297 dates, generally comprising six to seven depth-specific observations per profile. DOC concentrations were reported in mmol C m^{-3} and converted to mg C L^{-1} for comparison with model outputs. Measurements were subjected to quality-control screening, with non-positive concentrations and values exceeding 1,000 mmol C m^{-3} excluded from subsequent analyses. For the surface DOC series used for model evaluation, observations collected between 0 and 5 m depth were retained and, when more than one measurement was available on the same date, averaged to obtain a single representative surface DOC concentration for that sampling date.

2.3.2 Historical meteorological forcing

Historical meteorological forcing for both sites was obtained from the European Centre for Medium-Range Weather Forecasts ERA5 reanalysis dataset (Muñoz-Sabater et al., 2021). Daily values were extracted at a spatial resolution of 0.25° for the grid cell containing each lake or reservoir. The variables required by GLM included air

temperature, precipitation, relative humidity, wind speed, cloud cover, incoming shortwave radiation and incoming longwave radiation.

The extracted records were restricted to the corresponding historical simulation periods and processed to provide continuous daily time series. The use of the same reanalysis product at both sites provided internally consistent meteorological forcing despite their contrasting hydroclimatic settings.

2.3.3 Hydrological and inflow boundary conditions

Daily inflow boundary conditions were prepared for each site and included discharge, inflow water temperature and DOC concentration. These variables allowed GLM-AED to represent changes in water storage, heat delivery and external organic carbon loading.

For Lough Feeagh, the catchment contribution was represented through three inflow components: the combined Black and Srahrevagh catchments, the Glenamong catchment and the remaining direct catchment area (see Doyle et al. 2019 for a detailed description of the lake catchment and its inflows). These components represented catchment areas of 52.9, 17.5 and 13.6 km², respectively. A daily streamflow dataset of the Glenamong inflow covering 2002–2022 was available to support reescalation and preparation of the historical hydrological inputs, with the subset corresponding to 2005–2019 retained for this study. The inflow files contained discharge, water temperature and DOC concentration and were kept separate to preserve differences among the principal catchment contributions according to Doyle et al. (2019, 2023).

For Sau Reservoir, the Ter River was represented as the principal inflow. Daily boundary conditions included river discharge, water temperature and DOC concentration for the complete historical simulation period. The time series were regularised to a continuous daily interval before being incorporated into GLM-AED. Because the observed DOC profiles began in 1995, the inflow and meteorological inputs were extended backwards by three years to match. This extension was produced using a climatological approach (Murphy, 1992; Paíz et al., 2025b).

2.3.4 Lake and reservoir morphology

Site-specific morphological data were used to define the relationship between water depth, surface area and volume in GLM. These relationships determine the volume and area of each modelled layer and allow water-level changes to be represented consistently with the physical form of each system.

For Lough Feeagh, the model configuration used bathymetric information from the Marine Institute survey of the lake (Marine Institute, 2017).The resulting hypsographic curve represented its surface area and volume across the full depth range to a maximum depth of 46.8 m. The same bathymetric configuration had been applied in previous GLM studies at the site (e.g., Ayala et al., 2023; Paíz et al., 2025; Mercado-Bettín et al., 2026).

For Sau Reservoir, the model used a site-specific depth–area–volume relationship derived from the available reservoir bathymetric and operational information (Mercado-Bettín et al., 2021). This configuration accounted for changes in reservoir area and storage associated with fluctuations in water level and supported the representation of its maximum depth of approximately 70 m.

2.3.5 Reservoir operation and additional boundary data

Sau Reservoir required additional operational information because water withdrawals substantially influence its water balance, residence time and vertical structure. Daily outflow data were provided for three operational gates and incorporated separately into the model. Each time series described the volume of water withdrawn through the corresponding outlet, allowing GLM to remove water and associated heat and dissolved constituents at the configured withdrawal depths. The gate-operation records were regularised to daily values and aligned with the meteorological and inflow datasets. Their inclusion allowed the model to represent historical changes in reservoir storage and the effects of managed withdrawals on water temperature and DOC distribution.

2.4 Future climate projections and derived boundary conditions.

2.4.1 Climate forcing and scenario selection

Future climate forcing was obtained from phase 3b of the Inter-Sectoral Impact Model Intercomparison Project (ISIMIP3b) (Lange and Büchner, 2021). ISIMIP is an

international community of climate-impact modellers that develops consistent climate and socioeconomic forcing datasets, common simulation protocols and model outputs to support the comparison of climate-change impacts across sectors and spatial scales. ISIMIP3b specifically supports the quantification of climate-related risks under different levels of climatic change and socioeconomic development.

The ISIMIP3b atmospheric data are based on output from the Coupled Model Intercomparison Project Phase 6 (CMIP6), bias-adjusted and statistically downscaled to a regular global grid of 0.5° × 0.5° at a daily temporal resolution. For each study site, data were extracted from the grid cell containing the respective lake or reservoir. This approach provided a consistent climate dataset for both the historical reference and future simulations. An ensemble of five global climate models was used: GFDL-ESM4, IPSL-CM6A-LR, MPI-ESM1-2-HR, MRI-ESM2-0 and UKESM1-0-LL. For each model, nine daily atmospheric variables were obtained: mean, maximum and minimum near-surface air temperature; precipitation; near-surface wind speed; incoming shortwave and longwave radiation; relative humidity; and surface air pressure. These variables were processed and converted into the meteorological fields required by GLM-AED. The same five-model ensemble was used for both Lough Feeagh and Sau Reservoir.

Three Shared Socioeconomic Pathways were selected: SSP1-2.6, SSP3-7.0 and SSP5-8.5, referred to in the datasets as SSP126, SSP370 and SSP585. SSP1-2.6 represents a comparatively low-emission pathway characterised by stronger mitigation and more sustainable development. SSP3-7.0 represents a higher-emission pathway associated with regional rivalry and substantial challenges to mitigation and adaptation. SSP5-8.5 represents fossil-fuel-intensive development and very high greenhouse-gas emissions. The numerical component of each scenario indicates the approximate radiative forcing reached by 2100 and corresponds to the forcing levels associated with RCP2.6, RCP7.0 and RCP8.5, respectively. The three pathways were included to represent a broad range of climatic futures and to characterise uncertainty associated with differing socioeconomic and emissions trajectories.

2.4.2 Historical baseline and future periods

The most recent 30-year period available within the ISIMIP3b historical simulations, 1985–2014, was selected as the climatological baseline. This period immediately precedes the SSP projections, which begin in 2015, and allowed historical and future conditions to be evaluated using the same five-member climate-model ensemble (Lange and Büchner, 2021).

Future simulations focused on three 10-year periods: 2041–2050, 2061–2070 and 2091–2100. These periods were selected to represent changes during the middle and latter parts of the century while limiting the computational requirements associated with running every possible year, climate model and parameter configuration. Each period was simulated separately for the five GCMs and three SSPs, allowing projected changes to be evaluated relative to the 1985–2014 baseline and across increasingly divergent future climatic conditions.

2.4.3 Derived inflow boundary conditions

Direct observations cannot provide inflow discharge and DOC concentrations for future periods. In this study, daily inflow boundary conditions were generated for both sites using the Generalised Watershed Loading Functions Model coupled with its DOC module (GWLF-DOC) (Haith and Shoemaker, 1987; Naden et al., 2010; Schneiderman et al., 2010). The model simulates catchment water balance and the partitioning of water among hydrological pathways, together with the production and mobilisation of DOC from terrestrial stores. Its principal climate inputs are daily precipitation and air temperature, while land cover, land use and soil characteristics define the catchment configuration.

GWLF-DOC had previously been calibrated independently for both study areas (see Mercado-Bettín et al., 2026). For Feeagh, observed discharge was used to calibrate and validate the Glenamong inflow hydrological component during 2013–2018 and 2019–2023, respectively, while DOC-related observations from 2016–2023 were used to calibrate the DOC component. The resulting R^2 and NSE values were 0.64 during hydrological calibration, 0.60 during validation and approximately 0.45–0.47 for DOC calibration. For Sau, hydrological calibration and validation for the Ter River were based on observations covering 2008–2011 and 2011–2024, respectively, while the DOC

component was calibrated using 2008–2014 and validated using 2016–2018. The corresponding R^2 and NSE values were 0.66 during hydrological calibration, 0.42 during hydrological validation, 0.44 and 0.40 during DOC calibration, and 0.50 and 0.46 during DOC validation. These results indicated that the model provided an adequate representation of the broad hydrological and DOC dynamics required for generating the inflow boundary conditions.

For the future simulations, GWLF-DOC was driven separately by the daily precipitation and air-temperature series from each of the five GCMs under each of the three SSPs. This produced GCM- and scenario-specific daily series of inflow discharge and DOC concentration for the historical baseline and each future period. At Lough Feeagh, the generated boundary conditions for the Glenamong River were rescaled and adjusted to account for the other inflows as well (i.e., the Black and Srahrevagh inflow and the remaining direct catchment contribution). At Sau Reservoir, they represented the Ter River. The generated series followed the process representation and seasonal behaviour established during model calibration with consideration of their respective observational datasets as well. They were intended to reproduce broad climate-driven changes in discharge and terrestrial DOC delivery rather than the precise timing of individual future events. Maintaining separate inflow series for every GCM and SSP ensured that differences in precipitation and temperature were propagated through the catchment model before being incorporated into GLM-AED. Consequently, the inflow boundary conditions varied consistently with the climate ensemble rather than remaining fixed across future simulations.

2.4.4 Derived operational boundary conditions for Sau Reservoir

Future gate operations at Sau Reservoir could not be known because they will depend on future water availability, demand, infrastructure and management decisions. Daily withdrawal series were therefore generated using a climatological and water-availability-dependent approach based on the historical operational records.

The procedure preserved the principal seasonal operating patterns observed for the reservoir while accounting for simulated storage conditions. Historical relationships between reservoir volume and gate operation were used to represent differences in

withdrawal behaviour under relatively high and low water availability. When simulated reservoir storage was greater, the generated operations retained the withdrawal characteristics historically associated with higher-volume conditions. During lower-storage periods, operations were adjusted to reflect the corresponding historical behaviour and to avoid prescribing withdrawals that were inconsistent with the available water volume.

The resulting operational series were not identical among simulations. Differences in precipitation, inflow discharge and reservoir storage across GCMs and SSPs produced corresponding differences in the timing and magnitude of withdrawals. This allowed future operations to respond to the water balance simulated in each ensemble member while retaining characteristics derived from the historical record. These data should therefore be interpreted as internally consistent operational boundary assumptions rather than forecasts of future reservoir policy or water demand.

2.5 Modelling workflow

A six-step modelling workflow was implemented independently for Lough Feeagh and Sau Reservoir (Figure 4). The same general sequence was applied at both sites, while the input datasets, model configuration, calibration parameters and boundary conditions were adapted to their respective physical, hydrological and DOC dynamics.

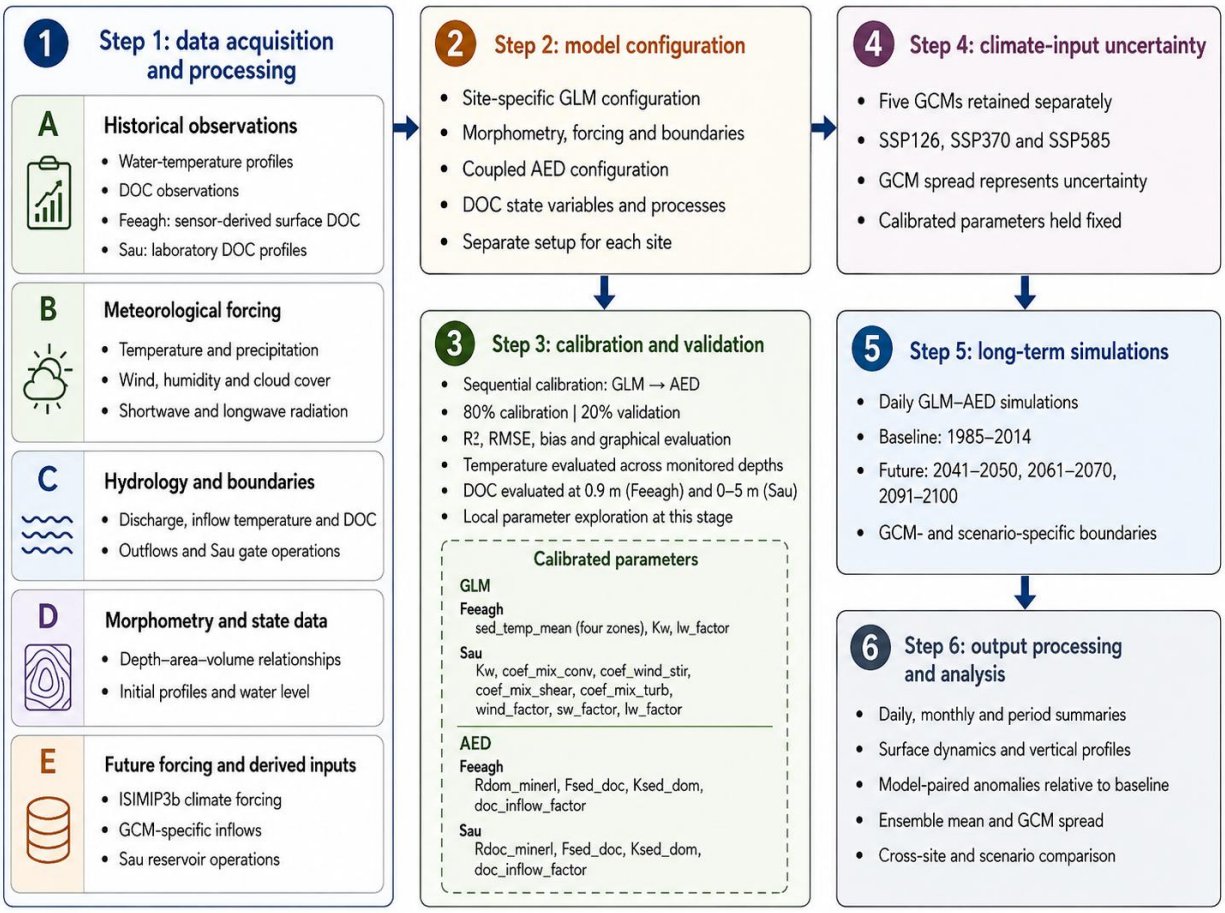


Figure 5. *Modelling workflow implemented at each study site. The workflow comprised six sequential steps.*

2.5.1 Data acquisition and processing

The historical observations and model input data described in Section 2.3, together with the future climate forcing and derived boundary conditions described in Section 2.4, were compiled for each site. These included the meteorological, hydrological, water-temperature, DOC, morphometric and operational datasets required for model configuration and evaluation. All time series were quality-checked, aligned to a common temporal structure and converted into the units and formats required by GLM-AED. Inflow discharge, inflow temperature and DOC concentrations were processed consistently for each site, while water-level, reservoir-volume and gate-operation data were incorporated where applicable.

2.5.2 Model configuration

GLM was configured separately for each water body. The site-specific hydrodynamic settings, including morphology, simulation period, initial water-column conditions, meteorological forcing, inflows, outflows and physical model parameters, were defined in the GLM namelist file (glm3.nml). The hydrodynamic configuration was coupled with the Aquatic EcoDynamics modules to simulate DOC. The corresponding state variables, process parameters, modules and biogeochemical settings were defined in the AED namelist file (aed2.nml). Boundary-condition files were linked to these configurations to provide the required daily meteorological, hydrological and DOC inputs. Separate configurations were retained for Lough Feeagh and Sau Reservoir because of their different morphometry, hydrological structure, monitoring information and operational characteristics. The final GLM and AED namelist files, together with the principal configuration parameters are provided in Supplementary Material A.

2.5.3 Model calibration and validation

Model calibration was conducted sequentially at both study sites. The hydrodynamic component was calibrated first and the resulting configuration was subsequently held fixed during calibration of dissolved organic carbon (DOC) with GLM-AED. This sequence was adopted to ensure that the principal physical controls on water-column temperature, stratification and vertical mixing were represented before modifying parameters governing DOC loading and in-lake biogeochemical processing. Parameter ranges and starting values were defined separately for Lough Feeagh and Sau Reservoir according to their respective configurations, previous applications, literature and site-specific physical and biogeochemical characteristics.

For both hydrodynamics and DOC, observations were divided chronologically according to their unique observation dates. The first 80% were used for parameter calibration and the remaining 20% were retained for independent validation; validation observations were not used in selecting the optimal parameter set. Model performance was subsequently quantified separately for both periods using the coefficient of determination (R^2), root mean squared error (RMSE) and graphical comparison of observed and simulated values. Daily and monthly representations were considered

because they provided complementary information on variability and broader seasonal behaviour.

For Lough Feeagh, hydrodynamic calibration used the complete set of water-temperature observations available at the 13 monitored depths. Simulated temperatures were extracted at the corresponding depths and compared directly with the daily observations. Six parameters were calibrated based on Paíz et al. (2025): the mean sediment temperatures (sed_temp_mean) of four sediment zones, corresponding to zone heights of 5, 15, 30 and 47 m; the light extinction coefficient (Kw); and the longwave-radiation scaling factor (lw_factor). The four sediment-temperature parameters regulate the thermal boundary conditions and heat exchange between the sediments and the overlying water column. They were allowed to vary independently while maintaining a physically consistent increase among sediment zones. Kw regulates the attenuation and vertical distribution of incoming shortwave radiation, whereas lw_factor scales the contribution of longwave radiation to the surface energy balance. The calibration objective combined daily RMSE, monthly RMSE and absolute daily bias, with respective weights of 0.70, 0.25 and 0.05. Parameter space was first explored using Latin Hypercube sampling and subsequently refined from the best-performing solution using the Nelder–Mead optimisation algorithm (Kripka et al., 2026).

The hydrodynamic calibration strategy for Sau Reservoir was adapted to its discrete vertical-profile dataset with similarities to the work undertaken by Mercado-Bettín et al. (2021). Measurements collected between the surface and 20 m were assigned to representative target depths at 2 m intervals, while observations between 25 and 55 m were assigned at 5 m intervals. When multiple observations from the same profile were associated with the same target depth, their mean temperature was retained (see Section 2.3.1). The surface group was represented by model output at 0.1 m. This standardisation allowed all available profiles to contribute consistently to the optimisation while preventing profiles with finer vertical sampling from receiving disproportionate weight. The calibration objective gave equal influence to the represented depths and combined the mean depth-specific daily RMSE, mean depth-specific monthly RMSE and overall absolute bias, with respective weights of 0.65, 0.25 and 0.10.

Eight hydrodynamic parameters were calibrated for Sau Reservoir: the light extinction coefficient (Kw); the coefficients controlling convective mixing (coef_mix_conv), wind-induced stirring (coef_wind_stir), shear mixing (coef_mix_shear) and turbulent mixing (coef_mix_turb); and scaling factors for wind speed (wind_factor), shortwave radiation (sw_factor) and longwave radiation (lw_factor). Kw, sw_factor and lw_factor regulate radiative forcing and the surface energy balance, while wind_factor accounts for uncertainty in the effective wind forcing experienced by the reservoir. The four mixing coefficients control distinct mechanisms contributing to the vertical redistribution of heat and were included because reservoir stratification and mixing are influenced by atmospheric forcing, inflow dynamics and managed withdrawals. As at Lough Feeagh, the parameter space was initially explored using Latin Hypercube sampling and subsequently refined around the best-performing solution using Nelder–Mead optimisation.

Following hydrodynamic calibration, the corresponding best-performing physical configuration was retained without further modification during DOC calibration. At both sites, four DOC-related quantities were calibrated: the DOM mineralisation rate (Rdom_minerl, referred to as Rdoc_minerl in some AED configurations), the reference sediment DOC flux (Fsed_doc), the oxygen half-saturation coefficient controlling sediment–water DOM exchange (Ksed_dom) and an additional dimensionless external DOC inflow factor (doc_inflow_factor). These parameters were selected to represent three complementary controls on in-lake DOC concentrations: DOC mineralisation, exchange of DOC across the sediment–water interface, and uncertainty in the magnitude of catchment-derived DOC loading. The same conceptual parameterisation was applied at both sites, although the parameter ranges, observational targets and calibration procedures were adapted to their contrasting environmental conditions.

For Lough Feeagh, DOC calibration used the fDOM-derived DOC observations collected at 0.9 m. Daily simulated concentrations were extracted at the same depth, while monthly means were used as the primary optimisation scale. Monthly observed concentrations were calculated from the measurements available within each month, whereas simulated monthly concentrations were calculated from all modelled days within the corresponding month. The calibration objective prioritised monthly RMSE and included additional

penalties for absolute bias and poor representation of the observed temporal pattern. Twenty-four initial parameter sets were evaluated, followed by 12 additional sets generated through local refinement around the best-performing initial solutions.

The Feeagh DOM mineralisation rate (Rdom_minerl) was allowed to vary between 0.001 and 0.05 d^{-1}. The reference sediment DOC flux (Fsed_doc) varied between 0 and 2 mmol C m^{-2} d^{-1}, while the oxygen half-saturation coefficient controlling sediment–water DOM exchange (Ksed_dom) varied between 20 and 100 mmol O_2 m^{-3}. The external DOC inflow factor (doc_inflow_factor) was allowed to vary between 1 and 3. External loading was represented through three catchment contributions: the combined Black and Srahrevagh inflow, the Glenamong inflow and the remaining direct catchment contribution (Doyle et al., 2019, 2023). Their relative contributions and temporal DOC dynamics were defined using available site-specific information and insights reported by Doyle et al. (2019). During calibration, the external DOC factor was applied consistently to the DOC concentrations of the three inflow components without modifying their discharge or temperature. This allowed uncertainty in the overall magnitude of catchment-derived DOC loading to be considered while preserving the observed temporal variability and relative differences among the individual inflows.

DOC calibration at Sau Reservoir differed principally in its observational target and the broader parameter space required to represent reservoir conditions. Although DOC profiles were available throughout the water column, the final calibration focused on source-water conditions in the upper reservoir. Only quality-controlled observations collected between 0 and 5 m were retained, and multiple measurements within this layer on the same sampling date were averaged to produce one representative surface DOC concentration. Non-positive concentrations and values exceeding 1,000 mmol C m^{-3} were excluded, and the retained laboratory measurements were converted from mmol C m^{-3} to mg C L^{-1}. Simulated surface DOC was correspondingly represented by the mean concentration extracted at 0.1, 1, 2, 3, 4 and 5 m.

The same four DOC controls were calibrated for Sau Reservoir, but substantially broader site-specific ranges were adopted. Rdoc_minerl varied between 1×10^{-8} and 5×10^{-4} d^{-1}, Fsed_doc between 0 and 40 mmol C m^{-2} d^{-1}, Ksed_dom between 100 and 15,000 mmol O_2 m^{-3}, and doc_inflow_factor between 0.30 and 25. Thirty-two initial DOC parameter

sets were evaluated, followed by 16 additional sets generated through local refinement around the four best-performing solutions. The calibration objective combined daily RMSE, monthly RMSE and absolute bias with terms evaluating the representation of observed variability and temporal correlation. An additional penalty discouraged configurations that produced an unrealistically compressed or nearly constant DOC signal.

Because the best-performing Sau GLM–AED simulation retained systematic differences in the magnitude and variability of surface DOC, a second calibration-only dynamic adjustment was evaluated after selecting the optimal DOC parameter set. This adjustment did not modify the calibrated hydrodynamic configuration or the four DOC-related parameters. Candidate transformations included the unadjusted simulation, scalar and affine corrections, monthly residual adjustments, variance-based and nonlinear amplification, empirical quantile mapping and a seasonal climatology combined with scaled model anomalies (Switanek et al., 2017). All transformations were fitted exclusively using observations from the 80% calibration period. The selected transformation combined the calibration-period monthly DOC climatology with modelled anomalies scaled by a factor of 0.75 (Beyer et al., 2020). It was subsequently applied without modification to the independent validation period and retained as the final Sau DOC calibration method for the long-term simulations.

For both sites, final model performance was reported independently for calibration and validation at daily and monthly resolutions using R^2, RMSE, mean bias and graphical comparisons of observed and simulated concentrations. Detailed parameter bounds, objective-function settings and implementation details are provided in Supplementary Material A.

2.5.4 Uncertainty assessment

Model parameterisation and climate input data were considered as sources of uncertainty at different stages of the modelling workflow. Local parameter uncertainty was examined during calibration and validation, whereas uncertainty in the long term projections was represented exclusively through differences among the climate input datasets.

Local parameter uncertainty was evaluated using ensembles centred on the best performing DOC parameter configuration identified for each site. The calibrated hydrodynamic configuration was retained without modification, while the four DOC related parameters were perturbed locally within their respective calibration ranges. The best performing parameter set was included explicitly in each ensemble, together with alternative configurations located around the optimum. Each configuration was evaluated against the calibration and validation observations using the same performance metrics and observational targets as the principal simulation. This procedure provided an indication of the sensitivity of simulated DOC dynamics to local differences in parameterisation without repeating the complete calibration search. These local parameter ensembles were used only to support the interpretation of calibration and validation performance and were not propagated through the long term simulations.

2.5.5 Long-term simulations

Long term simulations were conducted for each study site using the best performing GLM and AED configurations identified during calibration. All hydrodynamic and DOC related parameters were held fixed across the historical baseline, climate models, SSPs and future periods. Each configuration was driven independently using the meteorological, hydrological, DOC and operational boundary conditions associated with the corresponding global climate model. These included the site specific inflow conditions for both water bodies and the derived gate operations for Sau Reservoir.

The historical baseline from 1985 to 2014 was simulated separately for each of the five global climate models. Future simulations were subsequently conducted under SSP126, SSP370 and SSP585 for three periods (2041 to 2050, 2061 to 2070 and 2091 to 2100). This produced five historical baseline simulations and 45 future simulations for each study site, corresponding to 50 long term simulations per site.

Each simulation resolved the daily water balance, water temperature, thermal stratification, vertical mixing and hydrological exchanges using GLM. These physical conditions were coupled with AED to simulate DOC concentrations and their vertical distribution.

2.5.6 Output processing and analysis

Although GLM AED generated outputs at a daily resolution, the results were evaluated primarily at monthly, seasonal, annual and simulation period scales. Daily outputs were retained to verify individual simulations, examine temporal variability and generate the subsequent summaries. Water temperature and DOC were extracted at representative depths to characterise surface conditions and vertical profiles.

Future changes were calculated using a paired climate model approach (Du and Deng, 2022; Paíz et al., 2025a). For each GCM, the output from a given SSP and future period was compared with the historical baseline generated using that same GCM. Absolute anomalies were calculated by subtracting the corresponding historical value from the future value. Relative changes were also calculated as percentages where appropriate. This pairing was performed independently for all five GCMs before calculating any ensemble statistics. The five resulting anomalies were then averaged to obtain the ensemble mean change for each site, SSP, future period, month and representative depth. The spread among the paired GCM results was retained to characterise the variability associated with the climate input data. This procedure ensured that projected changes reflected differences between future and baseline conditions within each climate model rather than differences among the baseline climates represented by the models.

Particular emphasis was placed on DOC because it was the principal water quality variable addressed in this deliverable. Hydrodynamic outputs, including water temperature, water volume and vertical thermal structure, were analysed to contextualise the physical processes influencing the simulated DOC response (Ayala et al., 2020; Mesman et al., 2020). Surface dynamics, monthly seasonality and vertical concentration profiles were compared among the historical baseline, future periods and SSPs. The same processing and analytical structure was applied to Lough Feeagh and Sau Reservoir, allowing their projected responses to be evaluated within a consistent framework while preserving their respective physical, hydrological and operational characteristics.

3. Results

Results are presented in two main stages. First, the historical water-temperature and DOC dynamics of Lough Feeagh and Sau Reservoir are characterised and compared with the corresponding GLM-AED simulations to evaluate model calibration and validation. The second part of the results then evaluates projected changes in hydrodynamic and DOC conditions under the future climate scenarios and across the simulation ensemble.

3.1 Historical dynamics and model calibration

Historical dynamics and model performance were evaluated first for water temperature and subsequently for DOC, following the sequential calibration procedure described in Section 2.5.3. Results focus on the capacity of the calibrated models to reproduce the magnitude, vertical structure and broader seasonal and interannual variability observed at each site, with calibration and validation periods evaluated independently. The best performing hydrodynamic parameter configurations for Lough Feeagh and Sau Reservoir are reported in Supplementary Material A.

3.1.1 Temperature

Lough Feeagh exhibited a strong and recurrent seasonal thermal cycle throughout the historical period, superimposed on comparatively moderate interannual variability. The observed and simulated temporal and vertical thermal structures are presented in Figure 6. At 0.9 m, mean monthly observed temperature increased from 5.9 °C in February to 16.8 °C in July and remained above 15.0 °C through September. The highest individual surface observation was 22.6 °C in July 2013. Seasonal variability decreased progressively with depth, while the timing of maximum temperature shifted towards autumn. At 42 m, mean monthly temperature ranged from 5.7 °C in February to 12.3 °C in October, reflecting the delayed transfer of summer heat into deeper waters. Temperatures converged through much of the water column during winter, whereas summer differences between surface and deep water commonly exceeded 5.0 °C. Annual mean surface temperature ranged from 10.6 to 12.1 °C between 2005 and 2016.

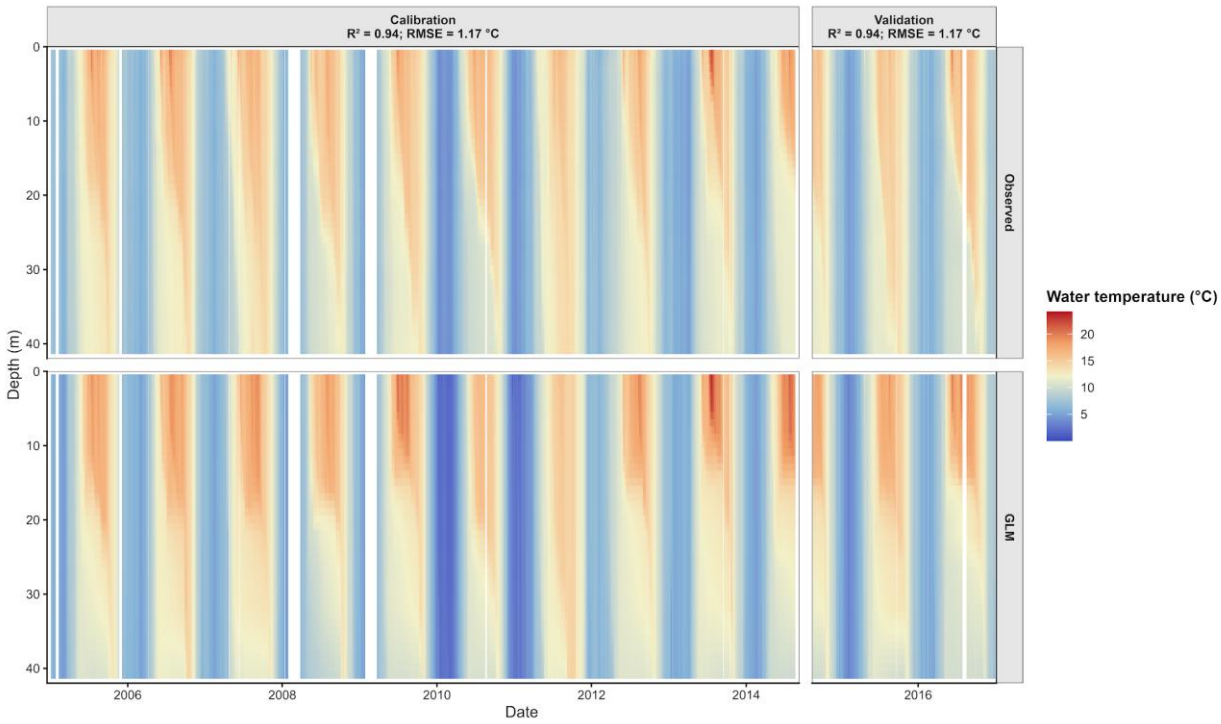


Figure 6. *Daily observed and simulated water temperature profiles at Lough Feeagh during GLM calibration and validation. Model performance are indicated for calibration and validation, respectively.*

The calibrated Feeagh model reproduced these dynamics consistently during both calibration and validation (Figures 6 and 7). Across all matched depths and dates, calibration produced an R^2 of 0.94 and an RMSE of 1.2 °C. Independent validation produced the same overall R^2 of 0.94 and an RMSE of 1.2 °C. Performance was particularly consistent between 0.9 and 14 m, where calibration R^2 values ranged from 0.95 to 0.96 and validation values from 0.98 to 0.99. RMSE values across these depths ranged from 1.1 to 1.4 °C. Between 16 and 32 m, calibration R^2 values ranged from 0.92 to 0.95 and validation values from 0.90 to 0.93, while RMSE remained between 0.8 and 1.1 °C. At 42 m, R^2 was 0.87 during calibration and 0.84 during validation, with respective RMSE values of 1.2 and 1.1 °C. Agreement remained high following temporal aggregation. Monthly calibration and validation produced R^2 values of 0.95 and 0.95, respectively, with corresponding RMSE values of 1.1 and 1.1 °C. Seasonal R^2 values were 0.96 during calibration and 0.97 during validation, while RMSE was approximately 1.0 °C in both periods. At the annual scale, RMSE decreased further to 0.6 °C during calibration and 0.5 °C during validation.

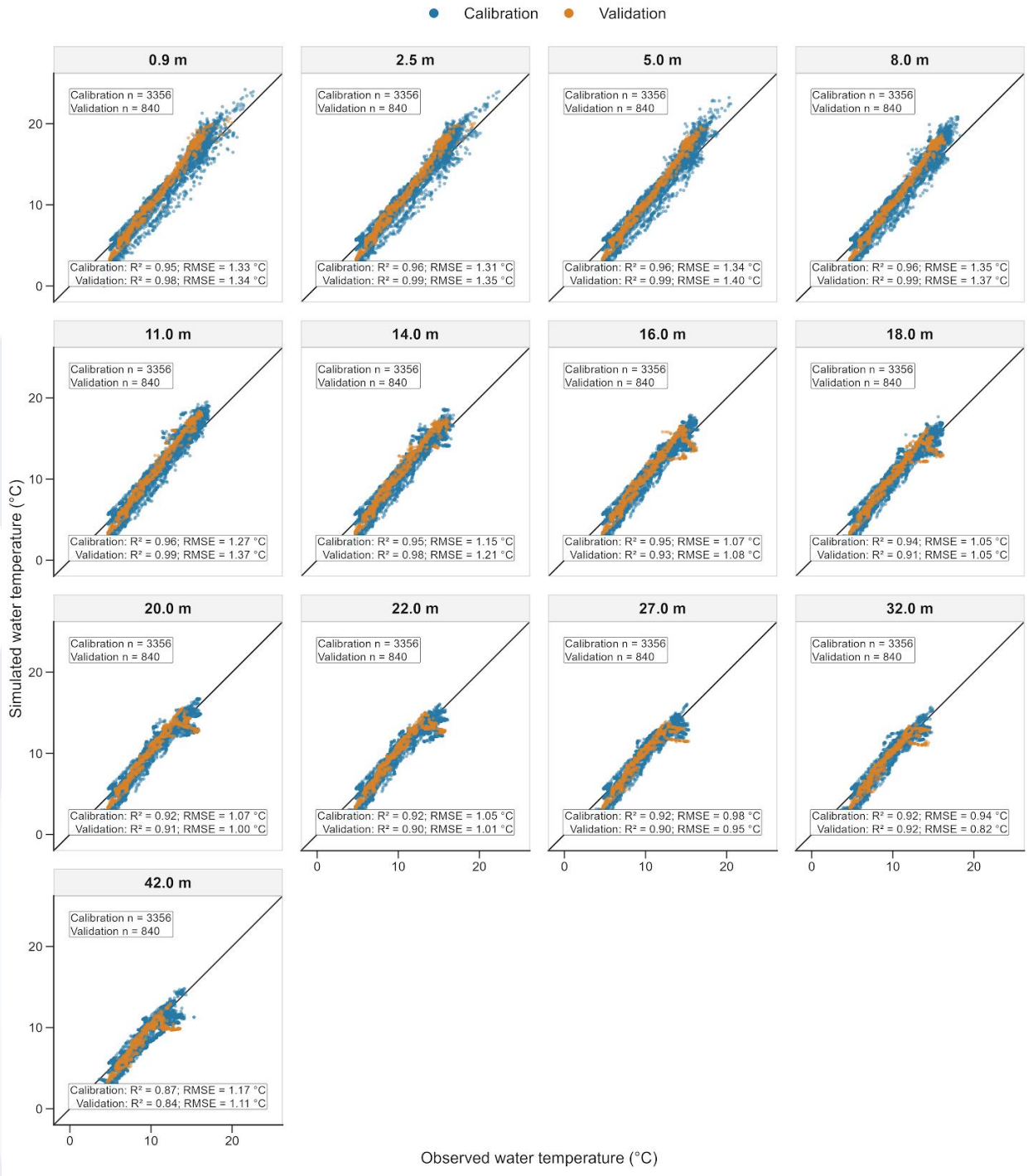


Figure 7. *Daily observed and simulated water temperature at different depths for Lough Feeagh during GLM calibration and validation. Model performance are indicated for calibration and validation, respectively.*

Sau Reservoir displayed a substantially stronger vertical and seasonal thermal gradient. The observed and simulated temperature profiles are shown in Figure 8. Mean monthly surface temperature was approximately 6.9 °C in January and February, increased rapidly during spring and reached 22.9 °C in June, 24.9 °C in July and 25.4 °C in August. The highest surface observation was 26.7 °C in July 2015. Seasonal temperature variation was progressively dampened with depth. At 30 m, mean monthly temperature ranged from 6.2 to 10.8 °C, while temperatures between 40 and 50 m generally ranged from 5.9 to 9.4 °C. The contrast between summer surface temperatures above 20.0 °C and persistently cooler deep water demonstrated the recurrent establishment of strong thermal stratification, followed by progressive cooling and vertical homogenisation during autumn and winter. The intensity and vertical extent of this structure varied among years over the 1997 to 2018 observational record, particularly in intermediate and deep waters.

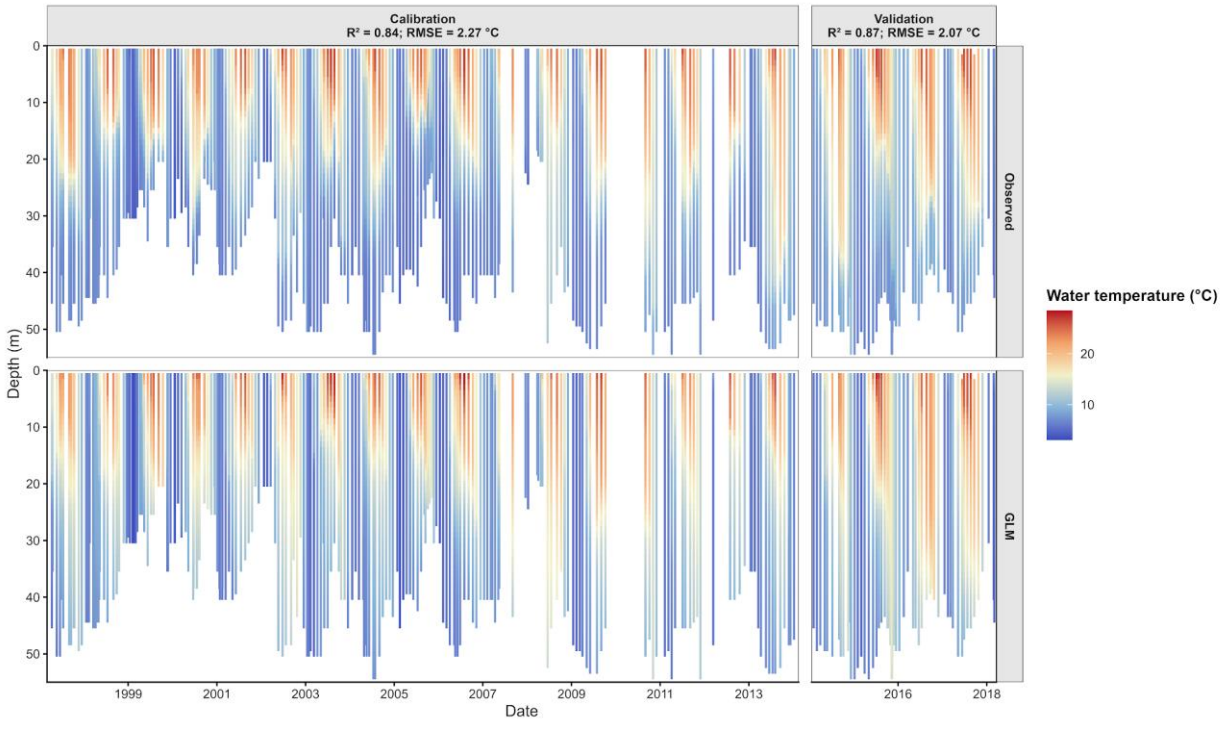


Figure 8. *Daily observed and simulated water temperature profiles at Sau Reservoir during GLM calibration and validation. Model performance are indicated for calibration and validation, respectively.*

The calibrated Sau model reproduced the dominant seasonal cycle and vertical thermal structure, although performance varied more strongly with depth than at Feeagh (Figures 8 and 9). Across all profile observations, calibration produced an R^2 of 0.84 and an RMSE of 2.3 °C. Independent validation produced an R^2 of 0.87 and an RMSE of 2.1 °C. Agreement was strongest between 0 and 10 m. Across these depths, calibration R^2 values ranged from 0.90 to 0.97, with RMSE values from 1.6 to 1.9 °C. Validation R^2 values ranged from 0.97 to 0.98, with RMSE values from 1.1 to 1.7 °C.

Performance decreased through intermediate and deep waters. Between 12 and 25 m, calibration R^2 ranged from 0.57 to 0.82, whereas validation R^2 ranged from 0.81 to 0.98. Corresponding RMSE values ranged from 2.3 to 2.9 °C during calibration and from 1.1 to 2.1 °C during validation. Between 30 and 55 m, calibration R^2 ranged from 0.33 to 0.57 and validation R^2 from 0.20 to 0.55. RMSE values across these depths ranged from 1.8 to 2.7 °C during calibration and from 2.9 to 3.4 °C during validation. The residual structure also changed with depth, with generally cooler simulated temperatures in the upper water column and warmer simulated temperatures below approximately 18 m.

Despite the reduced depth specific agreement in deeper waters, the broader temporal signal remained well represented following aggregation. Monthly R^2 values were 0.86 during calibration and 0.90 during validation, with RMSE values of 2.1 and 1.9 °C, respectively. Seasonal R^2 values were 0.88 and 0.89, with corresponding RMSE values of 1.9 and 1.8 °C. At the annual scale, R^2 values were 0.83 during calibration and 0.87 during validation, while RMSE decreased to 1.5 and 1.4 °C.

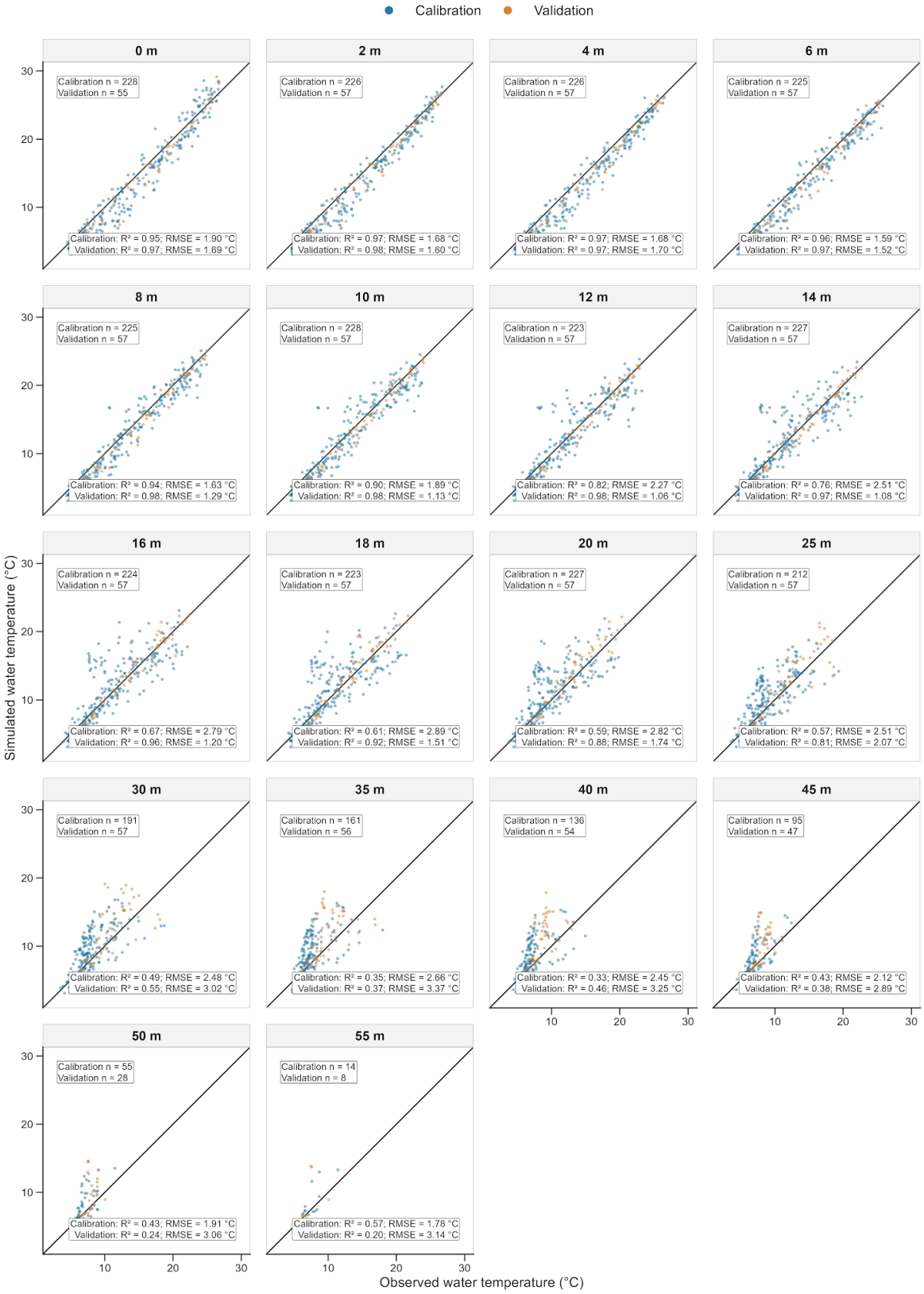


Figure 9. *Daily observed and simulated water temperature at different depths for Sau Reservoir during GLM calibration and validation. Model performance are indicated for calibration and validation, respectively.*

3.1.2 Dissolved organic carbon

Observed DOC at Lough Feeagh showed substantial seasonal and interannual variability between 2010 and 2019. Daily concentrations ranged from 6.8 to 15.3 mg C L^{-1}, with an overall mean of 10.5 mg C L^{-1}. The seasonal cycle was moderate relative to the interannual signal. Monthly climatological means were lowest in May (9.6 mg C L^{-1}) and highest in October (11.7 mg C L^{-1}), with generally higher concentrations from late summer through winter. More pronounced changes occurred among years. Annual mean DOC declined from 12.0 mg C L^{-1} in 2010 to 8.4 mg C L^{-1} in 2015, before increasing to 12.8 mg C L^{-1} in 2017. Concentrations subsequently declined to 10.9 mg C L^{-1} in 2018 and increased again to 11.6 mg C L^{-1} in 2019.

The calibrated Feeagh GLM AED configuration reproduced the broad magnitude and temporal evolution of DOC, although agreement with individual daily fluctuations was lower than that obtained for water temperature (Figures 10 and 11). During calibration, daily DOC produced an R^2 of 0.47 and an RMSE of 1.6 mg C L^{-1}. The observed and simulated means were 10.3 and 9.5 mg C L^{-1}, respectively, resulting in a bias of −0.8 mg C L^{-1}. During independent validation, R^2 was 0.29 and RMSE was 1.7 mg C L^{-1}. Observed and simulated means were 11.5 and 11.6 mg C L^{-1}, respectively, and the corresponding bias was 0.1 mg C L^{-1}.

Aggregation to monthly means resulted in an R^2 of 0.49 and an RMSE of 1.5 mg C L^{-1} during calibration. Validation produced an R^2 of 0.38 and an RMSE of 1.8 mg C L^{-1}, with observed and simulated monthly means of 11.6 and 12.1 mg C L^{-1}. The model represented the period of comparatively low DOC between 2013 and 2015 and the marked increase towards 2017, although differences remained in the magnitude and timing of individual peaks. The four calibrated DOC parameters associated with the best simulation are reported in Supplementary Material A.

The eleven-member local parameter ensemble produced a mean daily envelope width of approximately 1.2 mg C L^{-1}. This envelope contained 26% of the daily observations and 19% of the monthly observations. Most observations outside the envelope were above its upper limit, consistent with the tendency of the calibration simulations to underestimate some periods of elevated DOC.

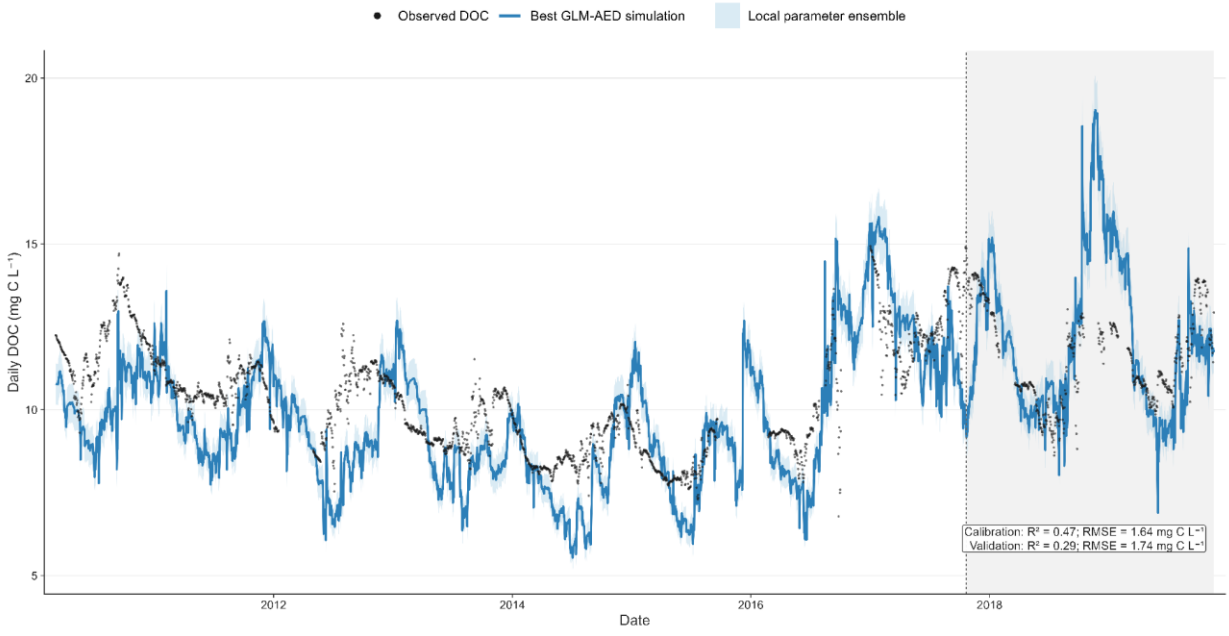


Figure 10. *Daily observed and simulated DOC concentration at the surface layer (0.9 m) for Lough Feeagh during GLM-AED calibration and validation. Model performance are indicated for the best parameter set obtained during calibration and employed during validation, respectively. The light blue band around the optimised run denotes the local parameter ensemble uncertainty band.*

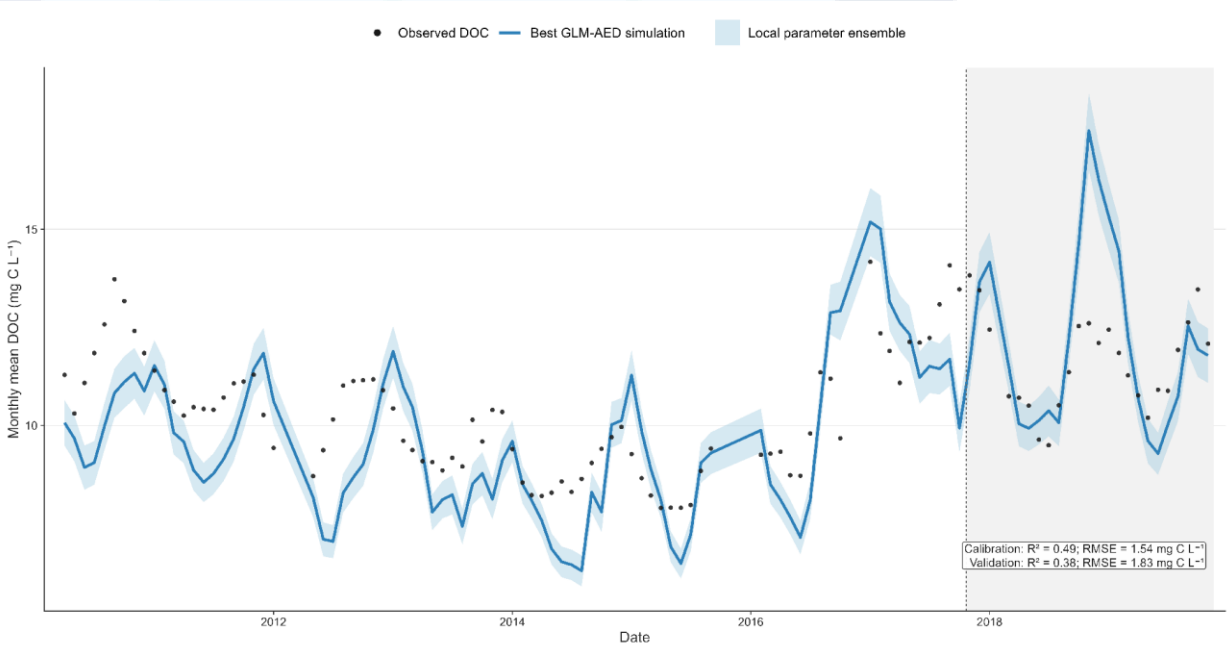


Figure 11. *Monthly observed and simulated DOC concentration at the surface layer (0.9 m) for Lough Feeagh during GLM-AED calibration and validation. Model performance are indicated for the best parameter set obtained during calibration and employed during validation, respectively. The light blue band around the optimised run denotes the local parameter ensemble uncertainty band.*

Surface DOC dynamics at Sau Reservoir differed substantially from those at Feeagh. Across the observations retained between 0 and 5 m, DOC ranged from 1.9 to 7.3 mg C L^{-1}, with a mean of 3.2 mg C L^{-1} and a median of 3.0 mg C L^{-1}. Most observations were concentrated between approximately 2.5 and 3.5 mg C L^{-1}, although episodic concentrations above 4.0 to 5.0 mg C L^{-1} occurred throughout the record. The highest concentrations were observed during its early years. In 1995, the annual mean reached 4.9 mg C L^{-1} and individual observations exceeded 7.0 mg C L^{-1}. Annual means subsequently varied predominantly between 2.4 and 3.8 mg C L^{-1}, with comparatively low values during 1997, 2007, 2013 and 2016.

A strong recurrent seasonal cycle was not evident at Sau. Monthly climatological means varied from 3.0 mg C L^{-1} in September and December to 3.5 mg C L^{-1} in April. Much of the observed variability was therefore associated with differences among years and individual sampling events rather than with a consistent seasonal pattern.

The initial physically calibrated GLM AED simulation substantially underestimated the magnitude of surface DOC. During calibration, the observed mean was 3.2 mg C L^{-1}, compared with a simulated mean of 1.0 mg C L^{-1}. This produced a bias of −2.3 mg C L^{-1}, an RMSE of 2.5 mg C L^{-1} and an R^2 of 0.03. A similar underestimation occurred during validation, when the observed and simulated means were 2.8 and 0.6 mg C L^{-1}, respectively. Validation bias was −2.2 mg C L^{-1}, RMSE was 2.3 mg C L^{-1} and R^2 was 0.03.

Following the dynamic adjustment described in Section 2.5.3, the selected estimate combined the monthly calibration climatology with simulated anomalies scaled by a factor of 0.75. The adjustment was fitted using only calibration observations and was subsequently applied without modification during validation. The resulting estimate reproduced the mean DOC concentration substantially more closely (Figures 12 and 13). During calibration, the observed and simulated daily means were both 3.2 mg C L^{-1}, with negligible bias, an RMSE of 0.9 mg C L^{-1} and an R^2 of 0.09. During validation, the observed and simulated means were 2.8 and 2.9 mg C L^{-1}, respectively. The corresponding bias was 0.1 mg C L^{-1}, RMSE was 0.7 mg C L^{-1} and R^2 was 0.02.

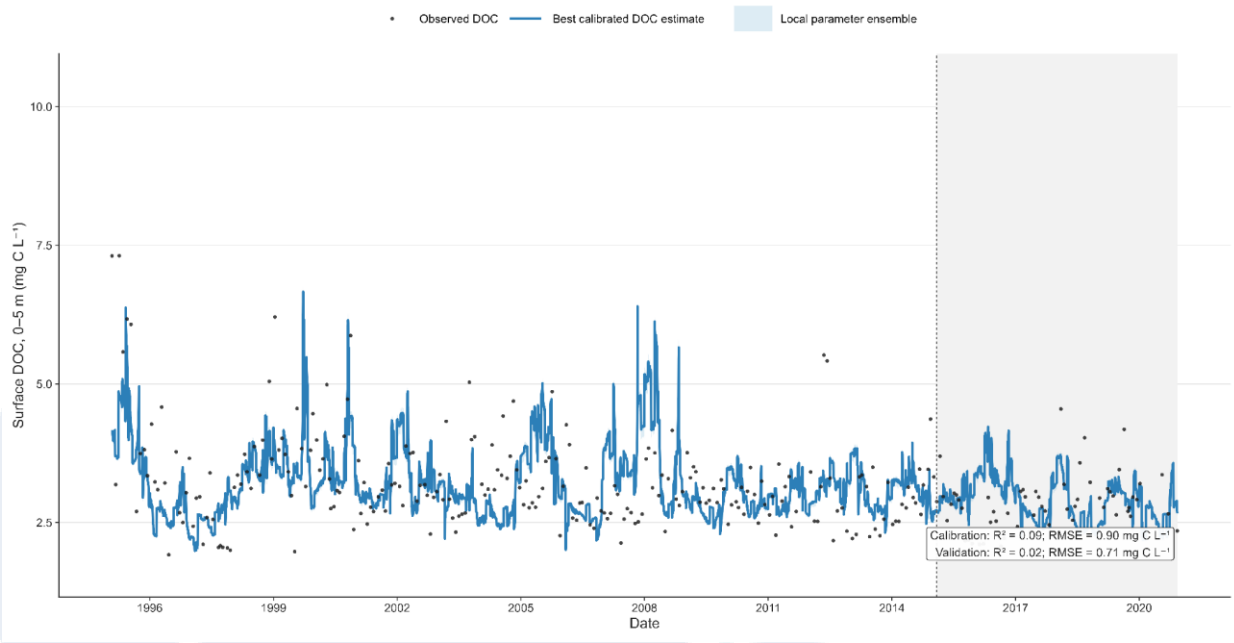


Figure 12. *Daily observed and simulated DOC concentration at the surface layer (0 – 5 m average) for Sau Reservoir during GLM-AED calibration and validation. Model performance are indicated for the best parameter set obtained during calibration and employed during validation, respectively. The light blue band around the optimised run denotes the local parameter ensemble uncertainty band.*

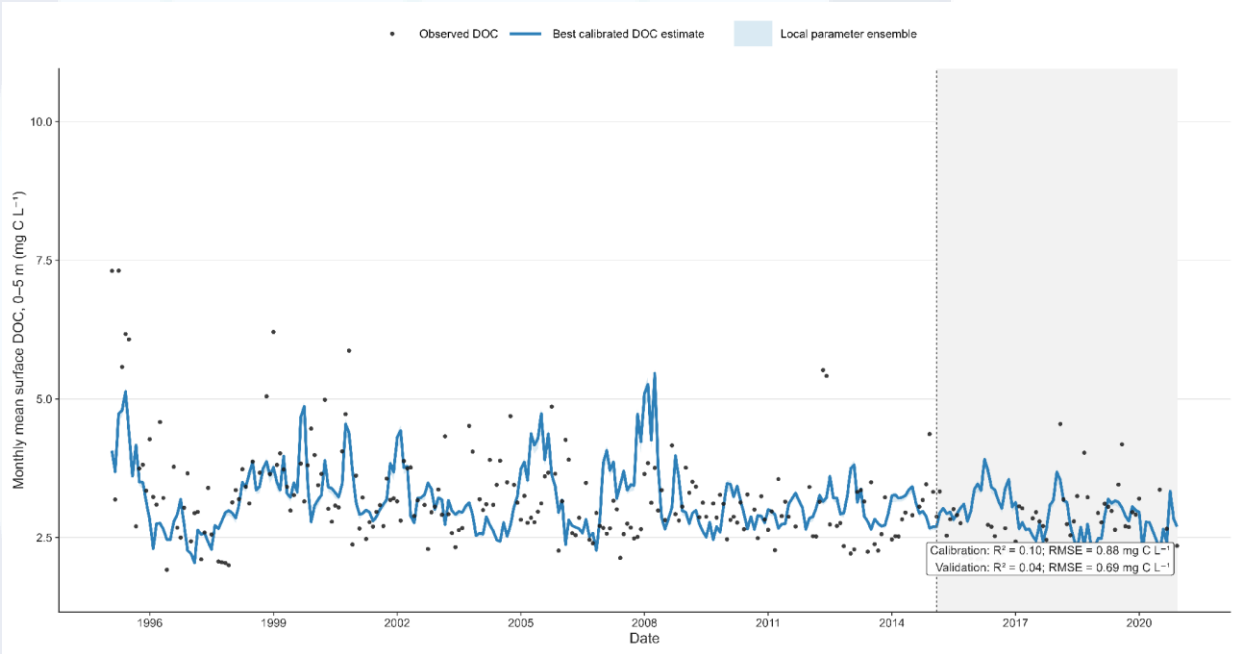


Figure 13. *Monthly observed and simulated DOC concentration at the surface layer (0 – 5 m average) for Sau Reservoir during GLM-AED calibration and validation. Model performance are indicated for the best parameter set obtained during calibration and employed during validation, respectively. The light blue band around the optimised run denotes the local parameter ensemble uncertainty band.*

At the monthly scale, calibration produced an R^2 of 0.10 and an RMSE of 0.9 mg C L^{-1}, while validation produced an R^2 of 0.04 and an RMSE of 0.7 mg C L^{-1}. The adjusted simulation therefore reproduced the overall DOC magnitude and broader temporal envelope more successfully than the unadjusted physical simulation. Nevertheless, the low R^2 values indicated that correspondence with the timing of individual observed fluctuations remained limited. The calibrated physical parameters and selected dynamic adjustment are reported in Supplementary Material A.

The Sau local parameter ensemble produced considerably less dispersion than the Feeagh ensemble. Its mean daily envelope width was approximately 0.2 mg C L^{-1} and it contained only 6% of the daily observations and 7% of the monthly observations. Observations outside the envelope were distributed almost evenly above and below it.

3.2 Future climate

The results presented in this section describe the projected meteorological conditions used to force the lake and reservoir simulations. The five-GCM ensemble projected changes in meteorological conditions at both study sites relative to the 1985–2014 historical-reference period. Projections were evaluated under SSP126, SSP370 and SSP585 for 2041–2050, 2061–2070 and 2091–2100. For each site, the annual distributions of three key meteorological drivers, mean air temperature, total precipitation and mean shortwave radiation, are presented as box plots containing individual values (Figures 14-16 and 20-22). The corresponding monthly figures show the five-GCM ensemble-mean seasonal cycles and allow comparison with the historical baseline. (Figures 17-19 and 23-25).

3.2.1 Lough Feeagh

The ensemble mean annual air temperature during the historical reference period was 9.2 °C (Figure 14). Under SSP126, mean temperature increased to 9.6 °C in both 2041 to 2050 and 2061 to 2070, before decreasing slightly to 9.4 °C in 2091 to 2100. These values represented increases of 0.4, 0.4 and 0.2 °C relative to the baseline, respectively. Under SSP370, temperature increased progressively to 10.1, 10.3 and 11.5 °C, corresponding to anomalies of 0.9, 1.1 and 2.3 °C. SSP585 produced the strongest

warming, with mean temperatures of 10.0, 10.7 and 12.2 °C and corresponding increases of 0.8, 1.5 and 3.0 °C.

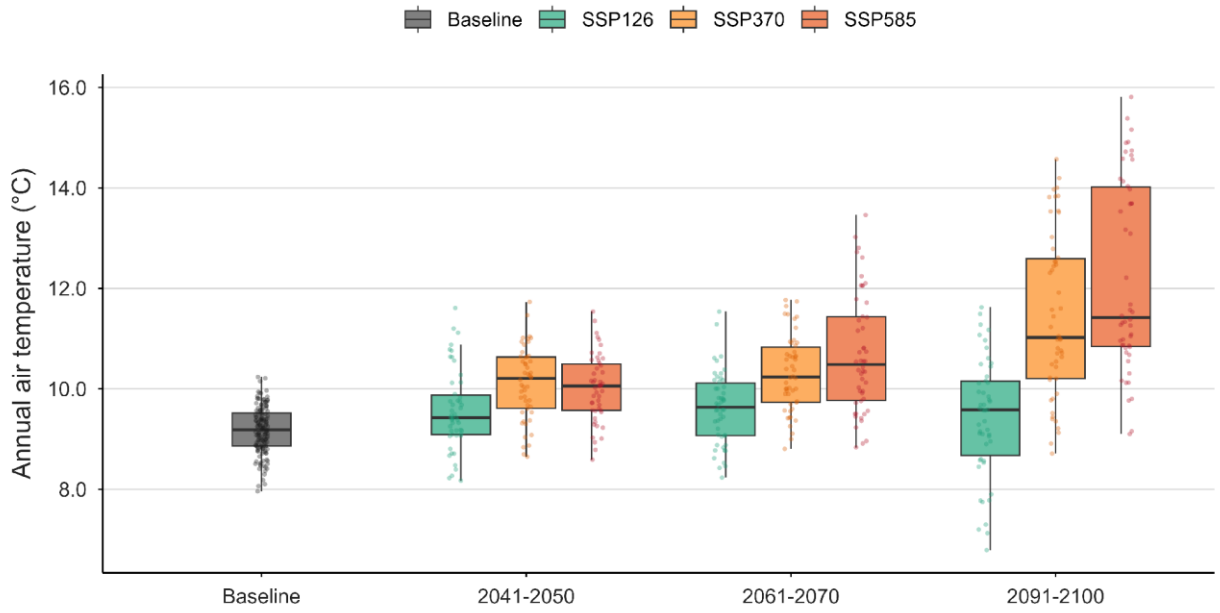


Figure 14. *Boxplot distributions of average annual air temperature for the baseline period, and for the SSP126, SSP370 and SSP585 scenarios during the three analysed independent future periods for Lough Feeagh.*

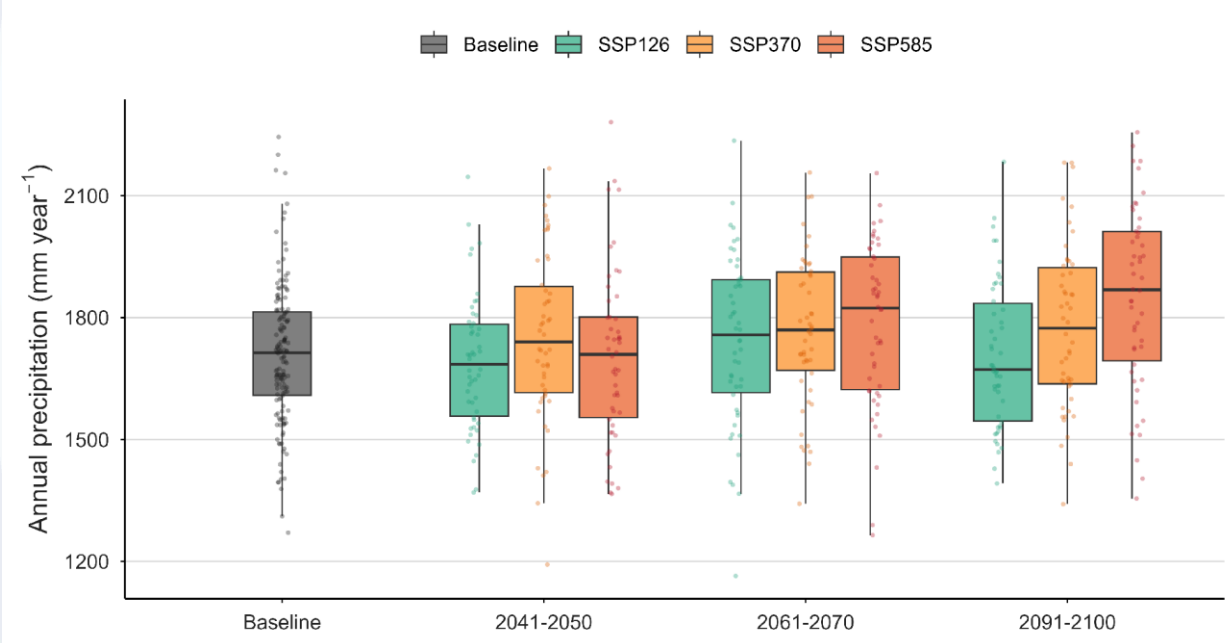


Figure 15. *Boxplot distributions of average annual precipitation for the baseline period, and for the SSP126, SSP370 and SSP585 scenarios during the three analysed independent future periods for Lough Feeagh.*



Figure 16. *Boxplot distributions of average annual shortwave radiation for the baseline period, and for the SSP126, SSP370 and SSP585 scenarios during the three analysed independent future periods for Lough Feeagh.*

The monthly cycles showed that warming was present throughout most of the year but became strongest during summer and autumn, particularly under the higher forcing scenarios (Figure 17). Under SSP585 in 2091 to 2100, mean temperature increased by 3.6 °C during summer and 3.7 °C during autumn. September showed the largest monthly anomaly, reaching approximately 4.1 °C. The distribution of annual temperatures also became wider towards the end of the century under SSP370 and SSP585, indicating increasing differences among GCMs and years.

Annual precipitation during the historical reference period was 1710.0 mm year^{-1} (Figure 15). Under SSP126, projected totals were 1687.7, 1743.5 and 1705.7 mm year^{-1} across the three future periods. These represented changes of −1.3, +2.0 and −0.3%, respectively. Under SSP370, precipitation increased to 1751.5, 1766.9 and 1776.4 mm year^{-1}, corresponding to increases of 2.4, 3.3 and 3.9%. Under SSP585, precipitation was initially close to the baseline at 1704.4 mm year^{-1}, before increasing to 1785.0 mm year^{-1} in 2061 to 2070 and 1849.4 mm year^{-1} in 2091 to 2100. The late century increase was therefore 139.4 mm year^{-1}, equivalent to 8.2%.

The annual changes were accompanied by a marked seasonal redistribution of precipitation (Figure 18). Summer conditions were generally drier than the historical reference, whereas winter and autumn became wetter in several projections. Under SSP585 in 2091 to 2100, mean precipitation increased by 39.9 mm month^{-1} during winter and 14.2 mm month^{-1} during autumn, but decreased by 13.8 mm month^{-1} during summer. January showed the largest positive anomaly at approximately 59.7 mm month^{-1}, whereas September decreased by approximately 19.7 mm month^{-1}.

Mean annual shortwave radiation during the historical reference period was 115.1 W m^{-2} (Figure 16). Future ensemble means ranged from 116.3 to 118.8 W m^{-2} and were therefore slightly higher than the baseline under every scenario and period. Under SSP126, values were 118.8, 117.4 and 117.6 W m^{-2} across the three periods. The corresponding values were 117.4, 116.3 and 117.9 W m^{-2} under SSP370 and 116.6, 116.3 and 116.4 W m^{-2} under SSP585. These changes represented increases of approximately 1.0 to 3.2%, without a consistent progression through time or with scenario intensity. The seasonal cycles of shortwave radiation remained similar to the historical reference, with the largest differences occurring around the spring and summer maximum (Figure 19). In 2091 to 2100, summer radiation increased by 8.4 W m^{-2} under SSP370 and 4.6 W m^{-2} under SSP585. The largest monthly increases occurred in June, reaching approximately 13.1 W m^{-2} under SSP370 and 8.4 W m^{-2} under SSP585. Winter values generally remained close to or slightly below the historical reference.

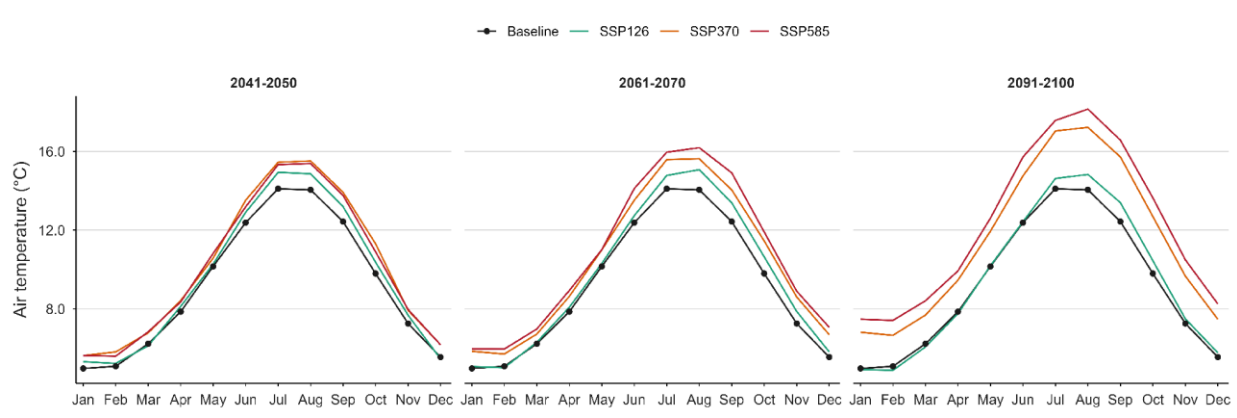


Figure 17. *Average calendar month air temperature value for the baseline period, and for the SSP126, SSP370 and SSP585 scenarios during the three analysed independent future periods for Lough Feeagh.*

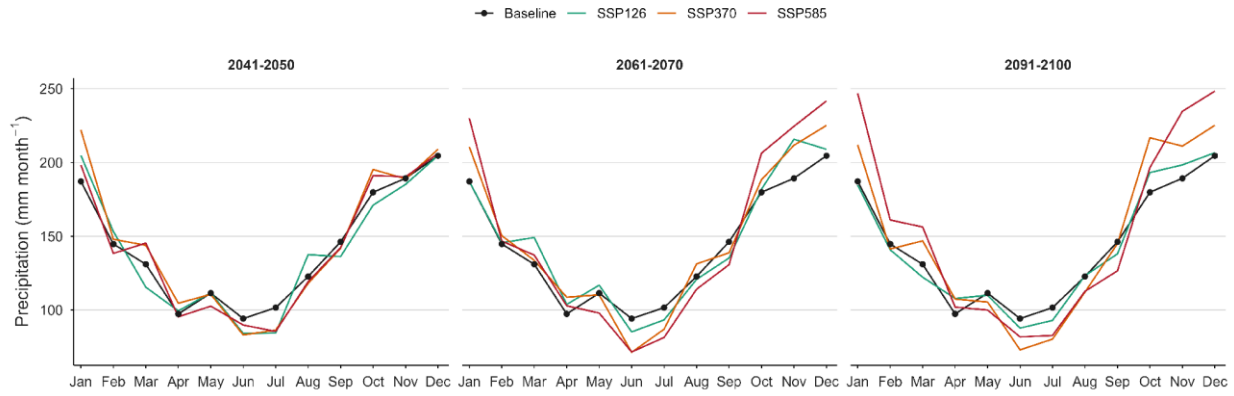


Figure 18. *Average calendar month precipitation value for the baseline period, and for the SSP126, SSP370 and SSP585 scenarios during the three analysed independent future periods for Lough Feeagh.*

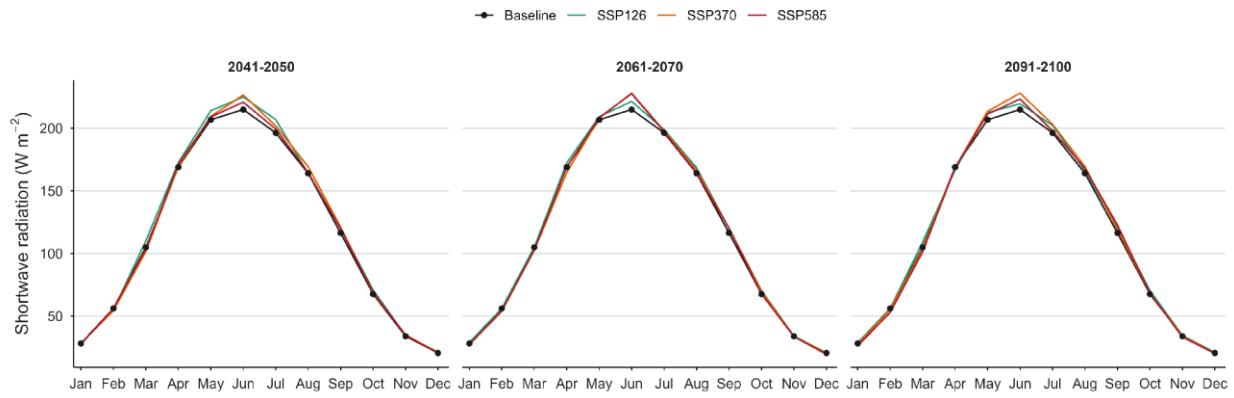


Figure 19. *Average calendar month shortwave radiation value for the baseline period, and for the SSP126, SSP370 and SSP585 scenarios during the three analysed independent future periods for Lough Feeagh.*

3.2.2 Sau Reservoir

The ensemble mean annual air temperature during the historical reference period was 8.9 °C (Figure 20). Under SSP126, mean temperature increased to 10.2 °C in 2041 to 2050, 10.3 °C in 2061 to 2070 and 10.1 °C in 2091 to 2100. These values represented increases of 1.3, 1.4 and 1.2 °C, respectively, indicating limited additional warming after the middle of the century under this pathway. Under SSP370, annual temperature increased progressively to 10.5, 11.4 and 12.9 °C, corresponding to changes of 1.6, 2.5 and 4.0 °C. The greatest warming occurred under SSP585, with mean temperatures of 10.5, 11.7 and 14.0 °C. The late century value represented an increase of 5.1 °C relative to the historical reference.

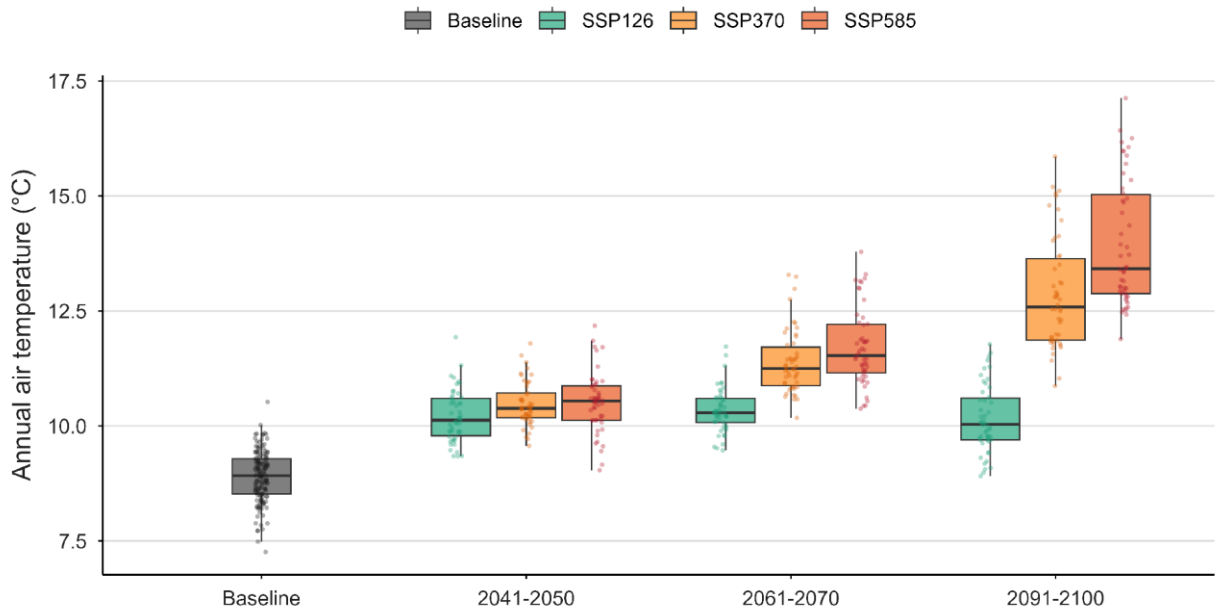


Figure 20. *Boxplot distributions of average annual air temperature for the baseline period, and for the SSP126, SSP370 and SSP585 scenarios during the three analysed independent future periods for Sau Reservoir.*

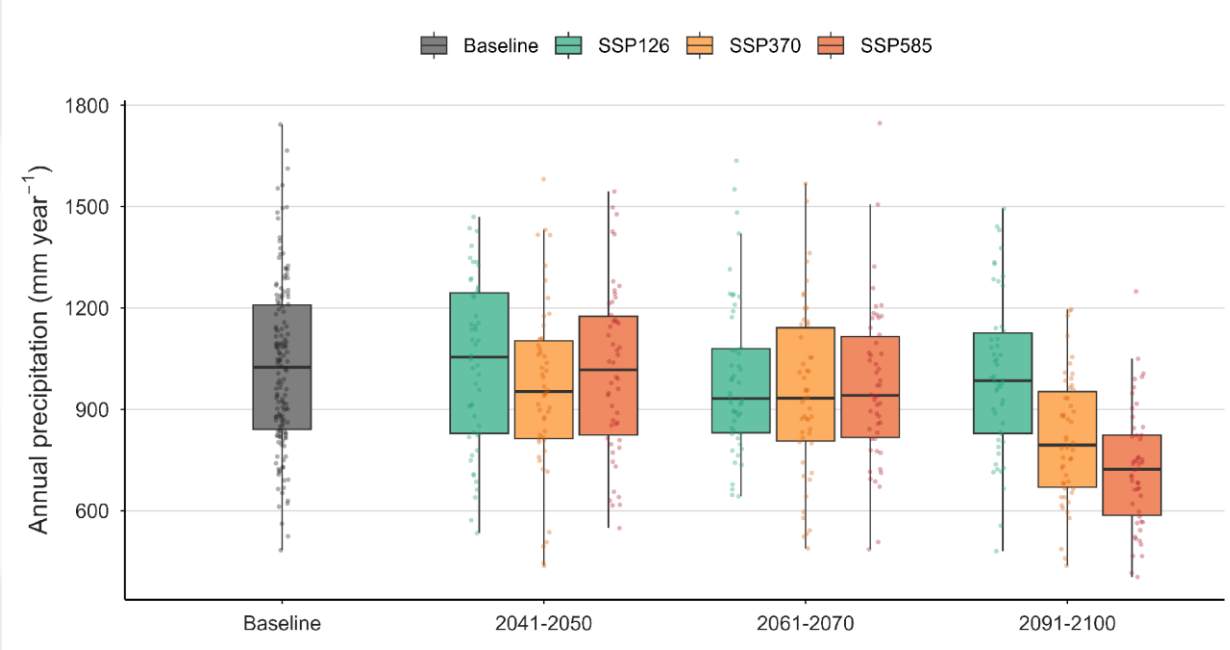


Figure 21. *Boxplot distributions of average annual precipitation for the baseline period, and for the SSP126, SSP370 and SSP585 scenarios during the three analysed independent future periods for Sau Reservoir.*

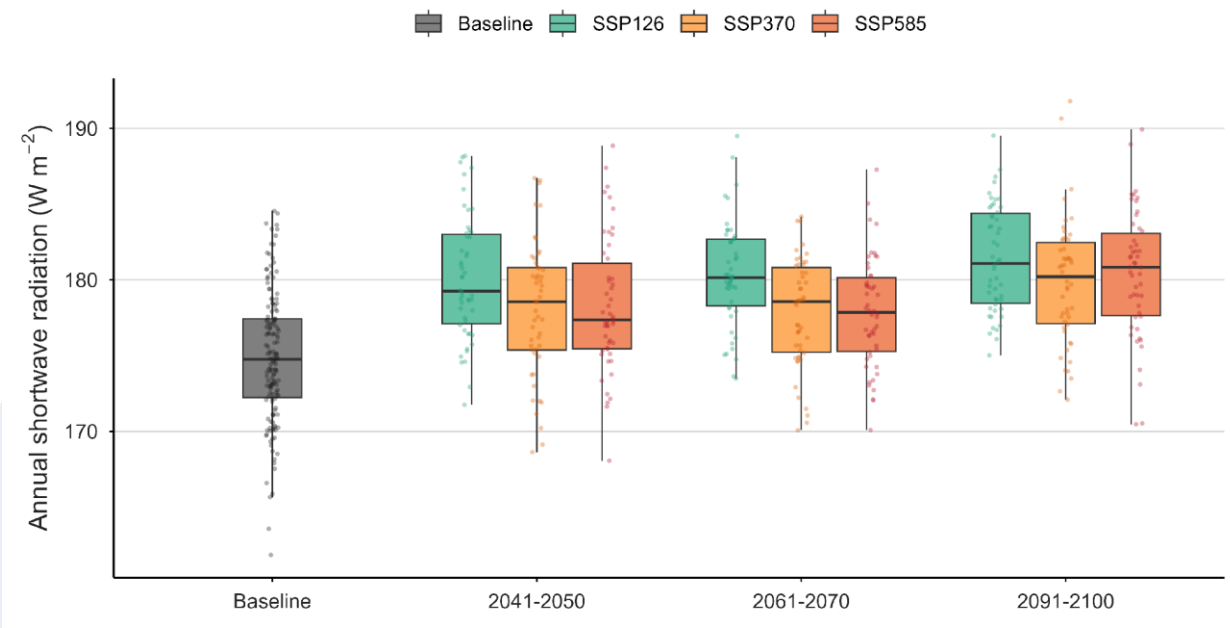


Figure 22. *Boxplot distributions of average annual shortwave radiation for the baseline period, and for the SSP126, SSP370 and SSP585 scenarios during the three analysed independent future periods for Sau Reservoir.*

Warming occurred throughout the year, although the magnitude was consistently greater during summer (Figure 23). Under SSP585 in 2091 to 2100, the mean anomaly reached 6.4 °C during summer and 5.2 °C during autumn. August showed the largest monthly increase at approximately 6.7 °C. Under SSP370 during the same period, summer temperature increased by approximately 5.0 °C. The annual distributions also became progressively wider under SSP370 and SSP585, reflecting greater variation among GCMs and years towards the end of the century.

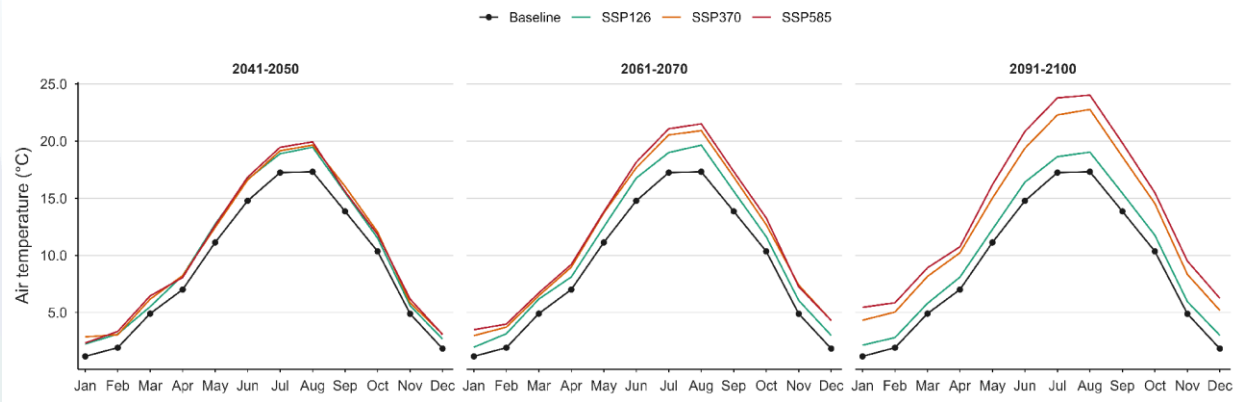


Figure 23. *Average calendar month air temperature value for the baseline period, and for the SSP126, SSP370 and SSP585 scenarios during the three analysed independent future periods for Sau Reservoir.*

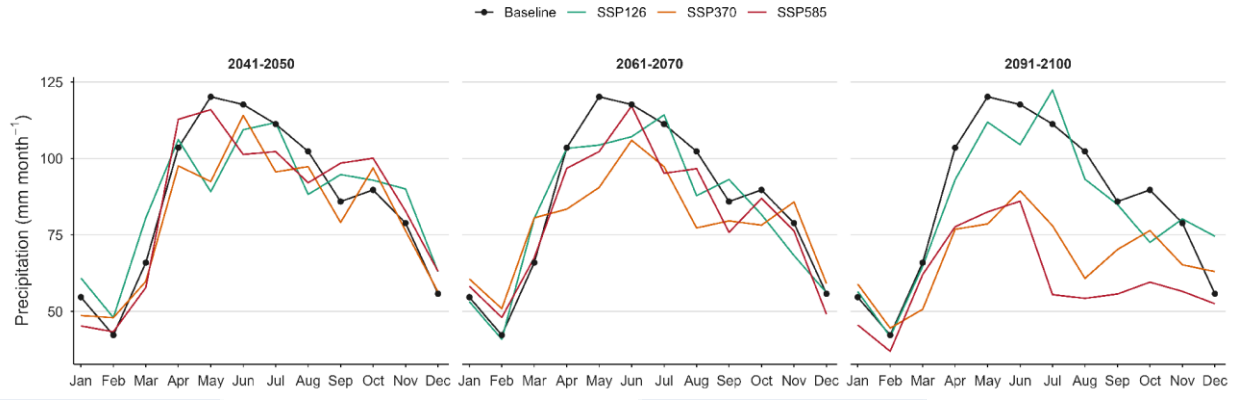


Figure 24. *Average calendar month precipitation value for the baseline period, and for the SSP126, SSP370 and SSP585 scenarios during the three analysed independent future periods for Sau Reservoir.*

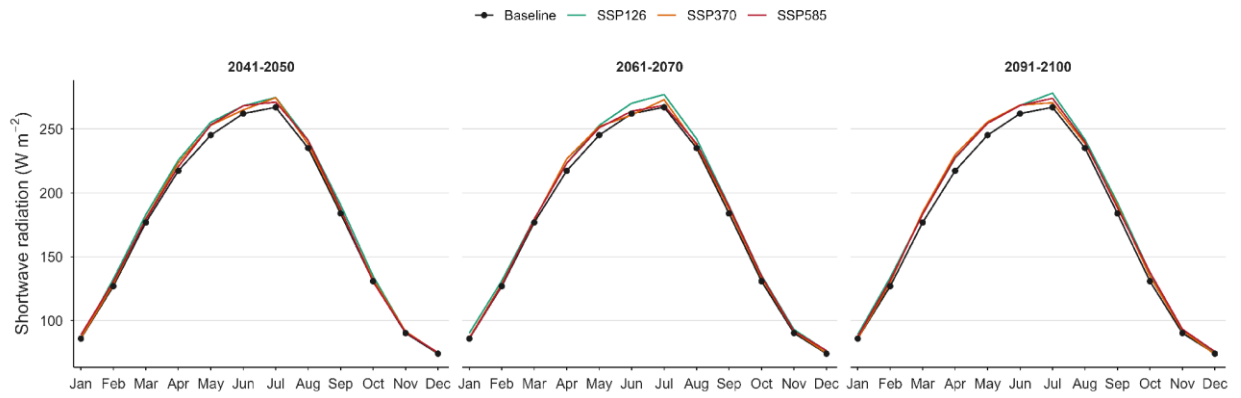


Figure 25. *Average calendar month shortwave radiation value for the baseline period, and for the SSP126, SSP370 and SSP585 scenarios during the three analysed independent future periods for Sau Reservoir.*

Annual precipitation during the historical reference period was 1028.1 mm year^{-1} (Figure 21). Under SSP126, precipitation increased slightly to 1034.8 mm year^{-1} in 2041 to 2050, equivalent to +0.7%, before decreasing to 990.6 and 1000.4 mm year^{-1} in the subsequent periods. These later values represented reductions of 3.6 and 2.7%, respectively. Drying was more pronounced under SSP370, with annual precipitation decreasing to 962.3, 949.4 and 812.8 mm year^{-1}. These changes corresponded to reductions of 6.4, 7.7 and 20.9%. Under SSP585, precipitation decreased to 1015.3 mm year^{-1} in 2041 to 2050, 970.1 mm year^{-1} in 2061 to 2070 and 724.9 mm year^{-1} in 2091 to 2100. The late century reduction was 303.1 mm year^{-1}, equivalent to 29.5%.

The monthly projections showed that drying was concentrated principally from spring to autumn (Figure 24). Under SSP370 in 2091 to 2100, winter precipitation remained slightly above the historical reference, with an average anomaly of +4.6 mm month^{-1}. In contrast, precipitation decreased by 27.8 mm month^{-1} during spring, 34.3 mm month^{-1} during summer and 14.2 mm month^{-1} during autumn. Under SSP585 in 2091 to 2100, precipitation was lower than the historical reference during every season. The mean reductions reached 22.5 mm month^{-1} in spring, 45.1 mm month^{-1} in summer and 27.6 mm month^{-1} in autumn. July experienced the largest monthly decrease, at approximately 55.8 mm month^{-1}.

Mean annual shortwave radiation during the historical reference period was 174.9 W m^{-2} (Figure 22). Higher annual values were projected under every scenario and period. Under SSP126, shortwave radiation increased to 180.1, 180.4 and 181.4 W m^{-2} across the three periods. The corresponding values were 178.1, 177.8 and 179.8 W m^{-2} under SSP370 and 178.3, 177.9 and 180.4 W m^{-2} under SSP585. These changes represented increases of approximately 1.7 to 3.7% relative to the historical reference. Although the overall seasonal form remained consistent, the largest shortwave radiation anomalies occurred during spring and summer (Figure 25). In 2091 to 2100, mean spring radiation increased by 10.4 W m^{-2} under SSP370 and 8.7 W m^{-2} under SSP585. The corresponding summer increases were 4.6 and 6.0 W m^{-2}. April showed the largest monthly anomaly, reaching approximately 12.6 W m^{-2} under SSP370 and 10.4 W m^{-2} under SSP585.

3.3 Response of thermal structures

The GLM simulations projected progressively warmer water-column conditions at both study sites, although the magnitude and vertical distribution of the changes differed substantially between Lough Feeagh and Sau Reservoir. Future thermal conditions are presented first as ensemble-mean monthly temperature profiles, followed by temperature anomalies relative to the historical simulations and, finally, by period-mean vertical profiles. The anomalies were calculated separately for each GCM relative to its

corresponding 1985–2014 historical simulation before being averaged across the ensemble.

3.3.1 Lough Feeagh

The future simulations retained the pronounced seasonal thermal structure characteristic of Lough Feeagh (Figure 26). Winter temperatures remained comparatively uniform throughout the water column, followed by rapid warming of the upper layers during spring. A distinct vertical temperature gradient developed from approximately April and was strongest between June and September. Surface temperatures generally reached their maximum in July, while warming at intermediate and deep layers was smaller and delayed. During autumn, surface cooling occurred before the release of heat stored at greater depths, producing comparatively warm intermediate and deep-water conditions after surface temperatures had begun to decline.

Differences among scenarios were relatively small during 2041–2050. Ensemble-mean maximum monthly surface temperatures ranged between 22.2 and 22.4 °C, with maxima occurring in July under all three SSPs. Scenario separation became clearer during 2061–2070 and was most pronounced during 2091–2100. In the final period, the maximum monthly surface temperature remained approximately 22.2 °C under SSP126, but increased to 23.6 °C under SSP370 and 24.4 °C under SSP585. Under SSP585, the maximum also shifted from July to August. The monthly profiles therefore indicated that the higher-emission scenarios produced both warmer summer conditions and a longer persistence of elevated temperatures into autumn.

The model-paired anomalies showed that warming was concentrated principally in the upper water column, while changes at depth were smaller (Figure 27). Under SSP126, period-mean surface temperature increased by 0.7 °C in 2041–2050, 0.8 °C in 2061–2070 and 1.1 °C in 2091–2100. Temperature at 42 m remained close to the corresponding historical simulations, with anomalies of approximately 0.0, 0.0 and 0.1 °C. The response under SSP126 was therefore moderate and showed limited progression after the middle of the century.

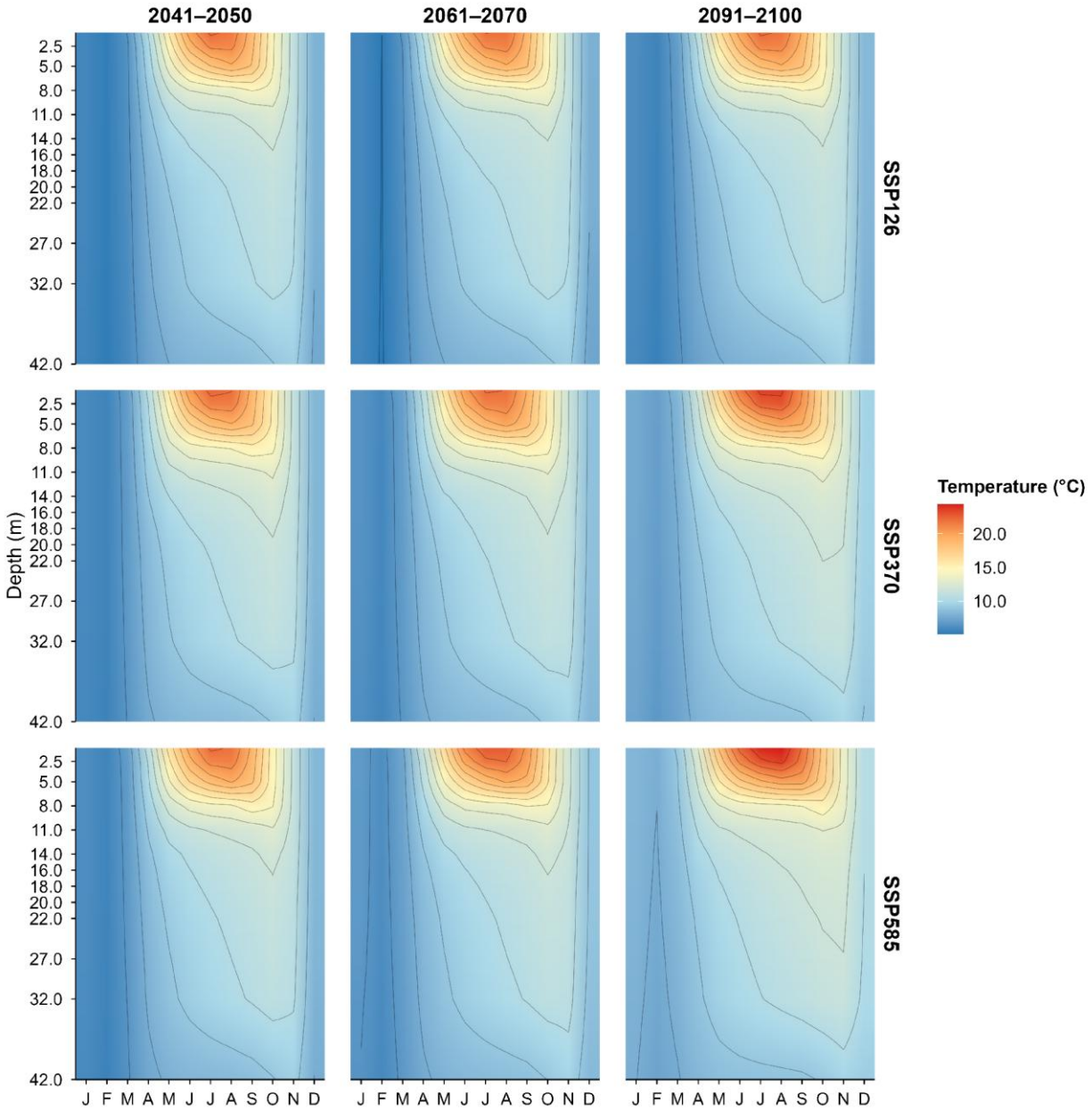


Figure 26. *Future projections of average calendar month water temperature profiles for Lough Feeagh for the SSP126, SSP370 and SSP585 scenarios during the three analysed independent future periods.*

Warming increased more clearly under SSP370 and SSP585. Under SSP370, period-mean surface anomalies increased from 1.0 °C in 2041–2050 to 1.2 °C in 2061–2070 and 2.4 °C in 2091–2100. Corresponding anomalies at 42 m were 0.3, 0.4 and 0.8 °C. Under SSP585, surface warming increased from 1.0 to 1.8 and 3.3 °C across the three periods, while deep-water warming increased from 0.2 to 0.4 and 1.0 °C. Monthly surface anomalies were largest during late summer and early autumn, reaching approximately 4.4 °C under SSP585 in 2091–2100. Warming was comparatively muted around the

seasonal thermocline, particularly at approximately 8 to 11 m during summer, indicating that the response involved a redistribution of vertical thermal structure rather than uniform warming at all depths.

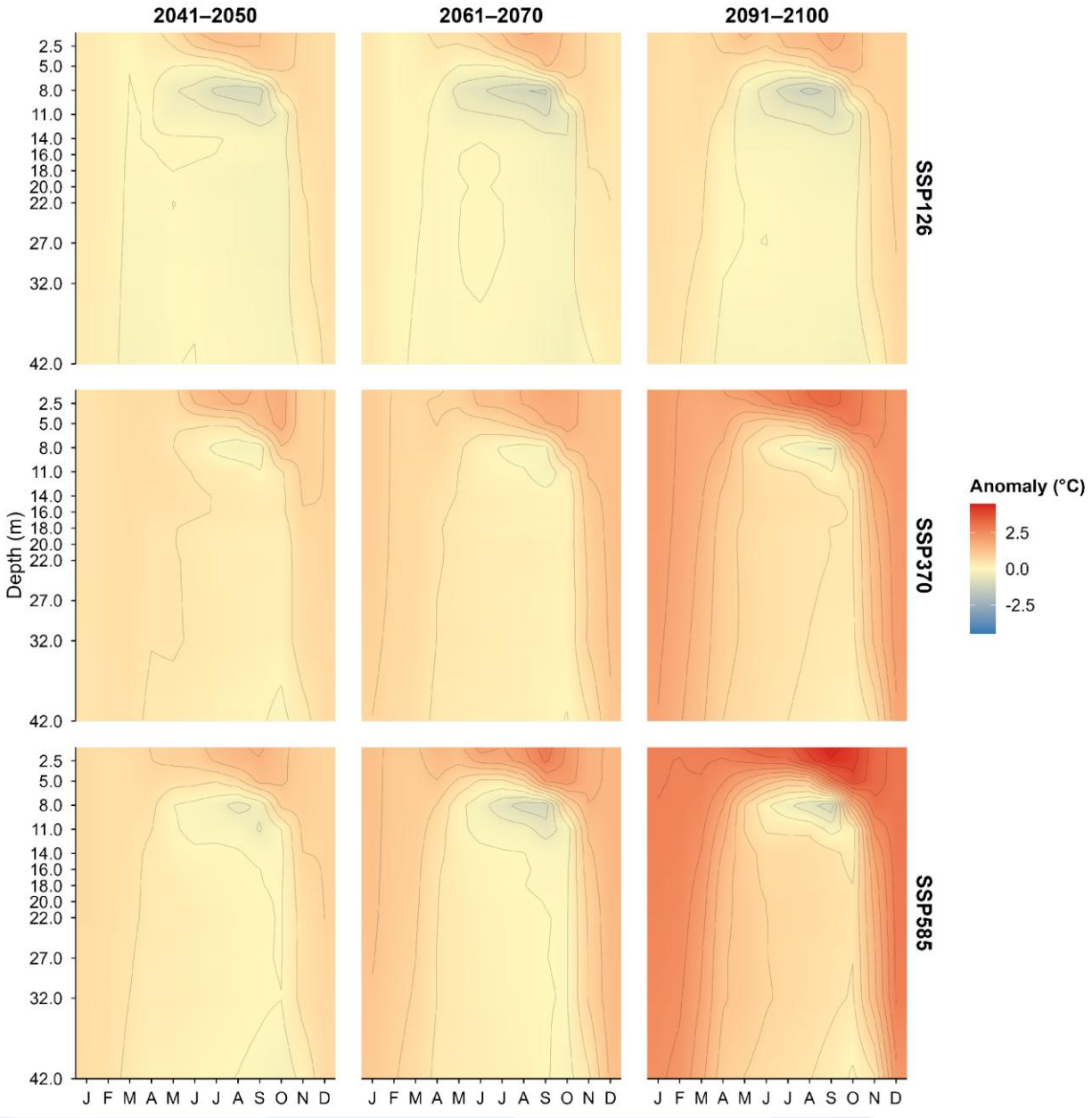


Figure 27. *Model-based anomalies of average calendar month water temperature profiles for Lough Feeagh for the SSP126, SSP370 and SSP585 scenarios during the three analysed independent future periods.*

The period-mean profiles further illustrated the stronger response of the upper water column (Figure 28). The historical simulations produced an ensemble-mean temperature of 12.6 °C at 0.9 m and 7.6 °C at 42 m, corresponding to a period-mean vertical difference

of 5.1 °C. During 2041–2050, mean surface temperatures increased to 13.3 °C under SSP126 and approximately 13.7 °C under SSP370 and SSP585. Deep-water temperatures remained between 7.6 and 7.8 °C. Differences among scenarios were therefore modest during the first future period.

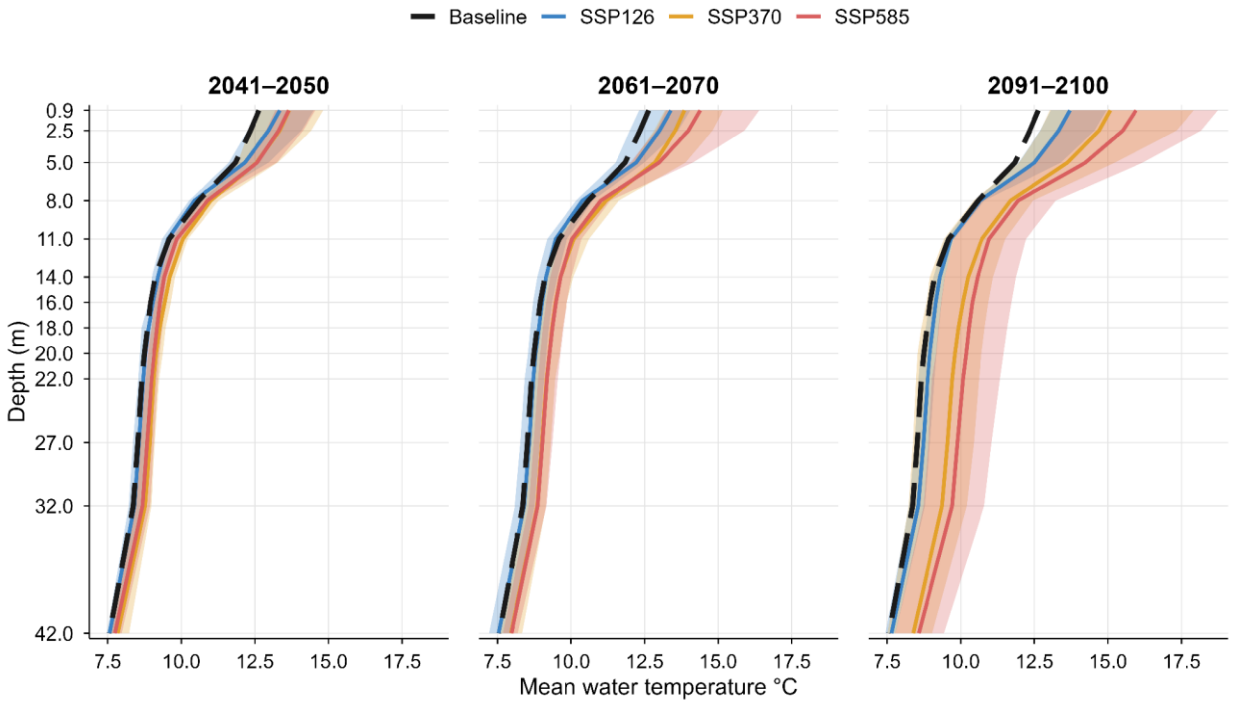


Figure 28. *Future projections of average water temperature at different depths for Lough Feeagh for the historical reference, and for the SSP126, SSP370 and SSP585 scenarios during the three analysed independent future periods. Light coloured bands denote GCM-derived uncertainty for each scenario, respectively.*

During 2061–2070, mean surface temperatures reached 13.4 °C under SSP126, 13.9 °C under SSP370 and 14.4 °C under SSP585. The corresponding temperatures at 42 m were 7.5, 8.0 and 8.0 °C. By 2091–2100, mean surface temperature was projected to reach 13.7 °C under SSP126, 15.1 °C under SSP370 and 16.0 °C under SSP585. Mean deep-water temperatures reached 7.7, 8.4 and 8.6 °C, respectively.

Because warming was consistently greater near the surface, the period-mean surface-to-deep temperature difference increased to 6.1 °C under SSP126, 6.7 °C under SSP370 and 7.4 °C under SSP585 by 2091–2100. The GCM range also widened under SSP370 and SSP585, particularly in the upper water column during the final period.

3.3.2 Sau Reservoir

Sau Reservoir exhibited a warmer and more strongly differentiated seasonal thermal structure than Lough Feeagh (Figure 29). Surface warming began rapidly during spring and produced a pronounced vertical gradient extending through much of the upper and intermediate water column. Maximum temperatures occurred near the surface in August, whereas the seasonal response became progressively smaller and delayed with increasing depth. Surface cooling began during autumn, but warmer water persisted at intermediate depths until later in the year. This general seasonal sequence was maintained under all scenarios and future periods.

During 2041–2050, ensemble-mean August surface temperatures were 28.7 °C under SSP126, 28.8 °C under SSP370 and 29.3 °C under SSP585. Scenario separation increased during 2061–2070, when August temperatures reached 28.8, 30.0 and 30.6 °C, respectively. The differences were greatest during 2091–2100. August surface temperature remained approximately 28.4 °C under SSP126 but increased to 31.7 °C under SSP370 and 32.7 °C under SSP585. Under the higher-emission scenarios, elevated temperatures also extended farther into the intermediate water column and persisted later into autumn.

Positive model-paired anomalies occurred across most months and depths, although the magnitude of warming decreased with depth (Figure 30). Under SSP126, period-mean surface temperature increased by 1.7 °C in both 2041–2050 and 2061–2070 and by 1.6 °C in 2091–2100. At 20 m, the corresponding anomalies were 0.8, 1.1 and 1.0 °C, while warming at 55 m was 0.8, 1.2 and 0.8 °C. As at Feeagh, SSP126 therefore produced sustained but comparatively stable warming without a progressive late-century increase.

Under SSP370, surface anomalies increased from 1.9 °C in 2041–2050 to 2.7 °C in 2061–2070 and 4.3 °C in 2091–2100. Warming at 20 m increased from 1.2 to 1.7 and 2.5 °C, while the corresponding anomalies at 55 m were 1.2, 1.5 and 2.4 °C. The response was greater under SSP585. Period-mean surface anomalies increased from 2.0 to 3.2 and 5.3 °C across the three periods. At 20 m, warming reached 1.2, 1.9 and 2.9 °C, while warming at 55 m reached 1.2, 1.8 and 3.1 °C. The strongest monthly anomalies occurred in the upper water column under SSP585 in 2091–2100, where warming approached or exceeded 6 °C during parts of summer and early autumn.

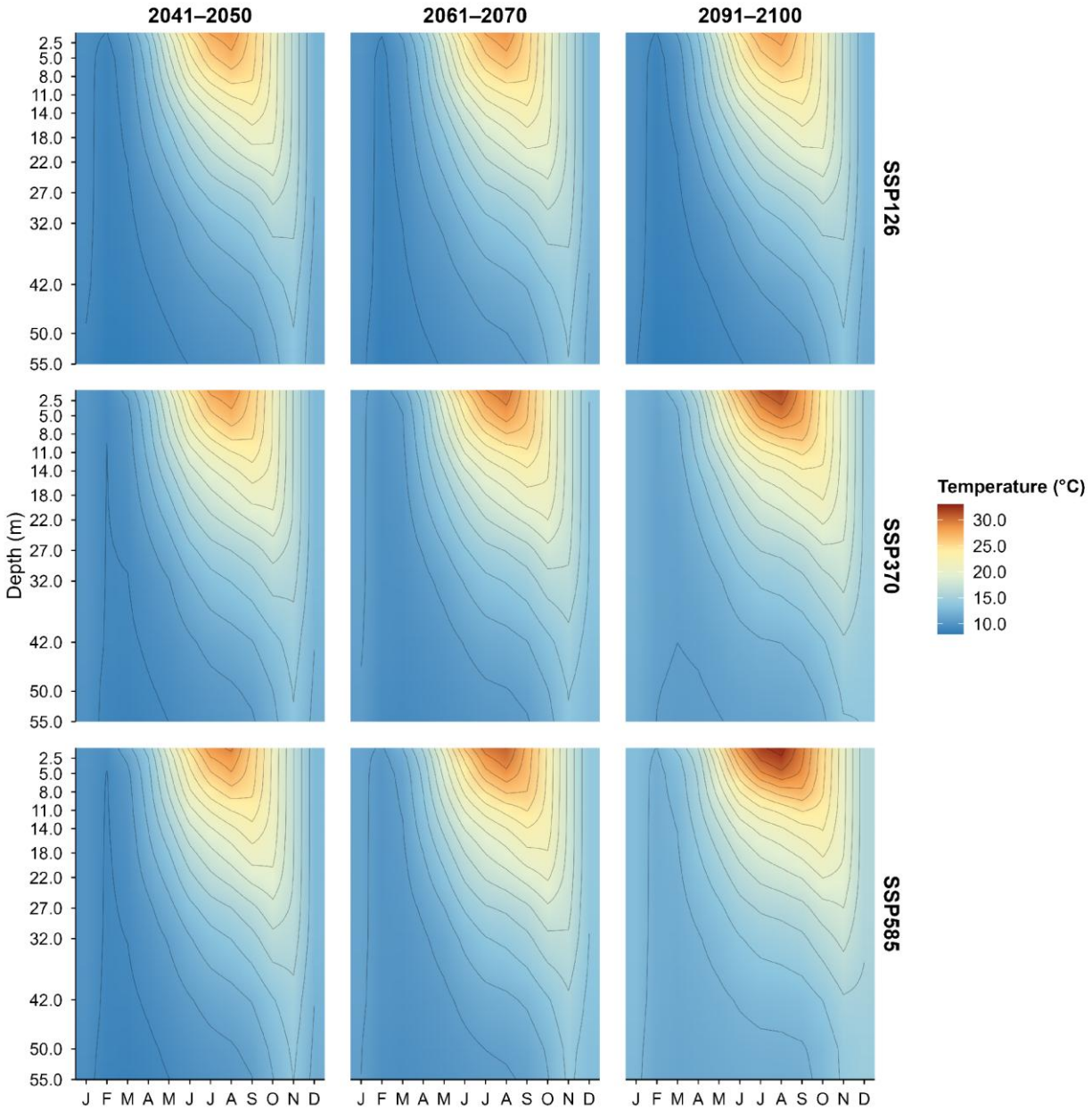


Figure 29. *Future projections of average calendar month water temperature profiles for Sau Reservoir for the SSP126, SSP370 and SSP585 scenarios during the three analysed independent future periods.*

The period-mean profiles demonstrated that warming extended throughout the reservoir, while remaining strongest near the surface (Figure 31). The historical simulations produced an ensemble-mean temperature of 16.7 °C at 0.9 m, 13.3 °C at 20 m and 9.1 °C at 55 m. The corresponding surface-to-deep temperature difference was 7.7 °C. During 2041–2050, mean surface temperatures increased to 18.4 °C under SSP126,

18.6 °C under SSP370 and 18.8 °C under SSP585. Temperatures at 55 m reached approximately 9.8, 10.2 and 10.2 °C, respectively. During 2061–2070, surface temperatures reached 18.4 °C under SSP126, 19.4 °C under SSP370 and 19.9 °C under SSP585, while temperatures at 55 m increased to 10.3, 10.6 and 10.9 °C.

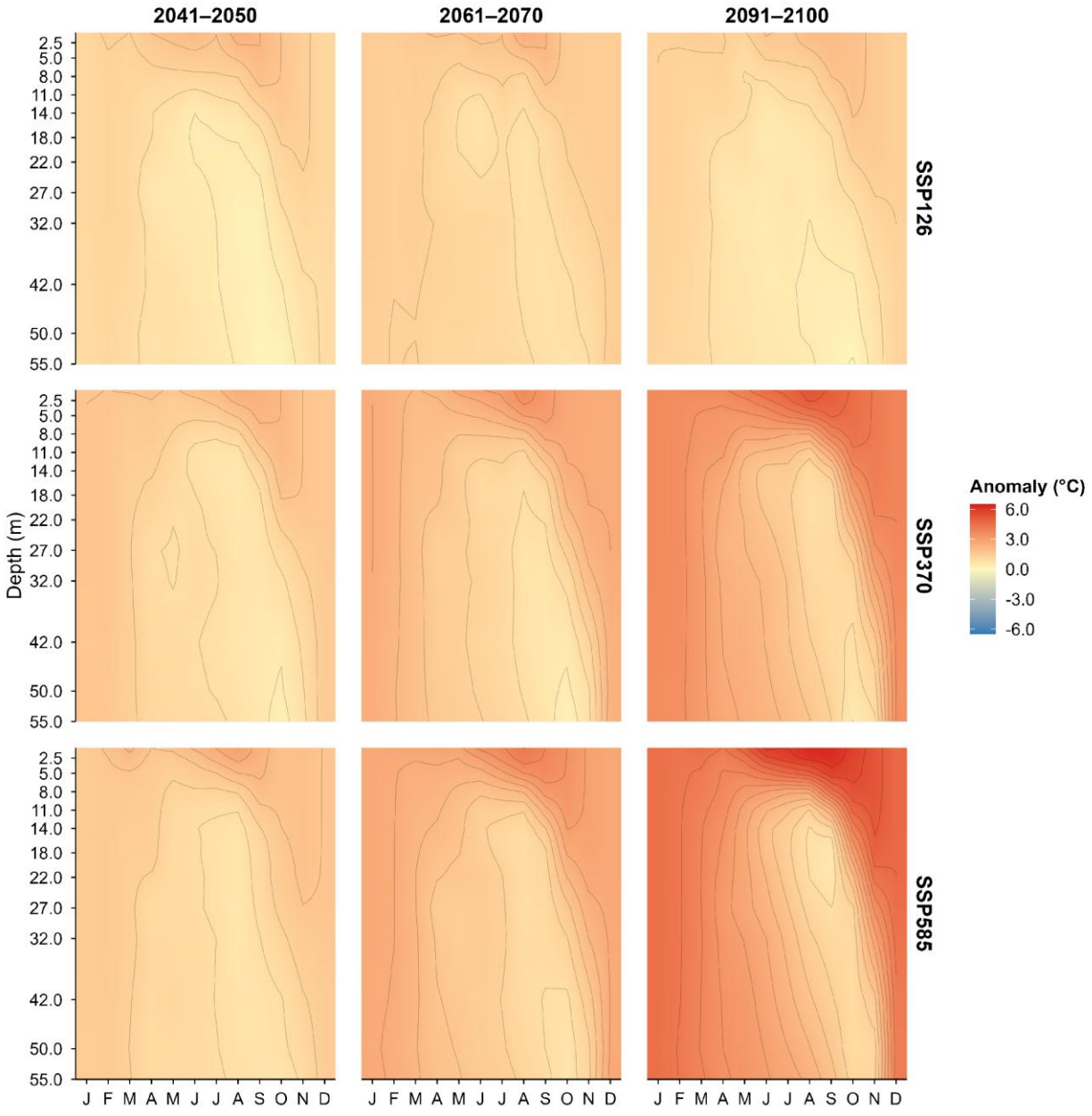


Figure 30. *Model-based anomalies of average calendar month water temperature profiles for Sau Reservoir for the SSP126, SSP370 and SSP585 scenarios during the three analysed independent future periods.*

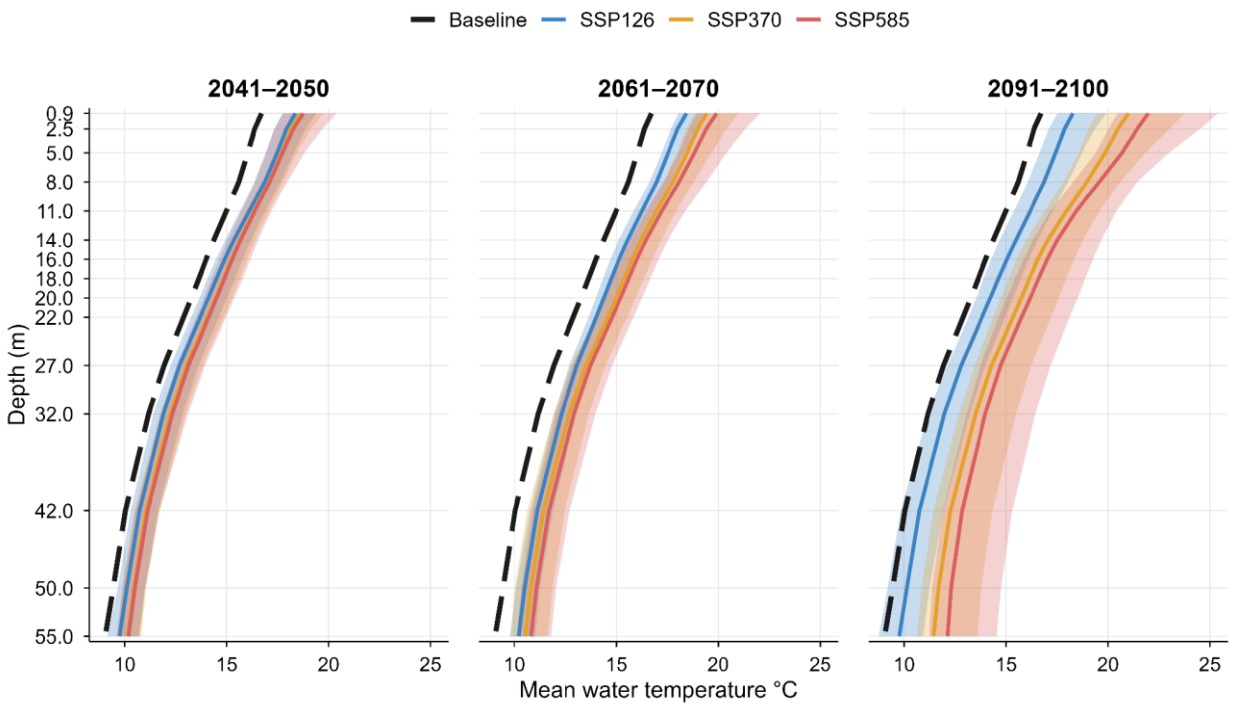


Figure 31. *Future projections of average water temperature at different depths for Sau Reservoir for the historical reference, and for the SSP126, SSP370 and SSP585 scenarios during the three analysed independent future periods. Light coloured bands denote GCM-derived uncertainty for each scenario, respectively.*

Scenario separation was most pronounced during 2091–2100. Mean surface temperature remained approximately 18.3 °C under SSP126 but increased to 21.0 °C under SSP370 and 22.0 °C under SSP585. At 20 m, the corresponding temperatures were 14.2, 15.7 and 16.2 °C, compared with a historical mean of 13.3 °C. At 55 m, mean temperatures reached 9.9 °C under SSP126, 11.5 °C under SSP370 and 12.2 °C under SSP585. The stronger surface response increased the period-mean surface-to-deep temperature difference from 7.7 °C during the historical period to 8.4 °C under SSP126, 9.5 °C under SSP370 and 9.8 °C under SSP585 by 2091–2100. The GCM ranges around the period-mean profiles also widened towards the end of the century, particularly under SSP370 and SSP585.

3.4 Future change in DOC concentrations

Future DOC responses were evaluated using annual mean surface concentrations, monthly seasonal cycles and vertical concentration profiles. Surface DOC represented 0.9 m at Lough Feeagh and the mean concentration between 0 and 5 m at Sau Reservoir.

3.4.1 Lough Feeagh

Mean surface DOC during the historical baseline was 10.5 mg C L^{-1}. Concentrations increased under every scenario and future period, although the magnitude and progression of change differed among scenarios (Figure 32 and 33). In 2041–2050, mean concentrations were 11.3 mg C L^{-1} under SSP126 and 11.1 mg C L^{-1} under both SSP370 and SSP585. The corresponding model paired anomalies were +0.7, +0.6 and +0.5 mg C L^{-1}, respectively. By 2061–2070, mean concentrations reached 11.1 mg C L^{-1} under SSP126, 11.4 mg C L^{-1} under SSP370 and 11.6 mg C L^{-1} under SSP585, corresponding to anomalies of +0.6, +0.9 and +1.0 mg C L^{-1}.

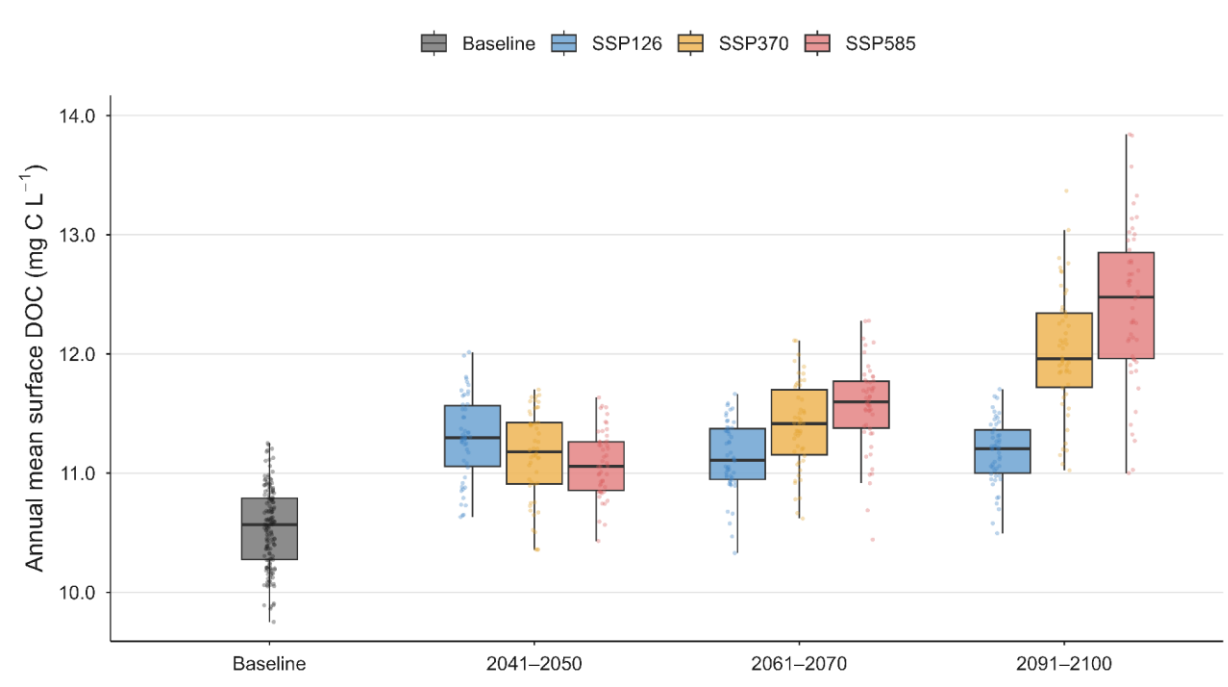


Figure 32. *Boxplot distributions of average annual surface DOC for Lough Feeagh for the baseline period, and for the SSP126, SSP370 and SSP585 scenarios during the three analysed independent future periods.*

Scenario differences became most pronounced by 2091–2100. Surface DOC remained comparatively stable under SSP126 at 11.2 mg C L^{-1}, representing an anomaly of +0.6 mg C L^{-1}. In contrast, concentrations increased to 12.0 mg C L^{-1} under SSP370 and 12.4 mg C L^{-1} under SSP585, with corresponding anomalies of +1.5 and +1.9 mg C L^{-1}. All five GCMs projected positive late century anomalies under SSP370 and SSP585. For SSP585, the individual GCM anomalies ranged from approximately +1.3 to +2.4 mg C L^{-1}, indicating greater climate model spread than under SSP126 (Figure 33).

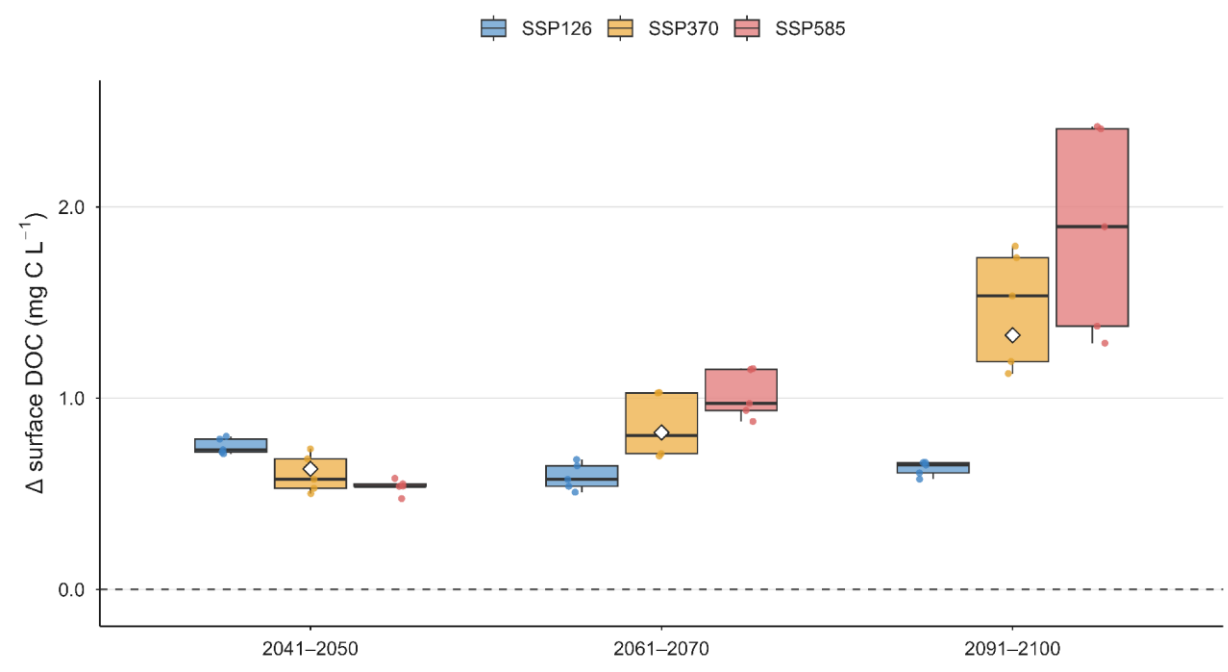


Figure 33. *Boxplot distributions of model-based anomalies of average annual surface DOC for Lough Feeagh for the baseline period, and for the SSP126, SSP370 and SSP585 scenarios during the three analysed independent future periods.*

The baseline seasonal cycle was characterised by higher concentrations during winter and autumn and lower concentrations during early summer. Monthly mean DOC decreased from 11.3 mg C L^{-1} in January to approximately 9.5 mg C L^{-1} in June and July, before increasing to 10.9 mg C L^{-1} in October (Figure 34). This seasonal pattern was retained in the future simulations, but the entire cycle generally shifted towards higher concentrations. Changes were comparatively uniform under SSP126, whereas SSP370 and SSP585 produced progressively larger autumn and winter increases. Under SSP585 in 2091–2100, ensemble mean surface DOC reached approximately 13.4 mg C L^{-1} in September and 14.0 mg C L^{-1} in October. These values were approximately 2.6 and 3.1 mg C L^{-1} above their corresponding baseline monthly means.

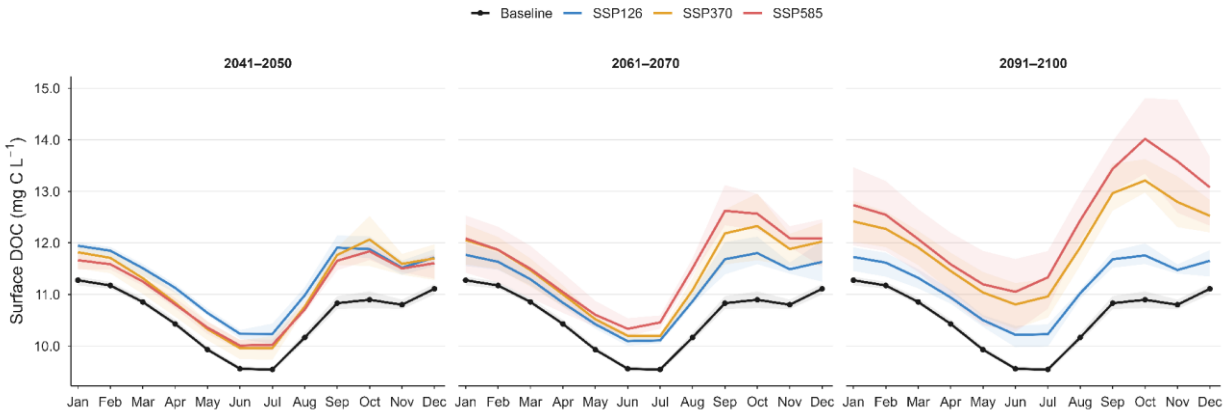


Figure 34. *Average calendar month DOC concentration value for the surface layer of Lough Feeagh for the baseline period, and for the SSP126, SSP370 and SSP585 scenarios during the three analysed independent future periods.*

Positive changes extended through most of the water column (Figures 35-37). The period mean profiles showed the largest scenario separation near the surface, although elevated concentrations persisted at greater depths. By 2091–2100, SSP370 and SSP585 produced consistently higher concentrations than the baseline throughout the modelled 42 m profile. Monthly anomalies were generally positive, with the largest increases concentrated in the upper water column during late summer and autumn. Localised areas with relatively small anomalies occurred around intermediate depths during autumn, but these did not alter the overall positive period mean response. Climate model spread also increased through time, particularly near the surface under SSP370 and SSP585 (Figure 37).

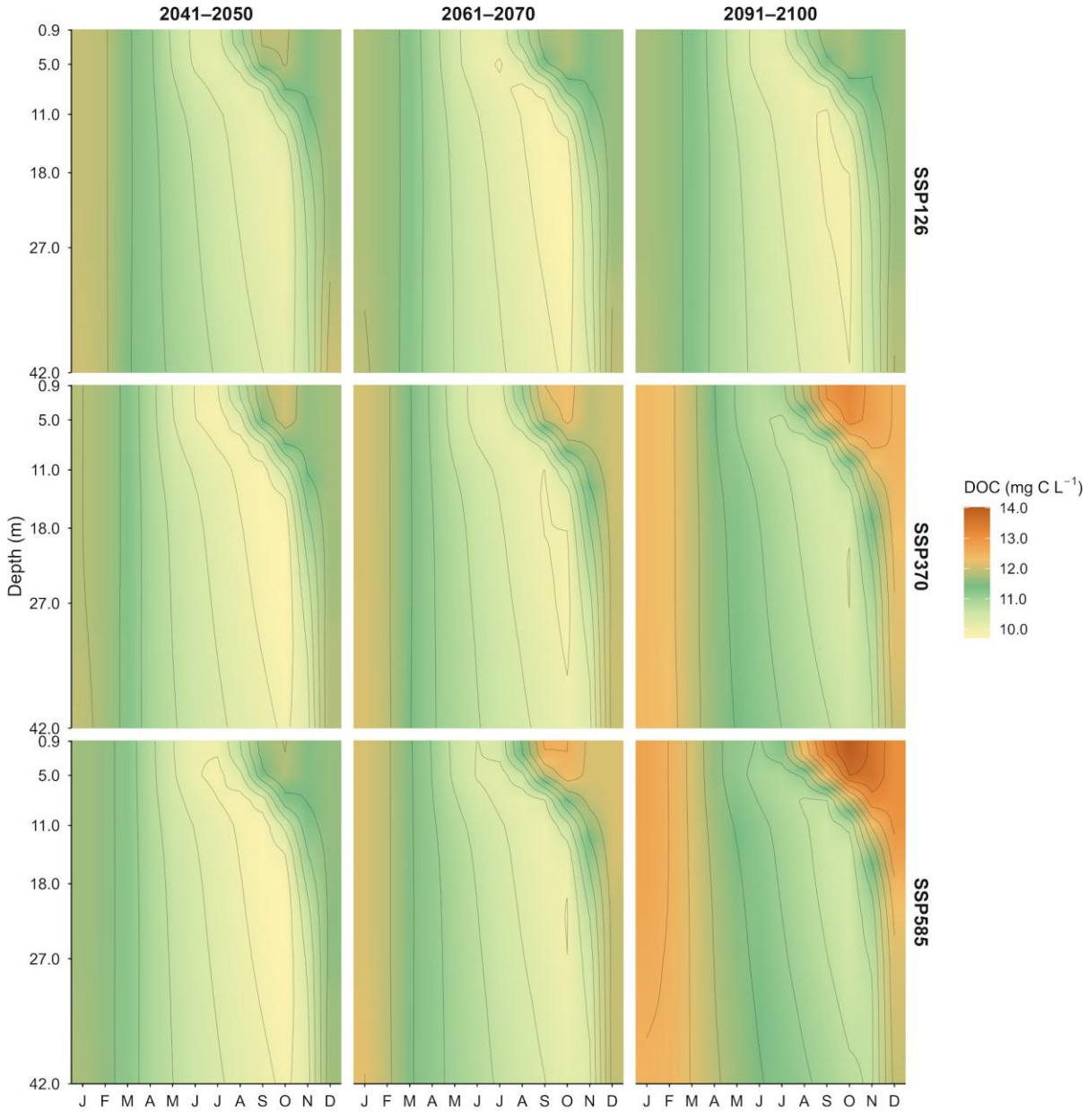


Figure 35. *Future projections of average calendar month DOC concentration profiles for Lough Feeagh for the SSP126, SSP370 and SSP585 scenarios during the three analysed independent future periods.*

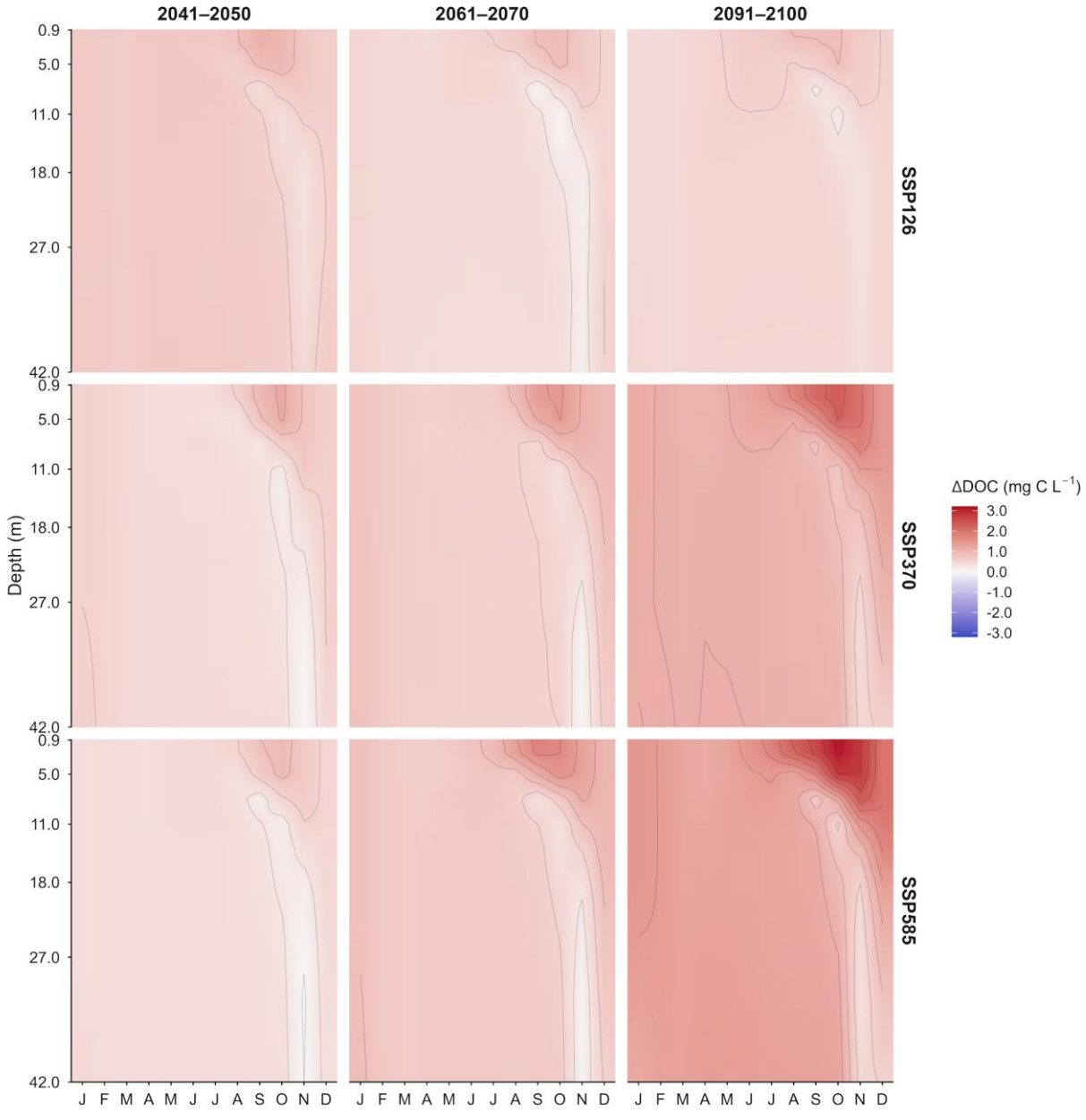


Figure 36. *Model-based anomalies of average calendar month DOC concentration profiles for Lough Feeagh for the SSP126, SSP370 and SSP585 scenarios during the three analysed independent future periods.*

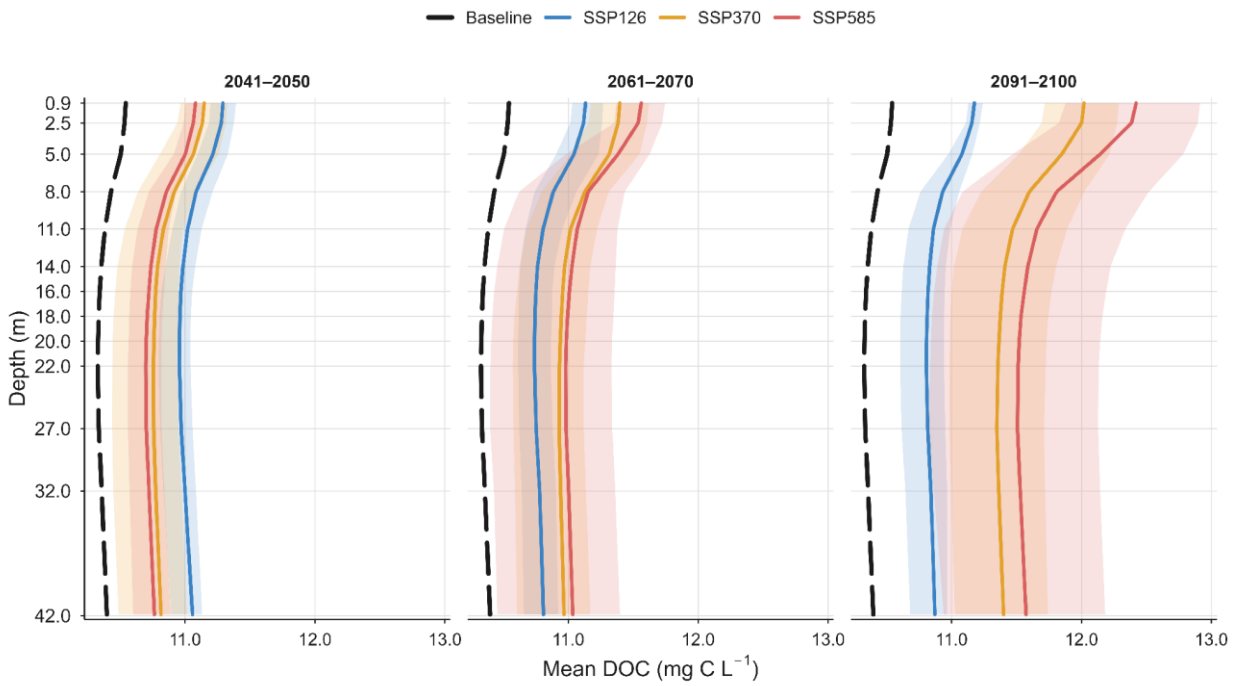


Figure 37. *Future projections of average DOC concentration at different depths for Lough Feeagh for the historical reference, and for the SSP126, SSP370 and SSP585 scenarios during the three analysed independent future periods. Light coloured bands denote GCM-derived uncertainty for each scenario, respectively.*

3.4.2 Sau Reservoir

Mean surface DOC during the historical baseline was 2.9 mg C L^{-1}. Near term changes were relatively small and varied among the five GCMs (Figures 38 and 39). In 2041–2050, mean concentrations were 3.1 mg C L^{-1} under SSP126, 3.2 mg C L^{-1} under SSP370 and 3.0 mg C L^{-1} under SSP585. These values represented ensemble mean anomalies of +0.1, +0.2 and +0.1 mg C L^{-1}, equivalent to increases of 4.4, 7.1 and 2.5%, respectively.

Surface DOC increased further under the higher forcing scenarios during the subsequent periods. In 2061–2070, mean concentrations were 3.1, 3.2 and 3.3 mg C L^{-1} under SSP126, SSP370 and SSP585, respectively. The corresponding anomalies were +0.1, +0.3 and +0.3 mg C L^{-1}. By 2091–2100, SSP126 remained close to the baseline at 3.0 mg C L^{-1}, whereas concentrations increased to 3.5 mg C L^{-1} under SSP370 and 3.9 mg C L^{-1} under SSP585. These late century changes corresponded to anomalies of +0.1, +0.5 and +1.0 mg C L^{-1}, or increases of 1.7, 17.3 and 33.3%, respectively. Climate model spread was largest under the higher forcing scenarios. Individual late century anomalies

ranged from +0.1 to +1.1 mg C L^{-1} under SSP370 and from +0.3 to +1.8 mg C L^{-1} under SSP585.

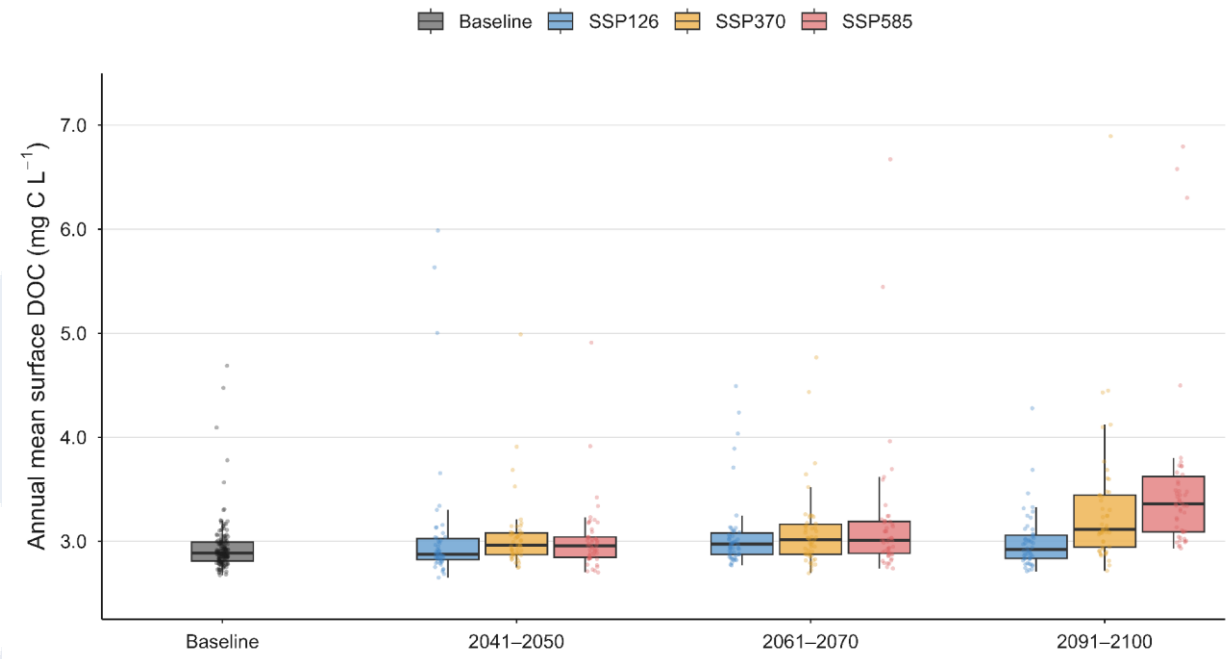


Figure 38. *Boxplot distributions of average annual surface DOC for Sau Reservoir for the baseline period, and for the SSP126, SSP370 and SSP585 scenarios during the three analysed independent future periods.*

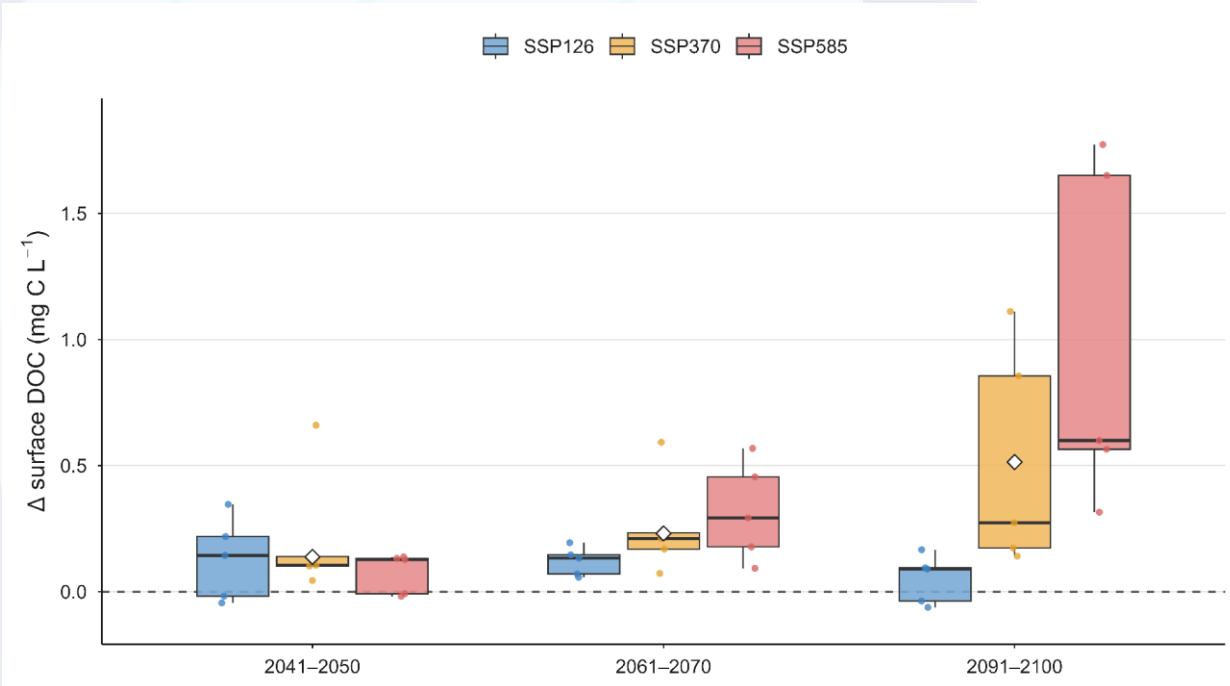


Figure 39. *Boxplot distributions of model-based anomalies of average annual surface DOC for Sau Reservoir for the baseline period, and for the SSP126, SSP370 and SSP585 scenarios during the three analysed independent future periods.*

The baseline surface seasonal cycle was comparatively weak. Monthly mean concentrations ranged from approximately 2.7 mg C L^{-1} in September to 3.3 mg C L^{-1} in April (Figure 40). This pattern remained broadly similar under SSP126, with relatively small changes throughout the year. More substantial seasonal departures developed under SSP370 and SSP585, particularly by 2091–2100. Under SSP585, surface DOC reached approximately 5.1 mg C L^{-1} in January, remained above 4.0 mg C L^{-1} during several spring and summer months and declined to approximately 3.4 mg C L^{-1} in December. The spread among GCMs was greatest during winter and early spring.

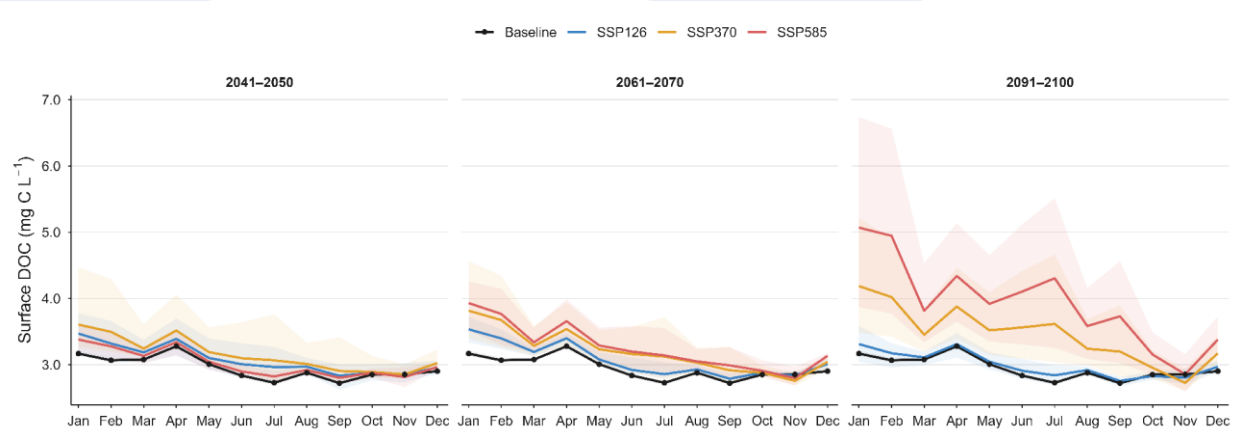


Figure 40. *Average calendar month DOC concentration value for the surface layer of Sau Reservoir for the baseline period, and for the SSP126, SSP370 and SSP585 scenarios during the three analysed independent future periods.*

The vertical DOC response at Sau was substantially larger than the corresponding surface change (Figures 41-43). Baseline period mean concentrations increased sharply below approximately 32 m and approached 18.0 mg C L^{-1} near the maximum evaluated depth of 55 m. This vertical gradient was retained in all future simulations. Changes were modest during 2041–2050, but concentrations in the deeper reservoir increased progressively under SSP370 and SSP585. By 2091–2100, period mean DOC near 55 m reached approximately 19.5 mg C L^{-1} under SSP370 and 20.8 mg C L^{-1} under SSP585, compared with relatively limited change under SSP126.

The monthly profiles showed that the largest deep-water concentrations generally occurred between July and October (Figure 41). Corresponding anomalies were concentrated below approximately 42 m and increased through time and with scenario intensity. Under SSP585 in 2091–2100, local monthly anomalies near the reservoir bed

exceeded 10.0 mg C L^{-1} during autumn (Figure 42). Smaller positive changes extended through much of the upper water column, while isolated negative anomalies occurred near the deepest layers in some near term and lower forcing simulations. The future response at Sau therefore combined relatively moderate changes in surface DOC with larger and more seasonally concentrated changes in the deeper reservoir.

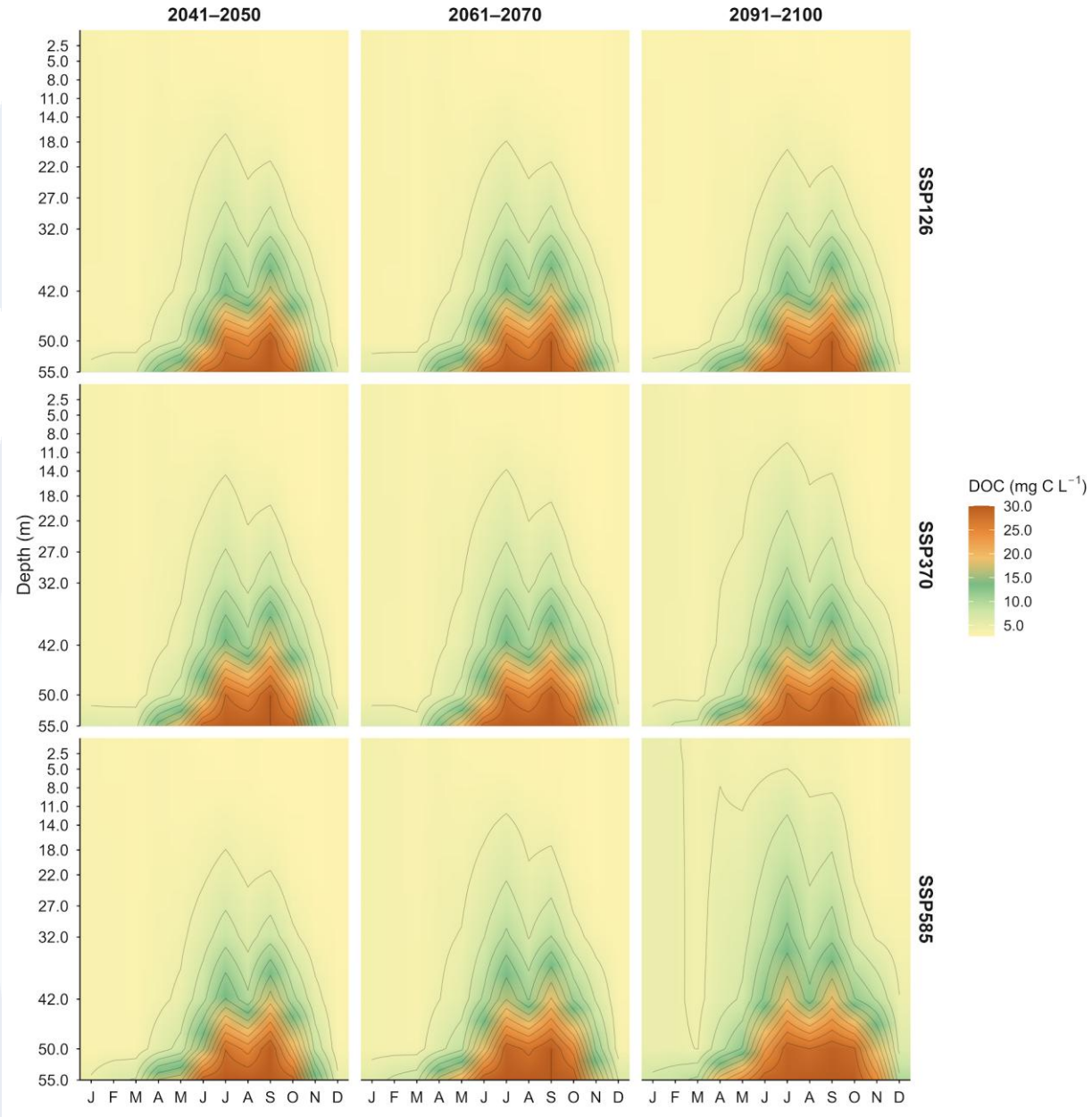


Figure 41. *Future projections of average calendar month DOC concentration profiles for Sau Reservoir for the SSP126, SSP370 and SSP585 scenarios during the three analysed independent future periods.*

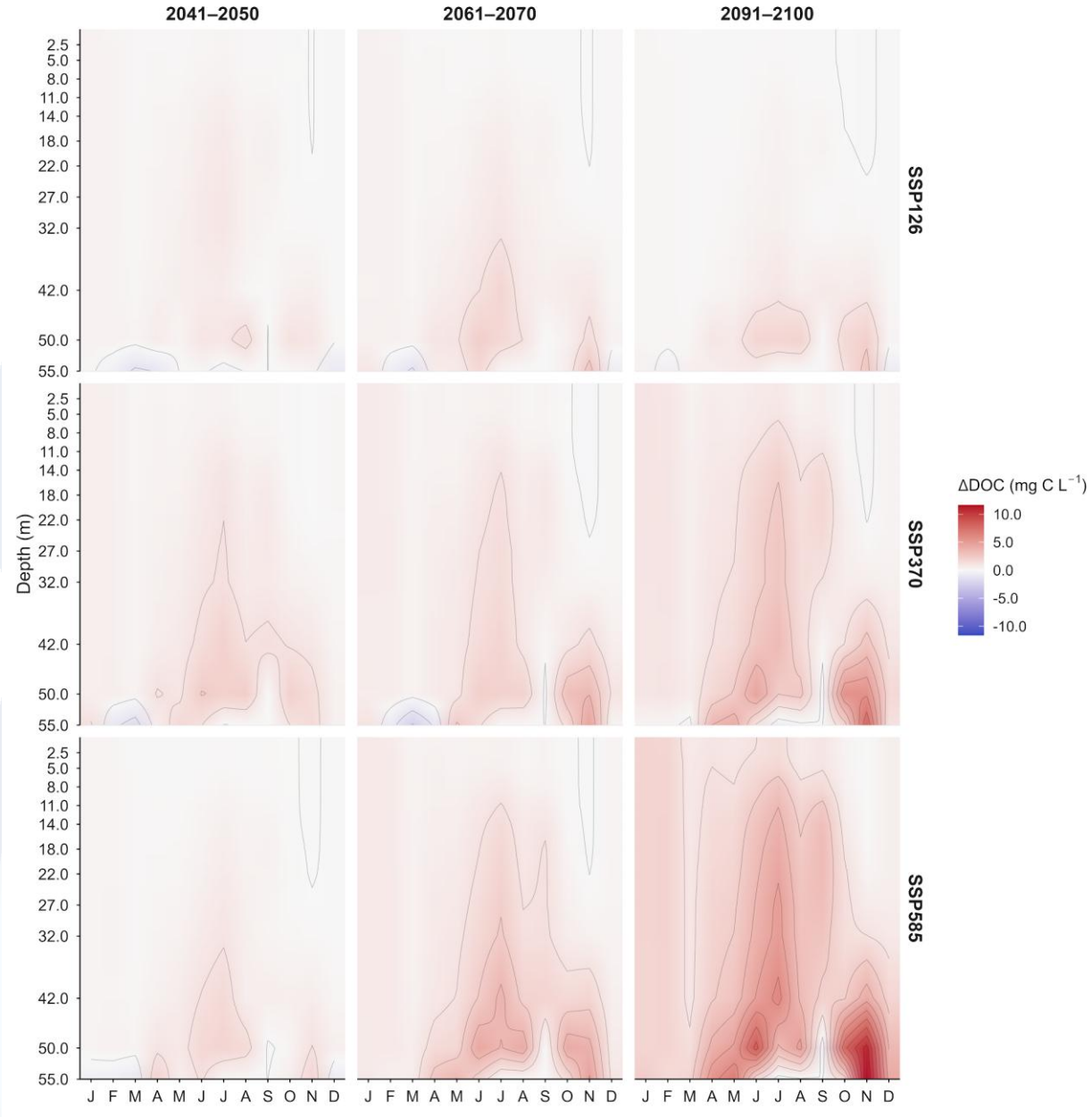


Figure 42. *Model-based anomalies of average calendar month DOC concentration profiles for Sau Reservoir for the SSP126, SSP370 and SSP585 scenarios during the three analysed independent future periods.*

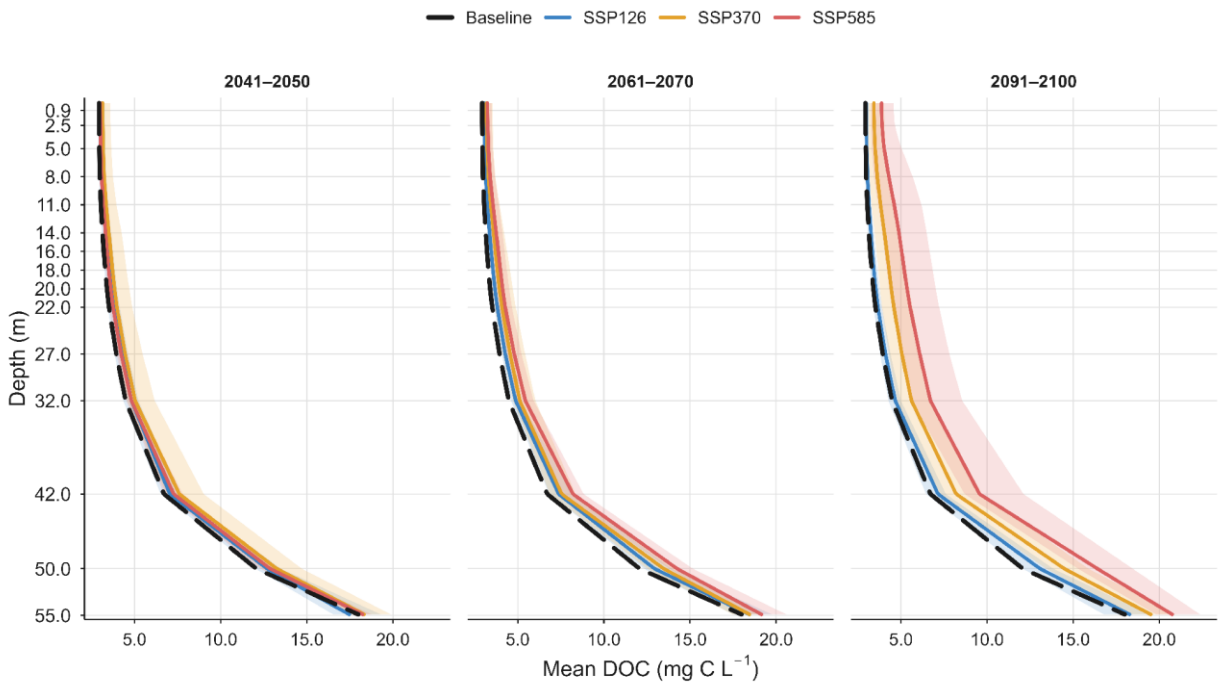


Figure 43. *Future projections of average DOC concentration at different depths for Sau Reservoir for the historical reference, and for the SSP126, SSP370 and SSP585 scenarios during the three analysed independent future periods. Light coloured bands denote GCM-derived uncertainty for each scenario, respectively.*

4. Discussion

This study applied a process-based modelling framework to two contrasting freshwater systems and examined how their thermal structure and DOC dynamics may respond to future climate conditions. Differences in calibration performance between the two sites, however, are important for interpreting the future projections. The model captured seasonal and interannual DOC variability more successfully at Feeagh, while at Sau it reproduced the broad range of surface DOC concentrations but had limited ability to match individual fluctuations. Although the hydrodynamic calibration at Sau provided a good basis for simulating thermal conditions, its DOC projections should be interpreted with caution. The projections indicated warmer conditions throughout the water column at both sites together with generally higher DOC concentrations. The magnitude and vertical distribution of these changes differed between sites, and the separation among scenarios became most evident towards the end of the century. Under SSP126, changes generally stabilised after the middle of the century. Under SSP370 and SSP585, warming and DOC enrichment continued, with the strongest responses occurring during the period from 2091 to 2100. This progression was particularly pronounced at Sau Reservoir, where the warmer and drier climate projected under the higher forcing scenarios produced a larger departure from historical conditions.

The thermal projections were among the clearest and most consistent results, and are in in line with other research on Feeagh and other freshwater systems (e.g., Mishra et al., 2011; Ayala et al., 2023; La Fuente et al., 2024). Mean water temperature increased at almost every evaluated depth, although surface and upper water responses were generally larger than those in deep water. By the end of the century under SSP585, mean surface temperature increased by approximately 3 °C at Feeagh and 5 °C at Sau, while the corresponding increases in deep water were approximately 1 and 3 °C. The contrast between surface and deep warming indicates that future change will not involve a uniform increase in water temperature across all depths. This will likely modify heat storage, the vertical distribution of temperature and the seasonal development of stratification (Mishra et al., 2011; Ayala et al., 2023; Atton Beckmann et al., 2026). These changes can also influence mixing, oxygen availability, evaporation and the timing of biological activity, with potential consequences for primary production, greenhouse gas

dynamics (e.g. methane emissions), habitat suitability and the occurrence of algal blooms (Woolway et al., 2020, 2022; Jansen et al., 2022; La Fuente et al., 2024). The larger warming response projected for Sau is consistent with the stronger atmospheric warming and declining precipitation projected for its catchment. Changes in water level and reservoir operations could also influence this response, but their future variability was simplified in the simulations and therefore cannot explain the differences projected here.

DOC also increased under most combinations of site, period and scenario, although its response was less uniform than that of temperature. At Feeagh, the historical mean surface concentration of approximately 10.5 mg C L^{-1} increased progressively under SSP370 and SSP585, reaching approximately 12.0 and 12.4 mg C L^{-1}, respectively, by the end of the century. Increases were especially evident during late summer and autumn, when the simulations also showed greater separation among GCMs. This is in line with related studies at this site that have focused on the catchment rather than the lake (Doyle et al., 2019; Paíz et al., 2025a). At Sau, the historical surface mean was lower, at approximately 2.9 mg C L^{-1}, and changes remained modest under SSP126. Larger increases emerged under SSP370 and SSP585, reaching approximately 3.5 and 3.9 mg C L^{-1} by the end of the century.

The contrasting DOC responses reflect differences in climate exposure, catchment characteristics, hydrological pathways and internal processing (Mercado-Bettín et al., 2026). Feeagh receives a substantial proportion of its organic matter from peat dominated catchments, where changes in soil moisture, temperature and runoff have been identified as being very important for the mobilisation and delivery of terrestrial carbon (Jennings et al., 2020; Ryder et al., 2014; Doyle et al., 2023; Paíz et al., 2025a). The projected seasonal enhancement of DOC during late summer and autumn may therefore represent the combined influence of warmer conditions, altered flow pathways and subsequent transport during wetter periods. At Sau, surface DOC remained within a comparatively narrow range during the first two future periods, but increased more strongly under the warmer and drier late century scenarios. The simulations suggest that changes in inflow supply, reservoir storage, residence conditions and internal redistribution may interact to shape this response (Marcé et al., 2021). These mechanisms cannot be separated completely within the present analysis, but their

combined representation provides a coherent basis for assessing how climate driven changes may propagate from the catchment to the source water body.

An important contribution of the framework is the explicit connection between physical lake and reservoir dynamics and DOC processing (Hounshell et al., 2026). Data driven approaches (e.g., machine learning) can provide skilful predictions when observations are abundant and future conditions remain close to those represented in the training data (Feigl et al., 2021; Sullivan, 2022; Zhu et al., 2022). However, their interpretation becomes more difficult when relationships change beyond the observed range (Beven, 2020). In contrast, the coupled GLM and AED framework represents water balance, heat exchange, mixing, inflow delivery and internal DOC transformations within a common structure (Hipsey et al., 2019). This does not remove model uncertainty, but it allows projected changes to be examined in relation to the processes that generated them (Beven, 2009, 2020; Bodner et al., 2021). The approach is therefore particularly useful for scenario analysis (Moore et al., 2008; Clark et al., 2010; Ledesma et al., 2012; Nissan et al., 2019), where the objective is to evaluate broad, internally consistent responses rather than reproduce the precise timing of individual future events.

The vertical DOC results at Sau require particular attention. The simulations produced comparatively high DOC concentrations near the bottom of the reservoir, especially during summer and autumn and under SSP370 and SSP585 towards the end of the century. This pattern was much stronger than the changes simulated at the surface and was not entirely supported by the available profile observations. It may partly reflect the accumulation and processing of organic matter near the sediment boundary (Downing et al., 2008; Kim et al., 2009), including sediment DOC release, GHG dynamics (e.g., methane release), and the delivery of material from a large drainage area (Zhang et al., 2023; Ma et al., 2024; Bodmer et al., 2025). It may also indicate limitations in the representation of sediment exchange, oxygen dependent processing or vertical transport (Bodmer et al., 2025; Eckland et al., 2026; Hounshell et al., 2026). Because the Sau calibration was deliberately focused on source water conditions from 0 to 5 m, the surface projections provide the most defensible basis for interpretation. The deep water results remain informative as an indication of possible internal accumulation, but their absolute magnitude should not be treated as a validated forecast.

Overall, the simulations describe a future in which both freshwater systems become warmer and, under most scenarios, more enriched in DOC (and therefore in DOM). The differences among scenarios were relatively limited during the first future period but became substantial by the end of the century. This delayed divergence is important for management because it indicates that decisions affecting future emissions and catchment resilience can materially influence the magnitude of long-term source water change (Kritzberg et al., 2020; Anderson et al., 2023). It also suggests that adaptation should not be based only on shifts in mean conditions. Changes in seasonality, climate model spread and the occurrence of high DOC periods may be also important for water treatment and operational planning.

4.1 Implications for water management

The projected increases in DOC have direct relevance for drinking water management because DOC represents a substantial component of DOM, an important DBP precursor. Nevertheless, DOC concentrations alone do not determine DBP formation. Molecular composition, reactivity, treatment conditions, disinfectant type and contact time also regulate the resulting DBP concentrations (Siddique et al., 2022; Pedregal-Montes et al., 2024; Costa et al., 2026). The projections should therefore be interpreted as an indication of changing precursor pressure. The combined increase in source water temperature and DOC suggests that treatment systems may face more demanding and variable conditions, particularly under SSP370 and SSP585 towards the end of the century.

The scenario comparison provides a clear management signal. SSP126 consistently produced the smallest late century changes and, at both sites, a narrower departure from historical conditions. SSP370 and SSP585 generated larger increases in temperature and DOC, together with greater variation among GCMs. Mitigation that limits the magnitude of global warming would therefore reduce the pressure placed on both catchments and treatment systems (Woolway et al., 2020; Nissan et al., 2019; Dahal et al., 2025). At the same time, adaptation remains necessary because measurable changes were projected even under SSP126. Management strategies should consequently combine long term emission reduction with site specific actions that improve source water resilience and treatment flexibility.

At Feeagh, catchment protection is especially important because the lake is closely connected to organic soils and peatland drainage (Ryder et al., 2014; Doyle et al., 2019; Fenner et al., 2021; Doyle et al., 2023). Measures that protect soil carbon, reduce erosion and limit rapid mobilisation of organic matter could help moderate future DOC delivery (Paíz et al., 2025a). Relevant actions include restoring or blocking artificial peat drains, maintaining riparian buffers, avoiding disturbance of organic soils and directing land use controls towards areas with a disproportionate influence on inflow water quality (Kritzberg et al., 2020). The projected increase during late summer and autumn also supports closer monitoring during periods when warm and relatively dry conditions are followed by renewed runoff.

At Sau, management must account for both catchment inputs and reservoir operation. Source protection across the Ter catchment can reduce the delivery of organic matter and associated contaminants (Marcé et al., 2008), while monitoring within the reservoir can identify changes in the vertical distribution of DOC (Marcé et al., 2016). Operational flexibility may offer an additional response because intake depth, withdrawal timing and gate operation can be used as a means to determine which parts of the water column contribute to supplied water. However, the future operational series used in this study were based on internally consistent assumptions based on historical behaviour and simulated water availability. Consequently, the forecasts do not include projections of future management policy. The results can therefore support evaluation of possible operating conditions, but specific changes to gate or intake practice should be tested through dedicated operational scenarios that consider infrastructure, demand and water level constraints.

In addition, treatment adaptation could focus on organic matter removal before disinfection rather than relying on increased disinfectant application (Sohn and Kim, 2002; Alver et al., 2025). Depending on the existing treatment train, this may involve optimisation of coagulation, adsorption or other pretreatment processes, together with routine assessment of DOC character and DBP formation potential (Köhler et al., 2016; Siddique et al., 2022; Valenti-Quiroga et al., 2024). The seasonal results indicate that adaptation can be phased rather than applied uniformly throughout the year. Monitoring thresholds based on DOC, flow, water temperature and reservoir storage could be used

to intensify treatment or alter abstraction strategies when source water conditions begin to depart from their normal range (Howard et al., 2026). Such an approach would be particularly valuable during drought recovery, high runoff events or persistent warm periods, when the interaction among catchment mobilisation, residence time and processing within the water body may produce rapid changes (Warner and Saros, 2019; Xiao et al., 2024).

The increasing spread among climate models towards the end of the century also argues for adaptive rather than deterministic planning (Beven, 2009; Bodner et al., 2021). Infrastructure and operating procedures should be robust across a range of possible futures, including conditions that are warmer, drier or more variable than the ensemble mean. Measures that provide benefits under multiple scenarios, including catchment conservation, improved monitoring, treatment flexibility and contingency planning are therefore preferable to actions designed around a single projection (Beven, 2009; Hattermann et al., 2018; Nissan et al., 2019). Periodic reassessment will be important as new observations, climate projections and operational information are incorporated.

4.2 Modelling ahead

The contrasting calibration results at the two sites illustrate how observation type and model structure influence confidence in future projections. At Feeagh, high frequency sensor derived DOC observations provided a temporally consistent record that captured seasonal and interannual variability. The calibrated model reproduced a meaningful proportion of this variability at both daily and monthly scales. At Sau, the observational record was much longer and included valuable laboratory measurements, but it was assembled across several decades and reflected changes in sampling frequency, profile depth, equipment and possibly analytical practice. The final calibration reproduced the broad surface DOC magnitude and temporal envelope, but its ability to match individual fluctuations remained limited. Future DOC results at Sau should therefore be interpreted primarily as changes in broad distributions, seasonality and period means rather than precise temporal forecasts. The successful hydrodynamic calibration at Sau provides an important foundation for this interpretation (Clark et al., 2009; Hounshell et al., 2026). Despite the challenges associated with DOC, the model reproduced the dominant thermal cycle and vertical structure across a long observational record. This supports the

use of simulated temperature, stratification and mixing as physically coherent drivers of future DOC dynamics (Hounshell et al., 2026). It also shows that a long but irregular observational dataset can be highly informative when its depth structure and temporal alignment are handled explicitly. For water quality variables, however, additional continuous monitoring would substantially improve the separation of catchment signals, reservoir processing and operational effects.

The local DOC parameter ensembles used during calibration represented a focused assessment around the best performing solution. At both sites, and especially at Sau, the ensemble envelope did not contain many of the observed excursions. This indicates that variation in the four calibrated DOC quantities alone could not explain the complete observational range. Remaining differences may arise from unrepresented boundary variability, observation uncertainty, model structure or processes that were held fixed (Beven and Binley, 1992; Beven and Freer, 2001; Beven, 2009; Paíz et al., 2025a). The local ensemble was not propagated into the future simulations. Instead, the best GLM and AED parameter configurations were retained, and future uncertainty was represented by the five climate models and their associated meteorological and derived boundary conditions, an inclusion that generally drives most of the uncertainty in climate change impact assessments (Hattermann et al., 2018; Kundzewicz et al., 2018; Paíz et al., 2025a). Future work could extend this framework by propagating accepted parameter sets through the climate ensemble. Such an analysis would allow climate forcing and parameter contributions to be compared directly (Paíz et al., 2025a), although the computational demand would increase. Other uncertainty sources should also be examined, including bias correction, spatial downscaling, catchment model structure, land use change, future water demand and reservoir operation (Kundzewicz et al., 2018; Her et al., 2019b). An ensemble of alternative process-based models (La Fuente et al., 2024) could further reveal whether projected responses depend on a particular representation of mixing, sediment exchange or DOC transformations. These additions would be most valuable if they were designed to preserve transparent links between assumptions, processes and outputs (Lofton et al., 2023).

Improved monitoring would provide an equally important advance. Continuous optical sensors, supported by regular laboratory analysis, can capture rapid DOC changes that

are easily missed by intermittent sampling (Marcé et al., 2016; Jennings et al., 2020; Mercado-Bettín et al., 2026). At Feeagh, this type of record supported stronger calibration despite covering a shorter period. At Sau, coordinated monitoring of inflow DOC, surface source water, deep water, oxygen and operational withdrawals would help determine whether the simulated deep accumulation occurs and which processes regulate it. Measurements of DOM composition and reactivity would also allow future modelling to move beyond DOC concentration and assess changes in treatment relevance and DBP formation potential more directly.

Finally, it is arguable that the process-based modelling workflow implemented here is transferable because it combines site observations with globally available climate data and explicitly derived boundary conditions. Its value lies in providing a coherent representation of how catchment forcing, physical dynamics and water quality may change together. The results indicate potential trajectories and identify the conditions, seasons and parts of the water column in which change may be most pronounced in terms of thermal structure and water quality (here DOC). With careful interpretation, this framework can support assessments of drinking water vulnerability and adaptation across different lake and reservoir ecosystems.

5. Conclusions

This deliverable demonstrates the feasibility of using a process-based modelling workflow to reproduce historical lake/reservoir thermal and DOC dynamics, and to project their broad evolution under alternative climate change scenarios. The application of GLM-AED to Lough Feeagh and Sau Reservoir showed that such a framework can be adapted to freshwater systems with contrasting climatic, catchment, morphometric and operational characteristics.

The simulations projected progressive warming at both systems, with the largest changes generally occurring towards the end of the century under SSP370 and SSP585. These changes extended through the water column but varied with depth, season and site. Surface DOC concentrations also generally increased relative to the historical baseline, particularly under the higher forcing scenarios and during the period 2091–2100. The magnitude, seasonality and vertical distribution of these responses differed between the lake and reservoir and should be interpreted alongside the uncertainty associated with both the underlying model assumptions and the future climate inputs employed in this study. The spread across simulations driven by different climate models illustrates a range of potential outcomes within the selected 5-GCM ensemble. Our findings also highlight the value of local water quality monitoring and the importance of hydrodynamic conditions, catchment inputs and reservoir operations in shaping estimations in future DOC dynamics. This information can support the evaluation of adaptation and mitigation strategies at these and potentially other sites, contributing to more resilient drinking water management and improved anticipation of conditions relevant to disinfection by-product formation and subsequent human exposure.

References

Adler, T., Underwood, K.L., Rizzo, D.M., Harpold, A., Sterle, G., Li, L., Wen, H., Stinson, L., Bristol, C., Stewart, B., Lini, A., Perdrial, N., Perdrial, J.N., 2021. Drivers of Dissolved Organic Carbon Mobilization From Forested Headwater Catchments: A Multi Scaled Approach. Frontiers in Water 3.

Alver, A., Baştürk, E., Kılıç, A., Altınışık Tağaç, A., 2025. Catalyst-driven strategies for organic matter and disinfection byproduct removal: Comparing adsorption, ozonation, and catalytic ozonation. Journal of Environmental Chemical Engineering 13, 118714. https://doi.org/10.1016/j.jece.2025.118714

Anderson, L.E., DeMont, I., Dunnington, D.D., Bjorndahl, P., Redden, D.J., Brophy, M.J., Gagnon, G.A., 2023. A review of long-term change in surface water natural organic matter concentration in the northern hemisphere and the implications for drinking water treatment. Science of The Total Environment 858, 159699. https://doi.org/10.1016/j.scitotenv.2022.159699

Atton Beckmann, D., Werther, M., Shatwell, T., Spyrakos, E., Hunter, P., Jones, I.D., 2026. How climate change erodes short-term lake-temperature predictability: Informing climate resilient lake forecasting. Water Research X 30, 100457. https://doi.org/10.1016/j.wroa.2025.100457

Ayala, A.I., Mesman, J.P., Jones, I.D., De Eyto, E., Jennings, E., Goyette, S., Pierson, D.C., 2023. Climate Change Impacts on Surface Heat Fluxes in a Deep Monomictic Lake. JGR Atmospheres 128, e2022JD038355. https://doi.org/10.1029/2022JD038355

Ayala, A.I., Moras, S., Pierson, D.C., 2020. Simulations of future changes in thermal structure of Lake Erken: proof of concept for ISIMIP2b lake sector local simulation strategy. Hydrology and Earth System Sciences 24, 3311–3330. https://doi.org/10.5194/hess-24-3311-2020

Beven, K., 2020. Deep learning, hydrological processes and the uniqueness of place. Hydrological Processes 34, 3608–3613. https://doi.org/10.1002/hyp.13805

Beven, K., Binley, A., 1992. The future of distributed models: Model calibration and uncertainty prediction. Hydrological Processes 6, 279–298. https://doi.org/10.1002/hyp.3360060305

Beven, K., Freer, J., 2001. Equifinality, data assimilation, and uncertainty estimation in mechanistic modelling of complex environmental systems using the GLUE methodology. Journal of Hydrology 249, 11–29. https://doi.org/10.1016/S0022-1694(01)00421-8

Beven, K.J., 2009. Environmental modelling : an uncertain future? : an introduction to techniques for uncertainty estimation in environmental prediction / Keith Beven. Routledge, London ;

Beyer, R., Krapp, M., Manica, A., 2020. An empirical evaluation of bias correction methods for palaeoclimate simulations. Climate of the Past 16, 1493–1508. https://doi.org/10.5194/cp-16-1493-2020

Blaurock, K., Beudert, B., Gilfedder, B.S., Fleckenstein, J.H., Peiffer, S., Hopp, L., 2021. Low hydrological connectivity after summer drought inhibits DOC export in a forested headwater catchment. Hydrology and Earth System Sciences 25, 5133–5151. https://doi.org/10.5194/hess-25-5133-2021

Bodmer, P., Bors, C., Liu, L., Lorke, A., 2025. Large sediment methane production potential in reservoirs compared to lakes and rivers. Limnology and Oceanography 70, 1561–1574. https://doi.org/10.1002/lno.70063

Bodner, K., Rauen Firkowski, C., Bennett, J.R., Brookson, C., Dietze, M., Green, S., Hughes, J., Kerr, J., Kunegel-Lion, M., Leroux, S.J., McIntire, E., Molnár, P.K., Simpkins, C., Tekwa, E., Watts, A., Fortin, M., 2021. Bridging the divide between ecological forecasts and environmental decision making. Ecosphere 12. https://doi.org/10.1002/ecs2.3869

Bruce, L.C., Frassl, M.A., Arhonditsis, G.B., Gal, G., Hamilton, D.P., Hanson, P.C., Hetherington, A.L., Melack, J.M., Read, J.S., Rinke, K., Rigosi, A., Trolle, D., Winslow, L., Adrian, R., Ayala, A.I., Bocaniov, S.A., Boehrer, B., Boon, C., Brookes, J.D., Bueche, T., Busch, B.D., Copetti, D., Cortés, A., De Eyto, E., Elliott, J.A., Gallina, N., Gilboa, Y., Guyennon, N., Huang, L., Kerimoglu, O., Lenters, J.D., MacIntyre, S., Makler-Pick, V., McBride, C.G., Moreira, S., Özkundakci, D., Pilotti, M., Rueda, F.J., Rusak, J.A., Samal, N.R., Schmid, M., Shatwell, T., Snorthheim, C., Soulignac, F., Valerio, G., Van Der Linden, L., Vetter, M., Vinçon-Leite, B., Wang, J., Weber, M., Wickramaratne, C., Woolway, R.I., Yao, H., Hipsey, M.R., 2018. A multi-lake comparative analysis of the General Lake Model (GLM): Stress-testing across a global observatory network. Environmental Modelling & Software 102, 274–291. https://doi.org/10.1016/j.envsoft.2017.11.016

Carey, C.C., Woelmer, W.M., Lofton, M.E., Figueiredo, R.J., Bookout, B.J., Corrigan, R.S., Daneshmand, V., Hounshell, A.G., Howard, D.W., Lewis, A.S.L., McClure, R.P., Wander, H.L., Ward, N.K., Thomas, R.Q., 2022. Advancing lake and reservoir water quality management with near-term, iterative ecological forecasting. Inland Waters 12, 107–120. https://doi.org/10.1080/20442041.2020.1816421

Chen, X., Lee, R.M., Dwivedi, D., Son, K., Fang, Y., Zhang, X., Graham, E., Stegen, J., Fisher, J.B., Moulton, D., Scheibe, T.D., 2021. Integrating field observations and process-based modeling to predict watershed water quality under environmental perturbations. Journal of Hydrology 602, 125762. https://doi.org/10.1016/j.jhydrol.2020.125762

Clark, J.M., Ashley, D., Wagner, M., Chapman, P.J., Lane, S.N., Evans, C.D., Heathwaite, A.L., 2009. Increased temperature sensitivity of net DOC production from ombrotrophic peat due to water table draw-down. Global Change Biology 15, 794–807. https://doi.org/10.1111/j.1365-2486.2008.01683.x

Clark, J.M., Bottrell, S.H., Evans, C.D., Monteith, D.T., Bartlett, R., Rose, R., Newton, R.J., Chapman, P.J., 2010. The importance of the relationship between scale and process in understanding long-term DOC dynamics. Science of The Total Environment 408, 2768–2775. https://doi.org/10.1016/j.scitotenv.2010.02.046

Costa, B., Morais, P.V., Batalha, M., Maniam, K.K., Paul, S., Meilmann, D., Durães, L., Martins, R., 2026. Water quality controls on toxic DBPs: A global multivariate assessment of THMs, HAAs, and HANs. Journal of Hazardous Materials 509, 142041. https://doi.org/10.1016/j.jhazmat.2026.142041

Cuddington, K., Fortin, M.-J., Gerber, L.R., Hastings, A., Liebhold, A., O'Connor, M., Ray, C., 2013. Process-based models are required to manage ecological systems in a changing world. Ecosphere 4, art20. https://doi.org/10.1890/ES12-00178.1

Dahal, D., Bhattarai, N., Silwal, A., Shrestha, S., Shrestha, B., Poudel, B., Kalra, A., 2025. A Review on Climate Change Impacts on Freshwater Systems and Ecosystem Resilience. Water 17, 3052. https://doi.org/10.3390/w17213052

DeMont, I., Stoddart, A.K., Gagnon, G.A., 2021. Assessing strategies to improve the efficacy and efficiency of direct filtration plants facing changes in source water quality from anthropogenic and climatic pressures. Journal of Water Process Engineering 39, 101689. https://doi.org/10.1016/j.jwpe.2020.101689

Diana, M., Felipe-Sotelo, M., Bond, T., 2019. Disinfection byproducts potentially responsible for the association between chlorinated drinking water and bladder cancer: A review. Water Research 162, 492–504. https://doi.org/10.1016/j.watres.2019.07.014

Dong, H., Zhang, S., Lin, J., Zhu, B., 2021. Responses of soil microbial biomass carbon and dissolved organic carbon to drying-rewetting cycles: A meta-analysis. CATENA 207, 105610. https://doi.org/10.1016/j.catena.2021.105610

Downing, B.D., Bergamaschi, B.A., Evans, D.G., Boss, E., 2008. Assessing contribution of DOC from sediments to a drinking-water reservoir using optical profiling. Lake and Reservoir Management 24, 381–391. https://doi.org/10.1080/07438140809354848

Doyle, B.C., de Eyto, E., Dillane, M., Poole, R., McCarthy, V., Ryder, E., Jennings, E., 2019. Synchrony in catchment stream colour levels is driven by both local and regional climate. Biogeosciences 16, 1053–1071. https://doi.org/10.5194/bg-16-1053-2019

Doyle, B.C., De Eyto, E., McCarthy, V., Dillane, M., Jennings, E., 2023. The organic carbon budget of an oligotrophic temperate peatland lake. Limnology & Oceanography 68, 544–556. https://doi.org/10.1002/lno.12292

Du, J., Deng, G., 2022. How Should a Numerical Weather Prediction Be Used: Full Field or Anomaly? A Conceptual Demonstration with a Lorenz Model. Atmosphere 13, 1487. https://doi.org/10.3390/atmos13091487

Eckland, A.C., Foster, M.A., Hurst, A.A., Beyene, M.T., Overeem, I., 2026. Reservoir sedimentation diminishes water storage and coastal delta resiliency. Nat Commun. https://doi.org/10.1038/s41467-026-76986-3

Evans, C.D., Chapman, P.J., Clark, J.M., Monteith, D.T., Cresser, M.S., 2006. Alternative explanations for rising dissolved organic carbon export from organic soils. Global Change Biology 12, 2044–2053. https://doi.org/10.1111/j.1365-2486.2006.01241.x

Evans, C.D., Monteith, D.T., Cooper, D.M., 2005. Long-term increases in surface water dissolved organic carbon: Observations, possible causes and environmental impacts. Environmental Pollution, Recovery from acidificationin the UK: Evidence from 15 years of acid waters monitoring 137, 55–71. https://doi.org/10.1016/j.envpol.2004.12.031

Feigl, M., Lebiedzinski, K., Herrnegger, M., Schulz, K., 2021. Machine-learning methods for stream water temperature prediction. Hydrology and Earth System Sciences 25, 2951–2977. https://doi.org/10.5194/hess-25-2951-2021

Fenner, N., Meadham, J., Jones, T., Hayes, F., Freeman, C., 2021. Effects of Climate Change on Peatland Reservoirs: A DOC Perspective. Global Biogeochemical Cycles 35, e2021GB006992. https://doi.org/10.1029/2021GB006992

Flem, B., Reimann, C., Birke, M., Banks, D., Filzmoser, P., Frengstad, B., 2015. Inorganic chemical quality of European tap-water: 2. Geographical distribution. Applied Geochemistry 59, 211–224. https://doi.org/10.1016/j.apgeochem.2015.01.016

Franklin, H.M., Doederer, K., Neale, P.A., Hayton, J.B., Fisher, P., Maxwell, P., Carroll, A.R., Burford, M.A., Leusch, F.D.L., 2021. Terrestrial dissolved organic matter source affects disinfection by-product formation during water treatment and subsequent toxicity. Environmental Pollution 283, 117232. https://doi.org/10.1016/j.envpol.2021.117232

Gonsior, M., Schmitt-Kopplin, P., Bastviken, D., 2013. Depth-dependent molecular composition and photo-reactivity of dissolved organic matter in a boreal lake under winter and summer conditions. Biogeosciences 10, 6945–6956. https://doi.org/10.5194/bg-10-6945-2013

Gonsior, M., Schmitt-Kopplin, P., Stavklint, H., Richardson, S.D., Hertkorn, N., Bastviken, D., 2014. Changes in Dissolved Organic Matter during the Treatment Processes of a Drinking Water Plant in Sweden and Formation of Previously Unknown Disinfection Byproducts. Environ. Sci. Technol. 48, 12714–12722. https://doi.org/10.1021/es504349p

Haith, D.A., Shoemaker, L.L., 1987. Generalized Watershed Loading Functions for Stream Flow Nutrients1. JAWRA Journal of the American Water Resources Association 23, 471–478. https://doi.org/10.1111/j.1752-1688.1987.tb00825.x

Hattermann, F.F., Vetter, T., Breuer, L., Su, B., Daggupati, P., Donnelly, C., Fekete, B., Flörke, F., Gosling, S.N., Hoffmann, P., Liersch, S., Masaki, Y., Motovilov, Y., Müller, C., Samaniego, L., Stacke, T., Wada, Y., Yang, T., Krysnaova, V., 2018. Sources of uncertainty in hydrological climate impact assessment: a cross-scale study. Environ. Res. Lett. 13, 015006. https://doi.org/10.1088/1748-9326/aa9938

Her, Y., Yoo, S.-H., Cho, J., Hwang, S., Jeong, J., Seong, C., 2019a. Uncertainty in hydrological analysis of climate change: multi-parameter vs. multi-GCM ensemble predictions. Sci Rep 9, 4974. https://doi.org/10.1038/s41598-019-41334-7

Her, Y., Yoo, S.-H., Cho, J., Hwang, S., Jeong, J., Seong, C., 2019b. Uncertainty in hydrological analysis of climate change: multi-parameter vs. multi-GCM ensemble predictions. Sci Rep 9, 4974. https://doi.org/10.1038/s41598-019-41334-7

Hipsey, M.R., Bruce, L.C., Boon, C., Busch, B., Carey, C.C., Hamilton, D.P., Hanson, P.C., Read, J.S., de Sousa, E., Weber, M., Winslow, L.A., 2019. A General Lake Model (GLM 3.0) for linking with high-frequency sensor data from the Global Lake Ecological Observatory Network (GLEON). Geoscientific Model Development 12, 473–523. https://doi.org/10.5194/gmd-12-473-2019

Hipsey, M.R., Bruce, L.C., Boon, C., Busch, B., Carey, C.C., Hamilton, D.P., Hanson, P.C., Read, J.S., De Sousa, E., Weber, M., Winslow, L.A., 2017. A General Lake Model (GLM 2.4) for linking with high-frequency sensor data from the Global Lake Ecological Observatory Network (GLEON) (preprint). Hydrology. https://doi.org/10.5194/gmd-2017-257

Hipsey, M.R., Bruce, L.C., Hamilton, D.P., 2014. GLM Manual v2 [WWW Document]. URL https://swan.science.uwa.edu.au/downloads/AED_GLM_v2_0b0_20141025.pdf (accessed 2.5.25).

Hipsey, M.R., Bruce, L.C., Hamilton, D.P., 2013. AED Manual v4 [WWW Document]. URL https://aed.see.uwa.edu.au/research/models/aed/Download/AED_ScienceManual_v4_draft.pdf (accessed 2.5.25).

Hounshell, A.G., Lewis, A.S.L., Howard, D.W., Wander, H.L., Lofton, M.E., Hanson, P.C., Carey, C.C., 2026. Dissolved organic carbon dynamics are driven by water temperature, primary production, and anoxia over 5 years of whole-ecosystem experiments in a eutrophic reservoir. Aquat Sci 88, 23. https://doi.org/10.1007/s00027-025-01252-5

Howard, D.W., Lofton, M.E., Thomas, R.Q., Delany, A.D., Breef-Pilz, A., Carey, C.C., 2026. Near-Term Forecasts of Dissolved Organic Matter Exhibit Consistent Patterns of Accuracy Across Multiple Freshwater Reservoirs. Journal of Geophysical Research: Biogeosciences 131, e2025JG009064. https://doi.org/10.1029/2025JG009064

Inácio, M., Barceló, D., Zhao, W., Pereira, P., 2022. Mapping lake ecosystem services: A systematic review. Science of The Total Environment 847, 157561. https://doi.org/10.1016/j.scitotenv.2022.157561

IPCC, Calvin, K., Dasgupta, D., Krinner, G., Mukherji, A., Thorne, P.W., Trisos, C., Romero, J., Aldunce, P., Barrett, K., Blanco, G., Cheung, W.W.L., Connors, S., Denton, F., Diongue-Niang, A., Dodman, D., Garschagen, M., Geden, O., Hayward, B., Jones, C., Jotzo, F., Krug, T., Lasco, R., Lee, Y.-Y., Masson-Delmotte, V., Meinshausen, M., Mintenbeck, K., Mokssit, A., Otto, F.E.L., Pathak, M., Pirani, A., Poloczanska, E., Pörtner, H.-O., Revi, A., Roberts, D.C., Roy, J., Ruane, A.C., Skea, J., Shukla, P.R., Slade, R., Slangen, A., Sokona, Y., Sörensson, A.A., Tignor, M., Van Vuuren, D., Wei, Y.-M., Winkler, H., Zhai, P., Zommers, Z., Hourcade, J.-C., Johnson, F.X., Pachauri, S., Simpson, N.P., Singh, C., Thomas, A., Totin, E., Arias, P., Bustamante, M., Elgizouli, I., Flato, G., Howden, M., Méndez-Vallejo, C., Pereira, J.J., Pichs-

Madruga, R., Rose, S.K., Saheb, Y., Sánchez Rodríguez, R., Ürge-Vorsatz, D., Xiao, C., Yassaa, N., Alegría, A., Armour, K., Bednar-Friedl, B., Blok, K., Cissé, G., Dentener, F., Eriksen, S., Fischer, E., Garner, G., Guivarch, C., Haasnoot, M., Hansen, G., Hauser, M., Hawkins, E., Hermans, T., Kopp, R., Leprince-Ringuet, N., Lewis, J., Ley, D., Ludden, C., Niamir, L., Nicholls, Z., Some, S., Szopa, S., Trewin, B., Van Der Wijst, K.-I., Winter, G., Witting, M., Birt, A., Ha, M., Romero, J., Kim, J., Haites, E.F., Jung, Y., Stavins, R., Birt, A., Ha, M., Orendain, D.J.A., Ignon, L., Park, S., Park, Y., Reisinger, A., Cammaramo, D., Fischlin, A., Fuglestvedt, J.S., Hansen, G., Ludden, C., Masson-Delmotte, V., Matthews, J.B.R., Mintenbeck, K., Pirani, A., Poloczanska, E., Leprince-Ringuet, N., Péan, C., 2023. IPCC, 2023: Climate Change 2023: Synthesis Report. Contribution of Working Groups I, II and III to the Sixth Assessment Report of the Intergovernmental Panel on Climate Change [Core Writing Team, H. Lee and J. Romero (eds.)]. IPCC, Geneva, Switzerland. Intergovernmental Panel on Climate Change (IPCC). https://doi.org/10.59327/IPCC/AR6-9789291691647

Jansen, J., Woolway, R.I., Kraemer, B.M., Albergel, C., Bastviken, D., Weyhenmeyer, G.A., Marcé, R., Sharma, S., Sobek, S., Tranvik, L.J., Perroud, M., Golub, M., Moore, T.N., Råman Vinnå, L., La Fuente, S., Grant, L., Pierson, D.C., Thiery, W., Jennings, E., 2022. Global increase in methane production under future warming of lake bottom waters. Global Change Biology 28, 5427–5440. https://doi.org/10.1111/gcb.16298

Jennings, E., de Eyto, E., Moore, T., Dillane, M., Ryder, E., Allott, N., Nic Aonghusa, C., Rouen, M., Poole, R., Pierson, D.C., 2020. From Highs to Lows: Changes in Dissolved Organic Carbon in a Peatland Catchment and Lake Following Extreme Flow Events. Water 12. https://doi.org/10.3390/w12102843

Jennings, E., Järvinen, M., Allott, N., Arvola, L., Moore, K., Naden, P., Aonghusa, C.N., Nõges, T., Weyhenmeyer, G.A., 2010. Impacts of Climate on the Flux of Dissolved Organic Carbon from Catchments, in: George, G. (Ed.), The Impact of Climate Change on European Lakes. Springer Netherlands, Dordrecht, pp. 199–220. https://doi.org/10.1007/978-90-481-2945-4_12

Kajan, K., Osterholz, H., Stegen, J., Gligora Udovič, M., Orlić, S., 2023. Mechanisms shaping dissolved organic matter and microbial community in lake ecosystems. Water Research 245, 120653. https://doi.org/10.1016/j.watres.2023.120653

Kim, S.W., Hong, S.K., Choi, E., 2009. Accumulation of organics in a water supply reservoir: Its cause, characteristics and implication on water quality management. Desalination and Water Treatment 2, 108–112. https://doi.org/10.5004/dwt.2009.158

Klante, C., Hägg, K., Larson, M., 2022. Understanding short-term organic matter fluctuations to optimize drinking water treatment. Water Practice and Technology 17, 2141–2159. https://doi.org/10.2166/wpt.2022.121

Köhler, S.J., Lavonen, E., Keucken, A., Schmitt-Kopplin, P., Spanjer, T., Persson, K., 2016. Upgrading coagulation with hollow-fibre nanofiltration for improved organic matter removal during surface water treatment. Water Research 89, 232–240. https://doi.org/10.1016/j.watres.2015.11.048

Kripka, M., de Medeiros, G.F., Kripka, R.M.L., 2026. Nelder-Mead Optimization Method, in: Encyclopedia of Engineering Optimization and Heuristics. Springer, Singapore, pp. 1–7. https://doi.org/10.1007/978-981-96-8165-5_47-1

Kritzberg, E.S., Hasselquist, E.M., Škerlep, M., Löfgren, S., Olsson, O., Stadmark, J., Valinia, S., Hansson, L.-A., Laudon, H., 2020. Browning of freshwaters: Consequences to ecosystem services, underlying drivers, and potential mitigation measures. Ambio 49, 375–390. https://doi.org/10.1007/s13280-019-01227-5

Kumari, M., Gupta, S.K., 2022. Cumulative human health risk analysis of trihalomethanes exposure in drinking water systems. Journal of Environmental Management 321, 115949. https://doi.org/10.1016/j.jenvman.2022.115949

Kundzewicz, Z.W., Krysanova, V., Benestad, R.E., Hov, Ø., Piniewski, M., Otto, I.M., 2018. Uncertainty in climate change impacts on water resources. Environmental Science & Policy 79, 1–8. https://doi.org/10.1016/j.envsci.2017.10.008

La Fuente, S., Jennings, E., Lenters, J.D., Verburg, P., Tan, Z., Perroud, M., Janssen, A.B.G., Woolway, R.I., 2024. Ensemble modeling of global lake evaporation under climate change. Journal of Hydrology 631, 130647. https://doi.org/10.1016/j.jhydrol.2024.130647

Lange, S., Büchner, M., 2021. ISIMIP3b bias-adjusted atmospheric climate input data (v1.1). https://doi.org/10.48364/ISIMIP.842396.1

Lavonen, E.E., Kothawala, D.N., Tranvik, L.J., Gonsior, M., Schmitt-Kopplin, P., Köhler, S.J., 2015. Tracking changes in the optical properties and molecular composition of dissolved organic matter during drinking water production. Water Research 85, 286–294. https://doi.org/10.1016/j.watres.2015.08.024

Ledesma, J.L.J., Köhler, S.J., Futter, M.N., 2012. Long-term dynamics of dissolved organic carbon: Implications for drinking water supply. Science of The Total Environment 432, 1–11. https://doi.org/10.1016/j.scitotenv.2012.05.071

Lofton, M.E., Howard, D.W., Thomas, R.Q., Carey, C.C., 2023. Progress and opportunities in advancing near-term forecasting of freshwater quality. Global Change Biology 29, 1691–1714. https://doi.org/10.1111/gcb.16590

Luo, J., Zhou, Q., Hu, X., Zeng, H., Deng, P., He, C., Shi, Q., 2022. Lake Chemodiversity Driven by Natural and Anthropogenic Factors. Environmental Science & Technology 56, 5910–5919. https://doi.org/10.1021/acs.est.1c08148

Ma, S., Yang, M., Wang, F., Luo, C., Xu, P., Ma, J., Chen, X., 2024. Autochthonous organic matter input in reservoirs: Limited methane oxidation in sediments fails to suppress methane emission. Science of The Total Environment 945, 174122. https://doi.org/10.1016/j.scitotenv.2024.174122

Marcé, R., George, G., Buscarinu, P., Deidda, M., Dunalska, J., de Eyto, E., Flaim, G., Grossart, H.-P., Istvanovics, V., Lenhardt, M., Moreno-Ostos, E., Obrador, B., Ostrovsky, I., Pierson, D.C., Potužák, J., Poikane, S., Rinke, K., Rodríguez-Mozaz, S., Staehr, P.A., Šumberová, K., Waajen, G., Weyhenmeyer, G.A., Weathers, K.C., Zion, M., Ibelings, B.W., Jennings, E., 2016. Automatic High Frequency Monitoring for Improved Lake and Reservoir Management. Environ. Sci. Technol. 50, 10780–10794. https://doi.org/10.1021/acs.est.6b01604

Marcé, R., Moreno-Ostos, E., Armengol, J., 2008. The role of river inputs on the hypolimnetic chemistry of a productive reservoir: implications for management of anoxia and total phosphorus internal loading. Lake and Reservoir Management 24, 87–98. https://doi.org/10.1080/07438140809354053

Marcé, R., Verdura, L., Leung, N., 2021. Dissolved organic matter spectroscopy reveals a hot spot of organic matter changes at the river–reservoir boundary. Aquat Sci 83, 67. https://doi.org/10.1007/s00027-021-00823-6

Marine Institute, 2017. Data Catalogue: Bathymetric Survey of Lough Feeagh, Co. Mayo. [WWW Document]. URL https://data.marine.ie/geonetwork/srv/eng/catalog.search#/metadata/ie.marine.data:dataset.1226 (accessed 6.7.24).

Mercado-Bettín, D., Clayer, F., Shikhani, M., Moore, T.N., Frías, M.D., Jackson-Blake, L., Sample, J., Iturbide, M., Herrera, S., French, A.S., Norling, M.D., Rinke, K., Marcé, R., 2021. Forecasting water temperature in lakes and reservoirs using seasonal climate prediction. Water Research 201, 117286. https://doi.org/10.1016/j.watres.2021.117286

Mercado-Bettín, D., Paíz, R., McCarthy, V., Jennings, E., De Eyto, E., Gallegos, A.M., Dillane, M., Garcia, J.C., Rodríguez, J.J., Marcé, R., 2026. A machine learning approach to driver attribution of dissolved organic matter dynamics in two contrasting freshwater systems. Biogeosciences 23, 2661–2685. https://doi.org/10.5194/bg-23-2661-2026

Mesman, J.P., Ayala, A.I., Adrian, R., De Eyto, E., Frassl, M.A., Goyette, S., Kasparian, J., Perroud, M., Stelzer, J.A.A., Pierson, D.C., Ibelings, B.W., 2020. Performance of one-dimensional hydrodynamic lake models during short-term extreme weather events. Environmental Modelling & Software 133, 104852. https://doi.org/10.1016/j.envsoft.2020.104852

Mishra, V., Cherkauer, K.A., Bowling, L.C., 2011. Changing thermal dynamics of lakes in the Great Lakes region: Role of ice cover feedbacks. Global and Planetary Change 75, 155–172. https://doi.org/10.1016/j.gloplacha.2010.11.003

Montenegro-Díaz, P., Crespo, P., Jaramillo, F., Ochoa-Sánchez, A., 2025. Water-related ecosystem services of lakes worldwide: a comprehensive meta-analysis. Environ. Res. Commun. 7, 112003. https://doi.org/10.1088/2515-7620/ae1d28

Moore, K., Pierson, D., Pettersson, K., Schneiderman, E., Samuelsson, P., 2008. Effects of warmer world scenarios on hydrologic inputs to Lake Mälaren, Sweden and implications for nutrient loads. Hydrobiologia 599, 191–199. https://doi.org/10.1007/s10750-007-9197-8

Muñoz-Sabater, J., Dutra, E., Agustí-Panareda, A., Albergel, C., Arduini, G., Balsamo, G., Boussetta, S., Choulga, M., Harrigan, S., Hersbach, H., Martens, B., Miralles, D.G., Piles, M., Rodríguez-Fernández, N.J., Zsoter, E., Buontempo, C., Thépaut, J.-N., 2021. ERA5-Land: a state-of-the-art global reanalysis dataset for land applications. Earth System Science Data 13, 4349–4383. https://doi.org/10.5194/essd-13-4349-2021

Murphy, A.H., 1992. Climatology, Persistence, and Their Linear Combination as Standards of Reference in Skill Scores. Weather and Forecasting 7, 692–698. https://doi.org/10.1175/1520-0434(1992)007%3C0692:CPATLC%3E2.0.CO;2

Naden, P.S., Allott, N., Arvola, L., Järvinen, M., Jennings, E., Moore, K., Nic Aonghusa, C., Pierson, D., Schneiderman, E., 2010. Modelling the Impacts of Climate Change on Dissolved Organic Carbon, in: George, G. (Ed.), The Impact of Climate Change on European Lakes. Springer Netherlands, Dordrecht, pp. 221–252. https://doi.org/10.1007/978-90-481-2945-4_13

Nissan, H., Goddard, L., De Perez, E.C., Furlow, J., Baethgen, W., Thomson, M.C., Mason, S.J., 2019. On the use and misuse of climate change projections in international development. WIREs Climate Change 10, e579. https://doi.org/10.1002/wcc.579

Paíz, R., Pierson, D.C., Lindqvist, K., Naden, P.S., de Eyto, E., Dillane, M., McCarthy, V., Linnane, S., Jennings, E., 2025a. Accounting for model parameter uncertainty provides more robust projections of dissolved organic carbon dynamics to aid drinking water management. Water Research 123238. https://doi.org/10.1016/j.watres.2025.123238

Paíz, R., Thomas, R.Q., Carey, C.C., de Eyto, E., Jones, I.D., Delany, A.D., Poole, R., Nixon, P., Dillane, M., McCarthy, V., Linnane, S., Jennings, E., 2025b. Near-term lake water temperature forecasts can be used to anticipate the ecological dynamics of freshwater species. Ecosphere 16, e70335. https://doi.org/10.1002/ecs2.70335

Pedregal-Montes, A., Jennings, E., Kothawala, D., Jones, K., Sjöstedt, J., Langenheder, S., Marcé, R., Farré, M.J., 2024. Disinfection by-product formation potential in response to variability in dissolved organic matter and nutrient inputs: Insights from a mesocosm study. Water Research 258, 121791. https://doi.org/10.1016/j.watres.2024.121791

Piai, L., Mei, S., van Gijn, K., Langenhoff, A., 2024. Effects of organic matter in drinking water and wastewater on micropollutant adsorption to activated carbon. Int. J. Environ. Sci. Technol. 21, 2547–2558. https://doi.org/10.1007/s13762-023-05132-z

Rodríguez-Cardona, B.M., Wymore, A.S., Argerich, A., Barnes, R.T., Bernal, S., Brookshire, E.N.J., Coble, A.A., Dodds, W.K., Fazekas, H.M., Helton, A.M., Johnes, P.J., Johnson, S.L., Jones, J.B., Kaushal, S.S., Kortelainen, P., López-Lloreda, C., Spencer, R.G.M., McDowell, W.H., 2022. Shifting stoichiometry: Long-term trends in stream-dissolved organic matter reveal altered C:N ratios due to history of atmospheric acid deposition. Global Change Biology 28, 98–114. https://doi.org/10.1111/gcb.15965

Ryder, E., de Eyto, E., Dillane, M., Poole, R., Jennings, E., 2014. Identifying the role of environmental drivers in organic carbon export from a forested peat catchment. Science of The Total Environment 490, 28–36. https://doi.org/10.1016/j.scitotenv.2014.04.091

Ryder, E., Jennings, E., de Eyto, E., Dillane, M., NicAonghusa, C., Pierson, D.C., Moore, K., Rouen, M., Poole, R., 2012. Temperature quenching of CDOM fluorescence sensors: temporal and spatial variability in the temperature response and a recommended temperature correction equation. Limnology and Oceanography: Methods 10, 1004–1010. https://doi.org/10.4319/lom.2012.10.1004

Schneiderman, E., Järvinen, M., Jennings, E., May, L., Moore, K., Naden, P.S., Pierson, D., 2010. Modeling the Effects of Climate Change on Catchment Hydrology with the GWLF Model, in: George, G. (Ed.), The Impact of Climate Change on European Lakes. Springer Netherlands, Dordrecht, pp. 33–50. https://doi.org/10.1007/978-90-481-2945-4_3

Shan, K., Song, L., Chen, W., Li, L., Liu, L., Wu, Y., Jia, Y., Zhou, Q., Peng, L., 2019. Analysis of environmental drivers influencing interspecific variations and associations among bloom-forming cyanobacteria in large, shallow eutrophic lakes. Harmful Algae 84, 84–94. https://doi.org/10.1016/j.hal.2019.02.002

Siddique, M.S., Xiong, X., Yang, H., Maqbool, T., Graham, N., Yu, W., 2022. Dynamic variations in DOM and DBPs formation potential during surface water treatment by ozonation-nanofiltration: Using spectroscopic indices approach. Chemical Engineering Journal 427, 132010. https://doi.org/10.1016/j.cej.2021.132010

Sohn, J., Kim, H.-S., 2002. Modeling of chlorination disinfection by-products (DBPs) formation at the full-scale study. KSCE J Civ Eng 6, 89–100. https://doi.org/10.1007/BF02829039

Srivastav, A.L., Patel, N., Chaudhary, V.K., 2020. Disinfection by-products in drinking water: Occurrence, toxicity and abatement. Environmental Pollution 267, 115474. https://doi.org/10.1016/j.envpol.2020.115474

Sullivan, E., 2022. Understanding from Machine Learning Models. The British Journal for the Philosophy of Science 73, 109–133. https://doi.org/10.1093/bjps/axz035

Switanek, M.B., Troch, P.A., Castro, C.L., Leuprecht, A., Chang, H.-I., Mukherjee, R., Demaria, E.M.C., 2017. Scaled distribution mapping: a bias correction method that preserves raw climate model projected changes. Hydrology and Earth System Sciences 21, 2649–2666. https://doi.org/10.5194/hess-21-2649-2017

Valenti-Quiroga, M., Cabrera-Codony, A., Emiliano, P., Valero, F., Monclús, H., Martin, M.J., 2024. In-depth analysis of natural organic matter fractions in drinking water treatment performance: Fate and role of humic substances in trihalomethanes formation potential. Science of The Total Environment 954, 176600. https://doi.org/10.1016/j.scitotenv.2024.176600

Villanueva, C.M., Evlampidou, I., Ibrahim, F., Donat-Vargas, C., Valentin, A., Tugulea, A.-M., Echigo, S., Jovanovic, D., Lebedev, A.T., Lemus-Pérez, M., Rodriguez-Susa, M., Luzati, A., de Cássia dos Santos Nery,

T., Pastén, P.A., Quiñones, M., Regli, S., Weisman, R., Dong, S., Ha, M., Phattarapattamawong, S., Manasfi, T., Musah, S.-I.E., Eng, A., Janák, K., Rush, S.C., Reckhow, D., Krasner, S.W., Vineis, P., Richardson, S.D., Kogevinas, M., 2023. Global assessment of chemical quality of drinking water: The case of trihalomethanes. Water Research 230, 119568. https://doi.org/10.1016/j.watres.2023.119568

Wang, H., Liu, X., Hua, Y., Xu, H., Chen, Y., Yang, D., Dai, X., 2024. Formation of autotrophic nitrogen removal granular sludge driven by the dual-partition airlift internal circulation: Insights from performance assessment, community succession, and metabolic mechanism. Journal of Environmental Management 353, 120158. https://doi.org/10.1016/j.jenvman.2024.120158

Warner, K.A., Saros, J.E., 2019. Variable responses of dissolved organic carbon to precipitation events in boreal drinking water lakes. Water Research 156, 315–326. https://doi.org/10.1016/j.watres.2019.03.036

Wit, H.A. de, Stoddard, J.L., Monteith, D.T., Sample, J.E., Austnes, K., Couture, S., Fölster, J., Higgins, S.N., Houle, D., Hruška, J., Krám, P., Kopáček, J., Paterson, A.M., Valinia, S., Dam, H.V., Vuorenmaa, J., Evans, C.D., 2021. Cleaner air reveals growing influence of climate on dissolved organic carbon trends in northern headwaters. Environ. Res. Lett. 16, 104009. https://doi.org/10.1088/1748-9326/ac2526

Woolway, R.I., Denfeld, B., Tan, Z., Jansen, J., Weyhenmeyer, G.A., La Fuente, S., 2022. Winter inverse lake stratification under historic and future climate change. Limnology and Oceanography Letters 7, 302–311. https://doi.org/10.1002/lol2.10231

Woolway, R.I., Kraemer, B.M., Lenters, J.D., Merchant, C.J., O'Reilly, C.M., Sharma, S., 2020. Global lake responses to climate change. Nature Reviews Earth & Environment 1, 388–403. https://doi.org/10.1038/s43017-020-0067-5

Wu, J., Yao, H., 2024. Enhanced Role of Streamflow Processes in the Evolutionary Trends of Dissolved Organic Carbon. Environ. Sci. Technol. 58, 4772–4780. https://doi.org/10.1021/acs.est.3c09508

Wu, J., Yao, H., Chen, Xiaohong, Chen, Xingwei, 2023. Dynamics of dissolved organic carbon during drought and flood events: A phase-by-stages perspective. Science of The Total Environment 871, 162158. https://doi.org/10.1016/j.scitotenv.2023.162158

Xiao, R., Deng, Y., Xu, Z., Chu, W., 2024. Disinfection Byproducts and Their Precursors in Drinking Water Sources: Origins, Influencing Factors, and Environmental Insights. Engineering 36, 36–50. https://doi.org/10.1016/j.eng.2023.08.017

Xie, H., Ma, Y., Jin, X., Jia, S., Zhao, Xu, Zhao, Xianfu, Cai, Y., Xu, J., Wu, F., Giesy, J.P., 2024. Land use and river-lake connectivity: Biodiversity determinants of lake ecosystems. Environmental Science and Ecotechnology 21, 100434. https://doi.org/10.1016/j.ese.2024.100434

Zhang, Z., Meng, J., Chen, Zhaoying, Zhou, S., Zhang, T., Chen, Zhe, Liu, Y., Cui, J., 2023. Response of dissolved organic matter to thermal stratification and environmental indication: The case of Gangnan Reservoir. Science of The Total Environment 868, 161615. https://doi.org/10.1016/j.scitotenv.2023.161615

Zhu, M., Wang, J., Yang, X., Zhang, Y., Zhang, L., Ren, H., Wu, B., Ye, L., 2022. A review of the application of machine learning in water quality evaluation. Eco-Environment & Health 1, 107–116. https://doi.org/10.1016/j.eehl.2022.06.001

Zimmermann, K., Schoutteten, K., Liu, Z., Chen, W., Bérubé, P., Mohseni, M., Barbeau, B., 2025. Biological ion exchange for natural organic matter removal from drinking water. Water Research 283, 123722. https://doi.org/10.1016/j.watres.2025.123722

Supplementary Material A

Supplementary Material A is available in the following repository: https://doi.org/10.5281/zenodo.23019762. It includes the GLM and AED configuration files for Lough Feeagh and Sau Reservoir parameter sets and scripts used in the modelling workflow.

intoDBP will create innovative tools and strategies to improve water quality management for safe human use and a healthy environment. It focuses on catchment protection and forecasting, transformative drinking water treatment, and real-time monitoring to combat the effects of climate and global change. In particular, intoDBP focuses on pollution and risks related to disinfection byproducts (DBPs). By developing and applying advanced, integrated, and cost-effective sensors and analytical methods, intoDBP will expand knowledge on water quality and DBP precursors to better understand its formation and human exposure in Europe. intoDBP monitoring results will feed into numerical forecasting tools to predict source water changes and formulate climate change adaptation pathways at catchment and treatment scale. intoDBP also develops transformative options for advanced and cost-effective upgrade of water treatment and disinfection.

In the intoDBP consortium researchers, small and large enterprises, communication experts and public services join forces to generate interdisciplinary solutions, that will generate a renewed perspective of drinking water surveillance, support decision-making and governance, and increase system resilience. intoDBP will implement and validate its cross-cutting products in four complementary case studies from three European countries where compliance with DBP regulation currently is an acknowledged challenge. The direct and visible positive impact of intoDBP in the case studies will foster rapid product adoption at a European and global scale, thus strengthening Europe's position and role in the global water market.

Reaching out beyond the water sector itself, intoDBP will directly engage society through surveys to analyze exposure to DBPs, collect data about catchment protection initiatives, create awareness and promote sustainable consumer behavior such as reducing bottled water consumption.



intoDBP

Funded by
the European Union